# Development of Cavity-Backed Antennas for use in Communications Applications

Jeffrey S. Carrie

A thesis presented to

University of Manitoba

in partial fulfillment of the requirements for

the degree of Master of Science

Winnipeg, Manitoba, 1998

THE UNIVERSITY OF MANITOBA

FACULTY OF GRADUATE STUDIES

*****

COPYRIGHT PERMISSION PAGE

# DEVELOPMENT OF CAVITY-BACKED ANTENNAS FOR USE IN COMMUNICATIONS APPLICATIONS

BY

JEFFREY S. CARRIE

A Thesis/Practicum submitted to the Faculty of Graduate Studies of The University of Manitoba in partial fulfillment of the requirements of the degree of

MASTER OF SCIENCE

# ABSTRACT

In this thesis several antenna elements are designed for use in commercial and personal communications systems. The goal of the research is to model and fabricate working antennas capable of both linear and circular polarization for use in receive and transmit applications. A patch-fed cavity is developed for linearly polarized applications, while for circularly polarized antennas, the microstrip patch is replaced with a circularly polarized dielectric resonator. The cavity antenna produces a gain of 12 dB over a 700MHz bandwidth at K-Band (20GHz) and over a 1GHz bandwidth at Ka-Band (30GHz).

The research involves the simulation, design, testing and optimization of the antenna elements. Simulation involves the use of the Transmission Line Matrix (TLM) method to predict antenna performance. These simulations lead to the design of the antenna geometry which is fabricated and tested. Results of the initial design are discussed with respect to minimizing losses and improving antenna performance. The iterative optimization process leads to the final element.

# Table of Contents

# List of Figures

# List of Tables

# Acknowledgments

I would like to thank the following:

Professor Sebak for accepting me as a graduate student, encouraging my research efforts and allowing me the opportunity to conduct my research both at the University of Manitoba and at the Communications Research Centre in Ottawa.

The Directorate of Antennas and Integrated Electronics at CRC, with special thanks to Dr. David Roscoe and Dr. Neil Simons whose insights and expertise provided invaluable assistance and guidance. Thanks are also due to Dr. Apisak Ittipiboon, Dr. Aldo Petosa, Michel Cuhaci, Rene Douville, John Bradley, Carole Glaser, Brian Clarke, and Peter Clark all of whom helped support my research.

SPAR Aerospace, Industry Canada, InfoMagnetics and the individual members of the Ka-Band project for allowing me the opportunity to share in their research and their wealth of experience and support.

Dr. Karu Esselle of MacQuarie University for his work on my behalf.

My fellow graduate students at both the University of Manitoba and at the Communications Research Centre for making my studies enjoyable and welcoming me to Ottawa.

My parents and siblings for passing on their wisdom, encouragement and sense of humour.

My loving wife Danielle for her constant support and trust.

My darling daughter Julia for always having a smile and just one more story to read.

# Introduction

## 1.0 Introduction

In reviewing a history of microwave communications, one can see a shift from larger conventional antennas to the printed microstrip antennas which finally gained acceptance in the 1970s. Although the performance of the conformal printed antennas paled in comparison to the more efficient, rugged collections of waveguides and horns, more and more research was devoted to the evolution of simple small bandwidth printed antennas. Industry and education both embraced the advantages of thin profile, lightweight antennas whose simplicity in design, manufacture and cost outweighed their apparent shortcomings. Research could be devoted to overcoming the obstacle of lower antenna efficiency; surface wave and radiation losses could be minimized and techniques could be developed to increase the bandwidth of the radiating device. The implementation of amplifiers and simple circuit elements could also improve performance. It is in this spirit that the following work is presented. In developing antennas for commercial and personal communication applications, the creation of novel and innovative designs is required to meet future demands. In addition to the physical fabrication of the device, the development of mathematical models to accurately predict device performance is crucial to timely optimization of the antenna geometry. In this thesis, both simulation and physical testing are undertaken to develop antennas for use in various communication applications. Insight and understanding were culled from a long list of predecessors too numerous to be listed as references here and it is hoped that this thesis joins this radiant body of knowledge and serves to illuminate future endeavours.

This thesis encompasses work done for the University of Manitoba as well as work on projects for the Communication Research Centre (CRC) in Ottawa and a co-operative project between SPAR Aerospace, CRC, The University of Manitoba, University of Waterloo and Carleton University. In each case the emphasis has been placed on the development and optimization of radiating elements for physical applications. This introduction serves to give an overview of some of the project requirements as well as providing background on the materials and tools required for the development of the radiating elements. Consideration is given to the project history, the software and hardware requirements in simulating proposed designs as well as the physical materials and structures used to construct the elements. Following chapters summarize the work which has been completed towards producing radiating elements for receive and transmit applications for both linear and circular polarization at both the K-band (20GHz) and Ka-Band (30GHz) operating frequencies.

Chapter 2 covers work performed for receive antenna applications, beginning with the early work performed in developing a low profile antenna. Starting with an oversized patch antenna, several candidates were tested and evaluated. Performance and design limitations resulted in the introduction of a cavity geometry which was then analyzed to produce the optimal performance. A combination of simulation and physical testing produced a linearly polarized element. The next stage in the evolution of the element was adaptation to circular polarization. Several simple modifications, which looked promising by simulation as well as the use of novel feeds proved to be less ideal in physical testing. As a result, yet another element was added to the overall geometry to produce a circularly

polarized element. This additional complexity required the use of more complex simulation with a transmission line matrix method.

The Transmission Line Matrix method employed is described in some detail in Chapter 2. The resulting designs were then fabricated and adjusted to produce the optimal geometry of the antenna. Comparisons between the physical and simulated geometries are made and an effort is made to explain the deviation between simulation and experiment.

Chapter 3 covers similar work performed for transmit antenna applications, the attempts to produce a linear polarized element from a simple scaled version of the receive antenna were not straightforward. Higher sidelobes in one of the principal planes led to a series of experiments attempting to reduce the unwanted effects. Once the linearly polarized element had been finalized efforts were then focused on creating the circularly polarized antenna. As with the receive antenna efforts, several candidates were examined and again the TLM software was utilized. Designs were then fabricated using both microstrip and stripline feeds. Chapter 3 presents several simulations and physical results performed in order to optimize the antenna for both feeds.

Finally, Chapter 4 summarizes the highlights from design to fabrication and through the optimization stages. Conclusions are drawn based on the comparisons between physical and simulated data and some final comments are made on the future work which is of interest.

## 1.1 Project Background

Much of the work contained in this thesis was performed as part of a co-operative effort with Spar Aerospace and select universities. The purpose of the project was to investigate future developments in space qualified antenna applications. The goal of the project was to develop a space compatible array for satellite use, capable of national coverage across a 1GHz bandwidth operating from 29-30GHz. Active phased array specifications and physical limitations were defined and based on these, a series of trade-offs were analyzed and agreed upon. From these agreements, specific objectives were then delegated to each of the partners in the project with the University of Manitoba group being in charge of element selection and optimization. Chapter 2 involves the optimization of receive antennas in the K-band. Initial efforts involved the use of oversized microstrip patches. By varying the geometry of the patch the antenna, parameters could be adjusted for frequency, gain, operating bandwidth and sidelobe levels.

Limitations of the design resulted in the introduction of the excited cavity geometry pictured in Figure 1.1 which would become the focal point of this investigation. The element is intended for use in a seven element array environment with a maximum inter-element separation of two free space wavelengths.

The cavity geometry was then fed by a variety of elements, including rectangular and circular microstrip patches as well as slot-coupled dielectric resonators. The evolution of the cavity backed antenna is traced in the following chapters. At the outset, the cavity geometry was simulated using a circular patch; parallel efforts at the Communications Research Centre led to the development of a linearly polarized rectangular patch-fed cavity.

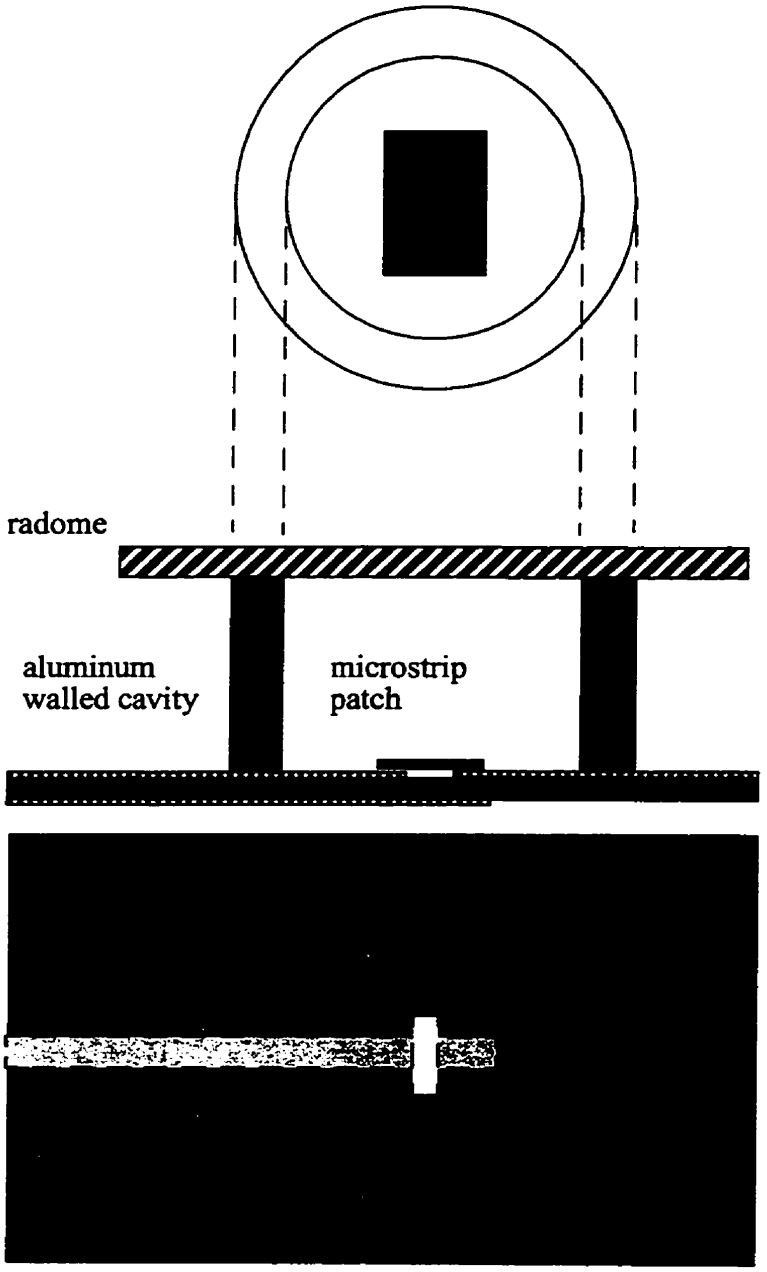


**Figure 1.1 Cavity backed antenna geometry**

Having achieved linear polarization, the next step was to modify the geometry for circular polarization. It was hoped that simple perturbations to the rectangular element would achieve circularly polarized results. Initial attempts involved alteration of the patch by bevelling the corners as achieved in [1]. Alternately, the use of a near square patch was investigated as well as several attempts at novel feeding techniques [2,3,4]. While modest success was achieved, the required specifications necessitated the introduction of an alternate feed element.

The choice of a resonating cross of medium dielectric was based on the dielectric resonator's ability to achieve circular polarization (CP) with low axial ratio, over a broad frequency band. Introduction of a dielectric radiating cross as achieved by Dr. Karu Esselle [5,6] assisted in increasing the performance. In order to simulate the effects of the cross, modifications were made to existing TLM software and these results were used in place of the Finite Difference Time Domain (FDTD) methods outlined by Dr. Esselle in [7]. The results of these simulations were early prototypes of radiating elements capable of producing CP both on their own as well as within the cavity geometry.

Chapter 3 outlines the process of duplicating the linear and circularly polarized elements in the Ka-band. While the experiments were anticipated to be a simple matter of scaling there were in fact several impediments to overcome. For the linear polarized element, a scaled version of the receive antenna as well as an empirically calculated patch showed less than ideal performance. The characteristics of concern were the high shoulders evident in the E plane pattern and several different methods were attempted to reduce their presence. Optimization of the linearly polarized element was successfully achieved and then the focus was shifted to the circularly polarized element. As with the receive antenna,

efforts were made with documented microstrip patch techniques however, once again the dielectric cross was chosen as the preferred element.

Simulation of an exact scaled version of the dielectric cross was not possible due to memory constraints related the meshing of the geometry within the source code. An approximate scaled geometry was analyzed which indicated that the antenna would not radiate CP.

As a result, the effects of altering the geometry height, width and arm lengths were investigated to attempt to equalize the field magnitudes and maintain a phase difference of 90 degrees. Several computer iterations produced two possible designs, one of which was deemed less sensitive to machining tolerances. Having achieved the optimal design in microstrip, the cavity geometry was subsequently modified for stripline feeding. As a final investigation, simulation was done with varying height of superstrate to show the effects of superstrate height on the matching to free space as well as the shift in operational frequency. These achievements are summarized in Chapter 4 along with some supplementary comments on future investigations.

## 1.2 Development Tools and Procedures

Simulation and fabrication of the antenna elements was achieved through the use of several materials and resources. Consideration was given to minimizing the total cost of development with the final design being space compatible. Early prototype designs of oversized patches and feeds were developed on a lower cost Rogers RT/Duroid with the end goal being to develop the feed as a stripline geometry using Rogers RT/Duroid 6002 having a relative permittivity of $\varepsilon_r$=2.94 with a very low coefficient of thermal expansion.

The model shop at the Communications Research Centre (CRC) was used extensively for fabrication of metal cavities which have been milled from aluminum with strict tolerances as well as for production of the miniature dielectric crosses. The dielectric crosses were constructed from Rogers RT/Duroid 6010 having a relative permittivity of $\varepsilon_r$=10.8. While tolerances for the lengths of the cross arms are easily controlled, the sharpness of the interior corners were difficult to ensure. In fact, there is a degree of rounding prevalent in the dielectric cross elements, which was determined to be insignificant as far as the performance of the cross was concerned. Connectors and launching blocks required for stability were also machined at CRC. Feed structures were plotted and out-sourced for photomask production with the etching of Duroid being done in-house. Precision markers were used throughout to ensure alignment of the structure. Several through holes were used to allow the feed substrates to be firmly attached to the metal ensuring rigidity of the structure and minimizing the possibility of air gaps. Finally the cavity element is topped with a superstrate of Alumina (having a relative permittivity of $\varepsilon_r$=9.9) machined to an appropriate thickness allowing the element to be matched to free space.

Simulations have been performed using several design tools. Originally, the cavity element was optimized using MBES, a CANCAD Technology package ideal for rotationally symmetric geometries using the Integral Equation techniques discussed in [8]. MBES was used to investigate the effect of middle and upper reflecting patches along with other perturbations to the geometry. These configurations were limited by the software only allowing one dielectric to be defined and therefore the entire potential of the exercise was never fully investigated. Shaker and Moheb have since followed up on this approach [9]. Initial investigations rejected the use of a reflective patch and it was decided to proceed with the

minimalist design of only one patch. While the University of Manitoba continued research on the circular patch, the project continued using the rectangular patch developed at CRC. The rectangular patch was later simulated using Panacea, a Transmission Line Matrix method described in[10] and summarized in Chapter 2.

Panacea was at that point intended solely as a check for the impedance matching of the cavity element while the simulation of the radiation pattern and axial ratio of circular polarization designs was intended for Ensemble. Ensemble uses a Method of Moments (MoM) approach to solve a Mixed Potential Integral Equation (MPIE). The software is well-suited to aperture coupled microstrip antennas and multi-layered structures including stripline and slotted ground planes. Ensemble was therefore intended to design and simulate the radiating patch element which would then be used within the cavity. As outlined in subsequent chapters, the simulated designs proved capable of achieving circular polarization, however the quality of the polarization was less than what had been desired. Several novel feeds and alternate radiating patch geometries failed to satisfactorily improve upon the present design which resulted in the use of an alternative radiating element to feed the cavity.

The dielectric cross developed by Esselle in [6] was simulated at MacQuarie University using a finite difference time domain (FDTD) technique and the results at 11GHz were then repeated for an individual aperture coupled cross at 19GHz. The TLM code was then altered to accommodate a dielectric element, in this case, the dielectric cross. Inclusion of the cross was difficult in that the cross was rotated fourty-five degrees and so the angular sides of the cross are not exact but stepwise approximate as detailed in chapter 2. These modifications proved successful in approximating the electrical performance also per-

formed at Macquarie University using their FDTD technique. This collaboration led to the element described in [11].

Using the Panacea code it was then possible to investigate both the performance of later designs at 30GHz as well as allowing us to simulate the entire cavity designs both in stripline and microstrip configuration. As noted in [12] the TLM method did tend to overestimate the length of the matching stub required in aperture coupling the element feedline.

In addition to producing the return loss performance of the feed, the transmission line matrix program was modified to produce far field transformations from the surface currents on the element. Computational memory requirements restricted the geometry tolerances to 0.2mm cell lengths and so physical testing and alterations were required to achieve more accurate dimensions.

In addition to the software described above, repeated use was also made of several other programs including Libra and Touchstone from EESOF which were used in investigation of feed structures as well as simple dimensional analysis for the electrical properties of the various materials used. Numerical computation was performed at both the University of Manitoba campus located in Winnipeg and the Communications Research Centre in Ottawa. Ensemble and Touchstone software was written for the PC and simulation times varied with the complexity of the geometry and meshing used. Panacea, MBES and Libra were all run on SUNOS SPARC20 and SOLARIS ULTRA SPARC workstations. Due to the fine spacing of the mesh, running Panacea on the full cavity geometry required nearly 300MB of RAM to run a simulation. The ULTRA SPARC is capable of running a full cavity simulation in four hours while the SPARC20 typically requires 8-10 hours. Both simu-

lations output a near field data file on the order of 85MB. From this output file the near to far field transformation for thirty frequency points can be relatively quickly calculated. That is, the transformation takes less than 10 minutes for each plane of interest.

This chapter has discussed the motivation for the project, the goals and the methodology in constructing the proposed antenna elements. In Chapter 2 we will examine the design, simulation, fabrication and optimization of the receive antenna elements. Included is some background into the TLM software (Panacea) used for simulation. Chapter 3 continues the evolution of the antenna elements as they are adapted for use in transmit applications. Chapter 4 reviews the project accomplishments, summarizes the contributions and suggests the future work which may be examined.

# Receive Antenna Elements

## 2.0 Receive Antenna Elements for use in 20GHz Applications

Early design work for the receive antennas was performed at C-Band with the intention of scaling the radiating elements for use at K-Band (~20GHz) for receive applications and later Ka-Band (~30GHz) for transmit applications. This chapter deals with the first efforts at producing a receive antenna. The cavity backed element is introduced as an alternative to the original design. Simulation of the geometry is first done using Dr. Kishk's MBES program and initial prototypes are tested using a circular patch. Dr. Roscoe's optimization of the 20GHz linear patch is then used as a stepping stone for the development of a circularly polarized element operating at 20GHz. The use of a rectangular patch results in dropping the use of the rotationally symmetric MBES program for Ensemble. The use of Ensemble allows us to investigate the results of perturbations to the patch in an effort to produce circular polarization. The Transmission Line Matrix method (TLM) based program Panacea is introduced for modeling the microstrip feed. Limited physical success results in the investigation of alternate feed arrangements to produce circular polarization. These efforts, while promising, do not provide the full capability required. These shortcomings are overcome by the introduction of the dielectric resonator as a feed element for the cavity, replacing the altered microstrip patch. The use of a circularly polarized dielectric cross is then investigated. In association with Dr. Karu Esselle and MacQuarie University, a K-Band element is produced using a Finite Difference Time Domain method. Operation is then validated through physical testing and duplicate simulation using Panacea. Finally the cross is designed into the cavity geometry and the entire structure is phys-

ically realized and optimized. Conclusions are drawn on the performance of the antenna and its discrepancy with respect to simulated expectations.

## 2.1 Linearly Polarized Elements

### 2.1.1 Preliminary Investigations

Early work on the Ka-Band project resulted in the development of oversized patches, of which one design is shown below in Figure 2.1. These elements were introduced by Dr. Herve Legay[13] whose investigations showed that the element properties could be altered through manipulation of the various slot widths, lengths and orientations.

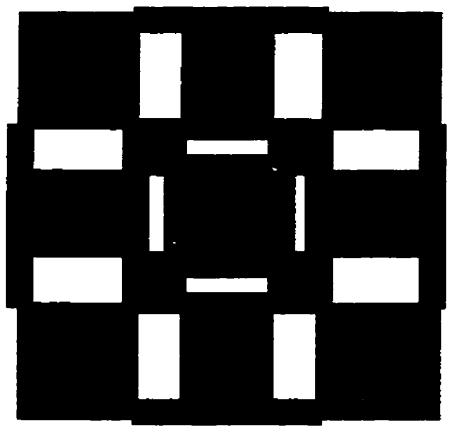

**Figure 2.1 EH143 Oversized microstrip patch**

The oversized patch is excited through an aperture coupled feedline as presented by Pozar[14]. This technique is chosen in order to remove the need for probe connections which typically require a larger physical area when used in an array environment. In addi-

tion the geometry, as shown in Figure 2.2 consists of two dielectric regions with a feed line coupling through a narrow slot in a shared ground plane. This approach allows more room for the feed network as well as isolating unwanted feedline radiation from the element. Physical testing was unsatisfactory in that the oversized aperture coupled patches had difficulty achieving the same performance as the probe excited elements, of which a typical radiation pattern is presented in Figure 2.3.

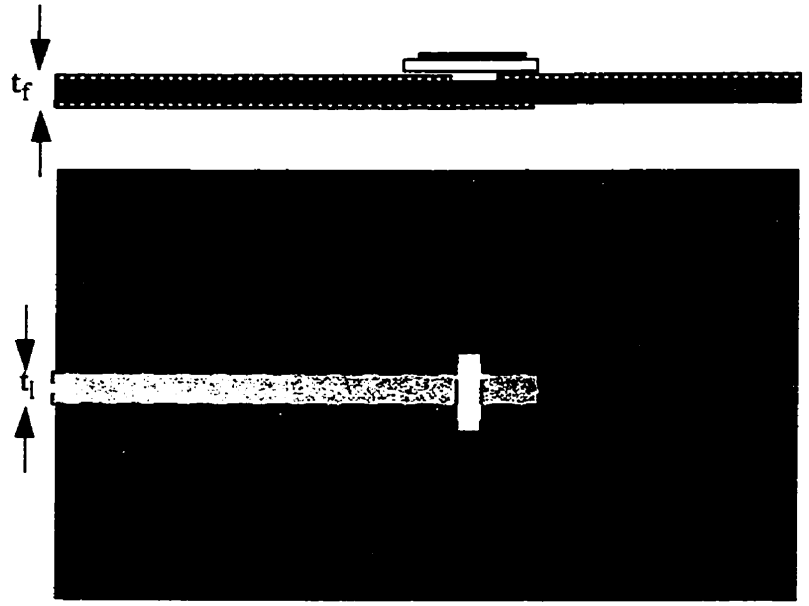


**Figure 2.2 Geometry of an aperture-coupled microstrip patch**

The performance discrepancy was assumed to be due to air gaps between the two dielectric layers and other difficulties with the oversized geometry. The decision was made to attempt a scaled version of the oversized patch for 30GHz, however, these efforts proved equally unsatisfactory. While the problems involved with alignment and coupling of the feed line were overcome, difficulties were encountered with the radiation pattern. Higher

sidelobes in one of the principal planes resulted in a lower than required gain. Suppression of the sidelobes through alteration of the slot geometry had resulted in a larger coupling variation over the desired frequency band. As a result the gain performance was not adequate over the entire operating band. Further optimizations were deferred in favour of a new element geometry.

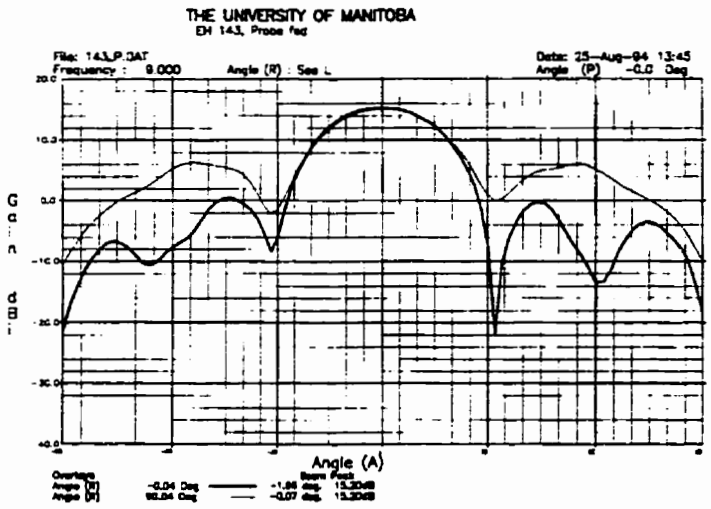


**Figure 2.3 Radiation Pattern of the Probe-Fed EH143 f=9.0GHz**

### 2.1.2 Introduction of the Patch-fed Cavity

In this configuration proposed by Dr. Shafai[15] and reproduced below in Figure 2.4, a single microstrip patch is placed inside a cavity approximately a half free-space wavelength in height with a diameter equivalent to 2 free space wavelengths and then covered with a dielectric radome. The radome electrical thickness is chosen to be slightly under a quarter wavelength. Inclusion of the radome is intended to cause a uniform field distribution across the aperture maximizing the element gain. The radome permits resonance as

the cavity is matched to free space and optimally provides maximum gain, a function of the cavity diameter. Current distribution and input impedance effects on a printed dipole have been investigated by Soares [16]. Increased relative permittivity of the radome allowed for stronger coupling to free space, and as a result, the dielectric radome was chosen to be manufactured out of Alumina with a relative permittivity ($\varepsilon_r$=9.9) much higher than the patch substrate. The radome therefore confines fringing effects close to the aperture, minimizing evanescent fields at the edge of the cavity. One of the benefits of this cavity design is reported in [17] where the bandwidth of a microstrip patch is increased from 4 to 8%. During optimization it was necessary to design the patch for a higher frequency since the cavity appeared to drop the overall operating frequency of the element.

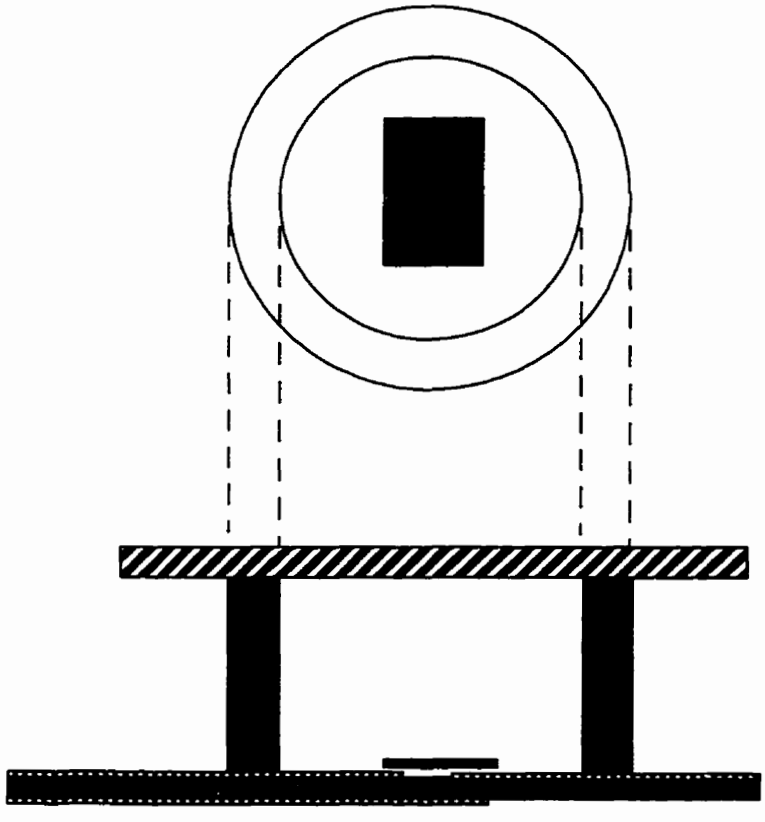

**Figure 2.4 Geometry of the Aperture-Coupled Patch-fed Cavity**

The microstrip patch typically designed as described in [1, 18] is also excited through the aperture coupled feedline as presented by Pozar[14] and simulated using techniques outlined by Saed [19]. Several numerical methods for analyzing cavity antennas and their application to circular polarization are discussed in the literature [20,21,22] along with works related to the microstrip and stripline feeds [23,24,25,26,27,28]. Numerical methods for multi-layered conditions such as presented by the appearance of the radome have been discussed in [29] which uses a moment method to determine the gain enhancement and alteration in impedance.

Initial simulation of the cavity backed microstrip patch geometry was performed using MBES which assumes a rotationally symmetric geometry as described by Kishk[8]. A cross section is defined as shown in Figure 2.5. An asymmetric mesh is typically used to produce more exact results in areas of interest, such as corners and boundaries between dielectric regions.

Using a dipole excitation to represent the source, the equivalence principle is invoked and the resulting matrix equations lead to the derivation of the far field $E_\theta$ and $E_\phi$ components which produce a radiation pattern similar to that seen in Figure 2.6.

In addition to the probe excited patch at the bottom of the cavity cross section, Figure 2.5 also shows an additional reflective patch underneath the dielectric radome. This patch was inevitably removed from the final design. MBES also allowed for the investigation of additional reflecting patches an alternate to the MPIE method discussed by Mosig et. al. [30].

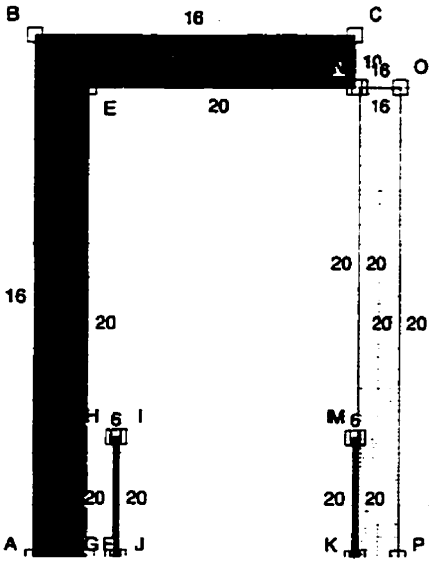


**Figure 2.5 MBES representation of the rotationally symmetric cavity**

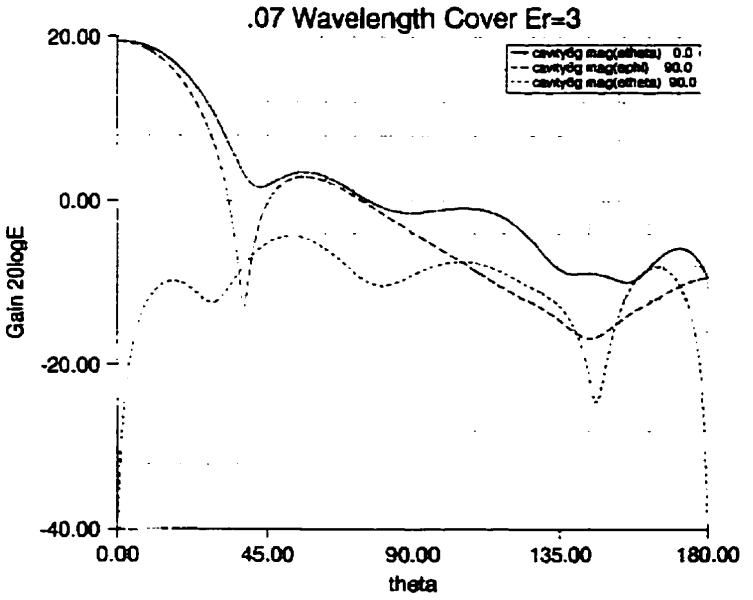


**Figure 2.6 MBES Simulated Radiation pattern**

Results of stacked patches have been investigated by Zavosh [31] who used the parasitic patch to reduce frequency variation of the input impedance which in turn enhanced the operating bandwidth. This increased bandwidth comes with the trade-off of reducing the antenna gain and so it was decided to proceed with the simpler single patch design. Further investigations have been undertaken to simulate the effects of stacked patches and predict the effect of high permittivity on gain, bandwidth, beamwidth and efficiency [17,30]. MBES limits the user to one non-unity dielectric constant and therefore a full investigation into dielectric spacers was not undertaken. Efforts were concentrated on the effects of the dielectric radome of different thicknesses.

For the case of an Alumina superstrate of $\varepsilon_r$=9.9, several simulations were run with varying thicknesses of dielectric cover. The results are captured in Figure 2.7 which shows a maximum gain for a dielectric thickness of approximately 0.08 free space wavelengths ($\lambda_0$). This translates roughly to a quarter guided wavelengths where:

$$\lambda g = \frac{\lambda 0}{\sqrt{\varepsilon r}}$$

which, substituting for the relative permittivity of Alumina and multiplying through the factor of 0.08 produces:

$$0.08 \times \lambda 0 = 0.08 \times \sqrt{9.9}\lambda g \approx 0.2517\lambda g$$

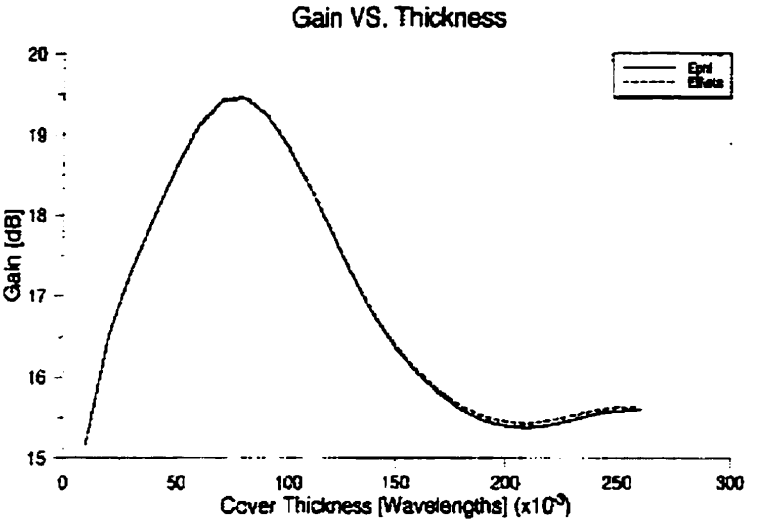


**Figure 2.7 MBES Simulated cavity gain as a function of radome thickness($\lambda_0$)**

Parallel work at the University of Manitoba and the Communications Research Centre has led to the optimization of a linear polarized radiating element for use at 19.7GHz. The entire structure is identical to that pictured in Figure 2.4. The microstrip patch is not circular, but rectangular, is built on 1/32" thick 5880 duroid ($\varepsilon_r$=2.33)and is 6mmx4.6mm in size. The feed line is built on 0.025" thick 6010 duroid ($\varepsilon_r$=10.2)and utilizes a 50Ω trace measuring 0.65mm wide and extending 0.76mm past the centre of a 5.1mmx0.6mm slot in the ground plane. The 0.737cm high cavity measures two wavelengths in diameter (2.035cm at 19.7GHz) and is covered by an alumina superstrate ($\varepsilon_r$=9.9), 0.040" thick (~1mm). This corresponds to a radome thickness of approximately 0.2 guided wavelengths, slightly lower than anticipated by the MBES simulations. Radiation patterns for the linear polarized element are shown for frequencies of 19.5GHz and 19.7GHz.

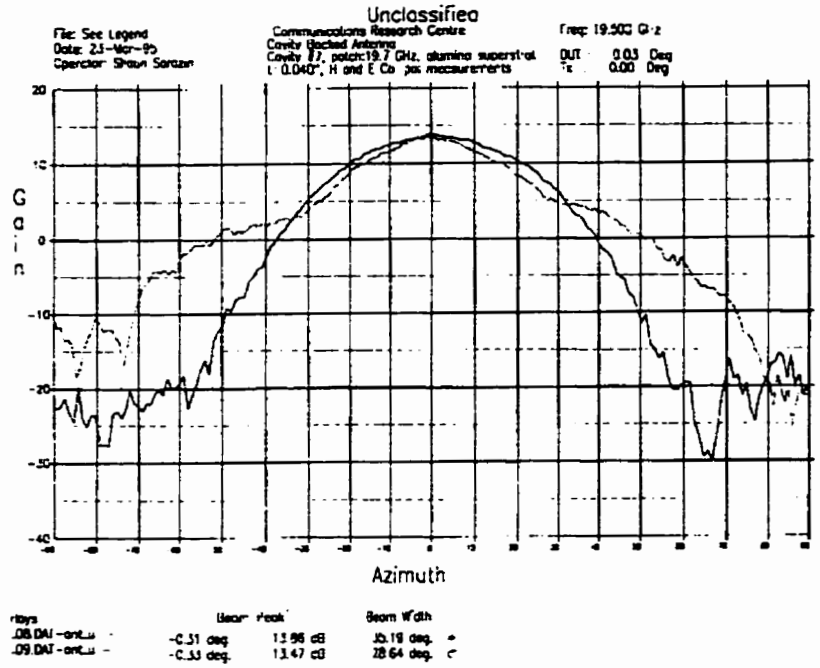


**Figure 2.8 Radiation pattern of the optimized Linear Polarized Cavity f=19.5GHz**

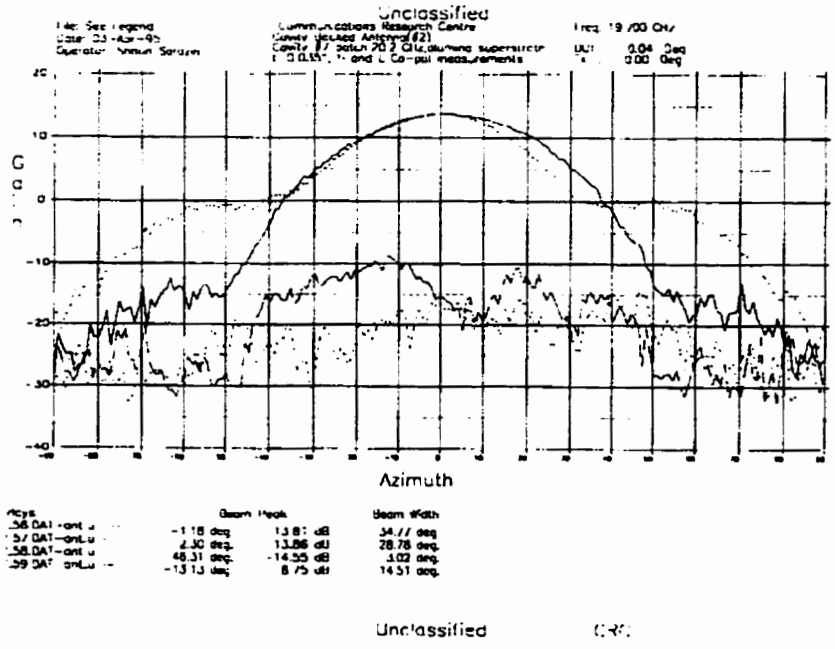


**Figure 2.9 Radiation pattern of the optimized Linear Polarized Cavity f=19.7GHz**

Beam symmetry is excellent between the two principal planes and cross-polarization levels are low. There is some concern about the height of the shoulders in the E-plane, however, they appear to be well behaved across the operating bandwidth. For the circularly polarized element the cavity diameter will need to be decreased to allow for its use in an array where the maximum element separation is two wavelengths. Further developments for millimeter wave applications have been investigated in [32] along with investigations into stacked microstrip patches[30].

The use of superconducting metals [33] has been investigated as a method of improving the feed coupling, but suffers from low operating bandwidth. This can be overcome with thicker substrates and other improved coupling techniques noted in [34].

### 2.1.3 The Transmission Line Matrix Method

The Transmission Line Matrix method uses a discrete uniform mesh of interconnected transmission lines where each transmission line has a characteristic impedance. By applying voltage pulses to the grid, the excitation then propagates through the grid as described by the algorithm with each pulse representing a discrete component of the field distribution. The details of the propagation and the mathematical algorithm have been covered in extensive literature. For an overview of two dimensional numerical analysis of generalized elements the reader is directed to [35]. A summary of this can be found in [12] with insight into the algorithms used for this thesis in [36, 37] based on works by Hoefer [38] and Johns[39]

Since TLM is capable of supporting transmission lines transverse electromagnetic (TEM) waves can therefore propagate. The E and H fields can then be found in terms of a voltage pulse v travelling in x and y. The 2-dimensional model described in[35] provides solutions based on Maxwell's equations with d/dz=0 and Hz=0.

The above technique assumes a homogeneous free space environment. This technique is then extended to material regions as in [40]. To summarize this work the permittivity can be realized with an open circuit terminated transmission line of admittance $Y_0$ and length equal to half the mesh size. This stub serves to reduce the wave propagation velocity.

Alternately, conductivity is realized using a match terminated transmission line of admittance $G_0$, again with a length equal to half the mesh size. Here the matched line reduces the amount of energy present in the TLM mesh for each time step.

In addition, boundary conditions are enforced by terminating the transmission lines with reflection coefficients halfway between the two node centres. The inclusion of absorbing boundary conditions serves to enforce the appropriate conditions on the field distributions along boundaries.

In order to analyze the structure of the linearly polarized aperture-coupled antenna, the geometry is meshed. Given the cubic nature of the meshing technique the circular cavity can either be defined as a stepwise approximation or replaced with a square cavity. For the purposes of analyzing the return loss, it is simpler to define a square cavity. A cubic space larger than the antenna of interest is chosen, a ground plane is defined in the z=0 plane. Simulating with a larger ground plane will improve the accuracy of the model, although larger geometries require longer computation times.

As shown in Figure 2.10, for a cavity of 1.8cm, (as will be used for simulating the geometry at 30GHz), a 3.6x3.6x0.86cm space was used. Given a mesh spacing of 0.2mm, the RAM requirements, given 18 line parameters multiplied by 4 bits per word multiplied by a factor of 2 (allowing for incident and reflected pulses) equates to over 200MB of RAM. Memory requirements therefore follow an $N^3$ relationship, so increasing the geometry size or shrinking the mesh size has a drastic effect on memory requirements as well as computation time. For this reason, a full cavity analysis of the antenna will only be performed at 30GHz and this chapter will only make use of the TLM code to simulate individual elements. A Gaussian pulse is used for the excitation and by placing observation points along the feed line we can monitor the z component of the electric field and subsequently the propagation as seen in Figure 2.11. Because the Gaussian pulse has a non-uniform energy content with respect to frequency we must normalize the frequency content of the observed field to the frequency content of the excitation. First we see the initial pulse passing the observation point at 0.08nsec, this is accompanied with a slight negative pulse created by dispersion along the feedline. The next positive pulse represents the reflection from the slot travelling back towards the source and that is soon followed by the reflection from the open circuit termination of the feed line. Successive reflections and some resonance from the microstrip patch settle out after approximately 3000 time steps (1 nanosecond). The TLM code calculates near field measurements based on the user's choice of observation space. The far field patterns can then be generated through a transformation from far near to far field as outlined in [25].

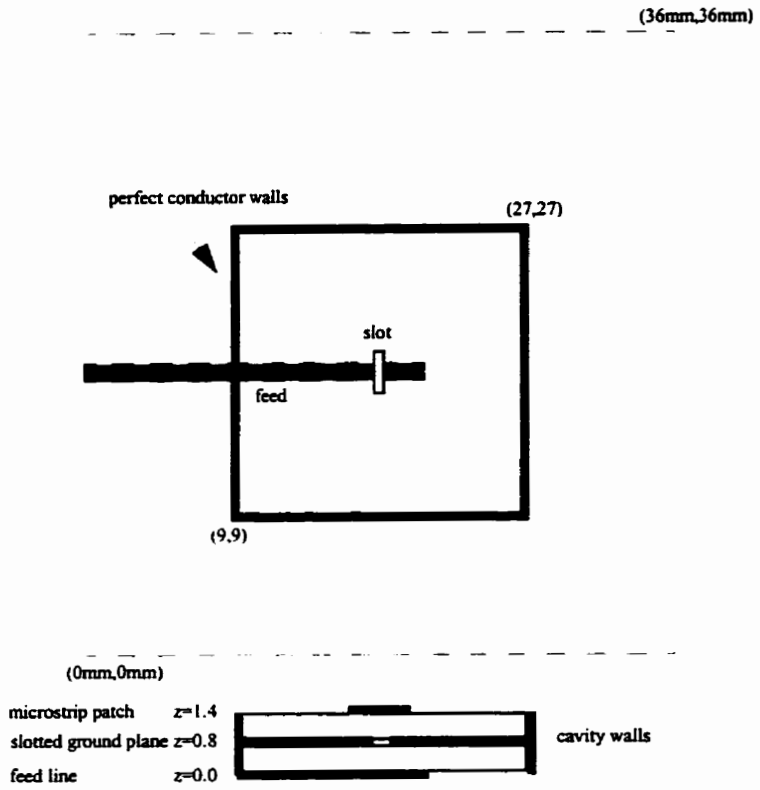


**Figure 2.10 Meshing of the Cavity Element, Mesh size=0.2mm, Nx=180, Ny=180**

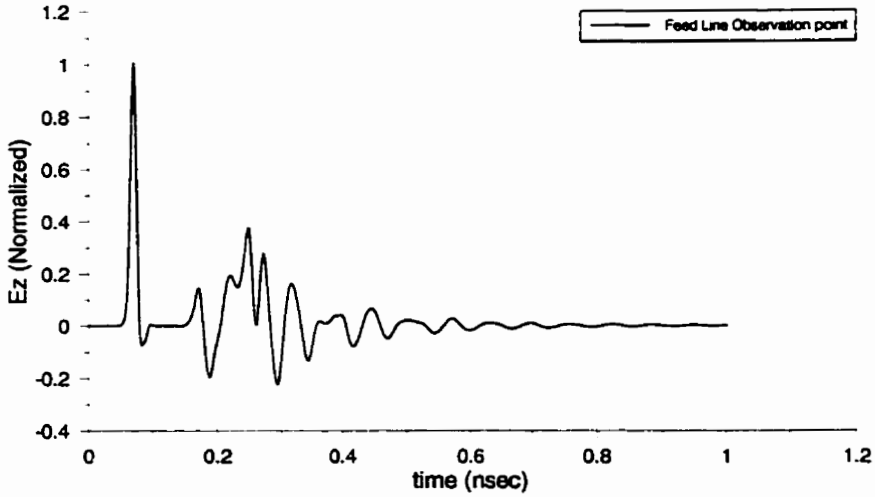


**Figure 2.11 Electric Field (Ez) observed along the microstrip feedline**

## 2.2 Circularly Polarized Elements Fed with Microstrip

For many communication applications it is necessary to radiate circular polarization. These antennas can typically be single or dual fed, although the presence of a second feed requires an external polarizer capable of producing the phase offset required. Classical methods of perturbing the single fed linear polarized element to produce circular polarization are outlined in [1] and [41,42,43,44,45]. Alternately, it is possible to produce an array of linear polarized elements which can be arranged to generate circular polarization [46]. Techniques for increasing the operating bandwidth of circularly polarized elements are also investigated in [47].

The purpose of this section is to minimize the feed design of a potential array element by producing a single-fed cavity element. Several classical techniques for producing circular polarization are attempted along with more novel adjustments of the aperture coupling. The most attractive solution is the introduction of an alternate radiating element.

### 2.2.1 Perturbation of the Linearly Polarized Element

The first step in developing the element for circular polarization was to attempt the adaptation of the existing linearly polarized model. In order to achieve Circular Polarization, bevelling of the patch corners was attempted. Using an exacto knife the 19.7GHz patch was bevelled slightly and tested on the network analyzer. The intent is to separate the generated mode into two orthogonal modes. Within the cavity, the antenna showed promising results with several thicknesses of dielectric radomes. Two resonances occurred which suggested the presence of two linear operating modes, with a Circularly Polarized band-

width likely existing between them. On the Smith Chart, these dual modes are shown as a resonant loop shrinking to a point. However, physical testing in the anechoic chamber showed that CP was not evident. Increased bevelling of the patch proved to be unhelpful.

While single probe feeding techniques are prone to low operating bandwidths, it was hoped that the low Q of the cavity would increase the axial ratio bandwidth to a usable level. To ensure that the cavity was not having a parasitic effect on the overall performance, an attempt was made to achieve CP using the patch alone, separate from the cavity structure. Axial ratios remained greater than 10dB, so while dual modes may have been operating, the phase difference between them was not adequate for CP to occur.

By itself the patch did not show a resonant loop at the expected frequency. It was postulated that the cuts made by hand may not have been exact enough and that the patches should be etched to ensure a smooth and precise bevelling. In the event quality of the cut was not accurate enough, several bevelled patches with different degrees of bevelling (2-8% of the patch area) were etched. The 2% bevelled patch showed the expected performance in the s-parameter analysis, suggesting the presence of two linear modes operating at 19.456GHz and 19.984GHz and the Smith Chart showed the resonant loop has shrunk to a corner as anticipated. However, as before, the physical results were less than impressive. All degrees of bevelling failed to produce a CP bandwidth upon testing them in the anechoic chamber. The measured Axial Ratio was poor whether the patch was operating alone or in the cavity.

Numerical simulations of the 6mmx4.6mm patch using Ensemble indicated that the patch seemed to be incapable of producing CP with a single probe feed with 45 degree cut bev-

els. Various bevelling techniques and feed positions were attempted with little success. Ensemble indicated that reasonable CP could be achieved by using a two probe method as well as by using a diagonally located feed on a square patch. Techniques for probe and slot feed locations are covered in [48].

Rather than increase the complexity of the design with dual feeds, which would be cumbersome in an array environment, alternate methods of generating CP were researched. Three different alternatives were explored, the possibility of a new slot-feed mechanism, adoption of a near square patch, and the utilization of a new element, specifically a dielectric radiating cross element.

### 2.2.2 Alternate Feed Techniques

Dual feed techniques for creating circular polarization [2,49,50] with aperture coupled patches are less attractive due to the increased complexity of the feed design in an array environment. Circular polarization has been achieved with single point feeding [41,51] although these are not techniques which have been performed with aperture coupling. Several slot architectures such as those pictured in Figure 2.12 were attempted in hopes of inducing circular polarization without the use of a second feed. Many of these were based on [3,4], where CP is generated with the use of a directly excited slot and a second slot which due to its proximity, is parasitically excited. Crossed slots fed by a single meandering line as in [52] were rejected due to size restraints. The results pictured in Figures 2.13-15 turned out to be unsatisfactory. Symmetric crossed slots with an offset feed showed the

most promise although the performance is quite rough. The potential for CP operation does appear but only over a fairly small bandwidth.

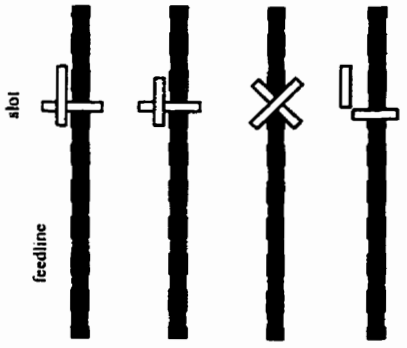


**Figure 2.12 Potential Alternate Feeds**

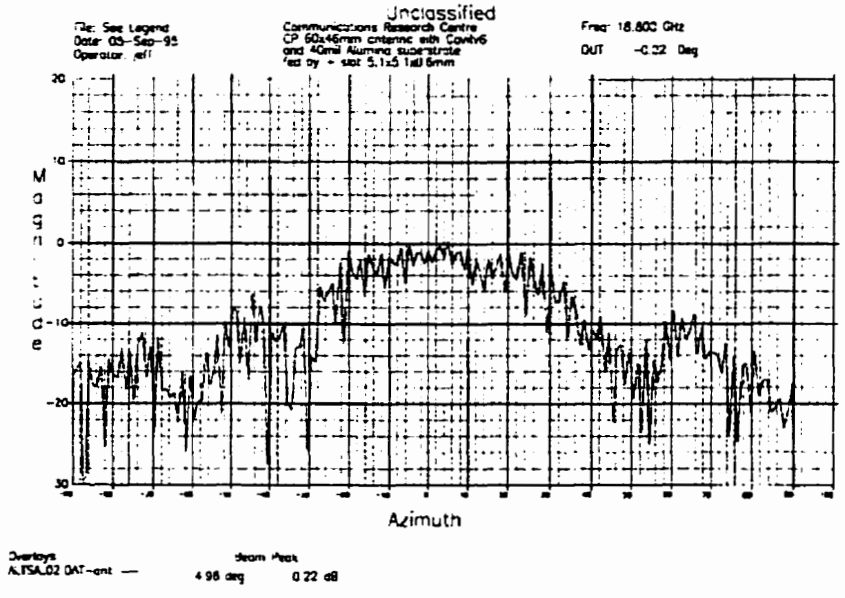


**Figure 2.13 Attempt at Producing Circular Polarization with crossed slots**

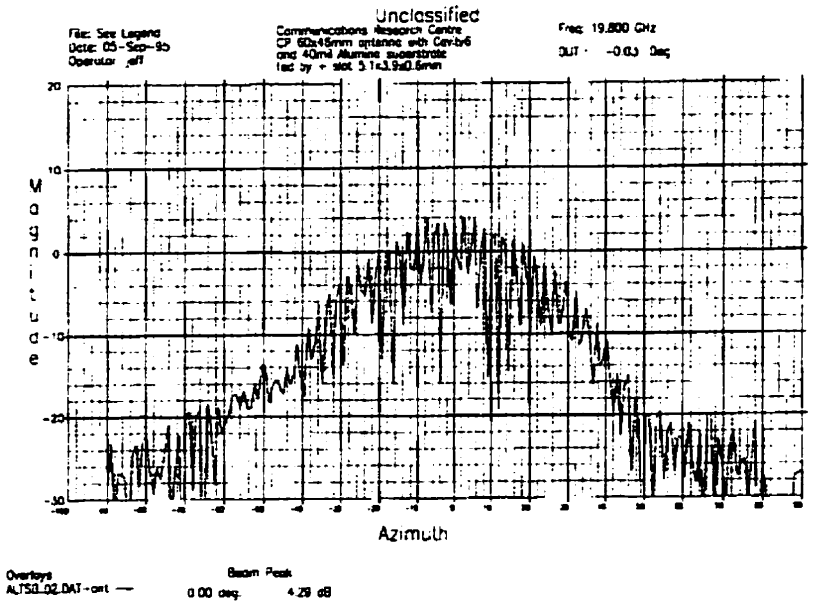


**Figure 2.14 Attempt at Producing Circular Polarization with asymmetric crossed slots**

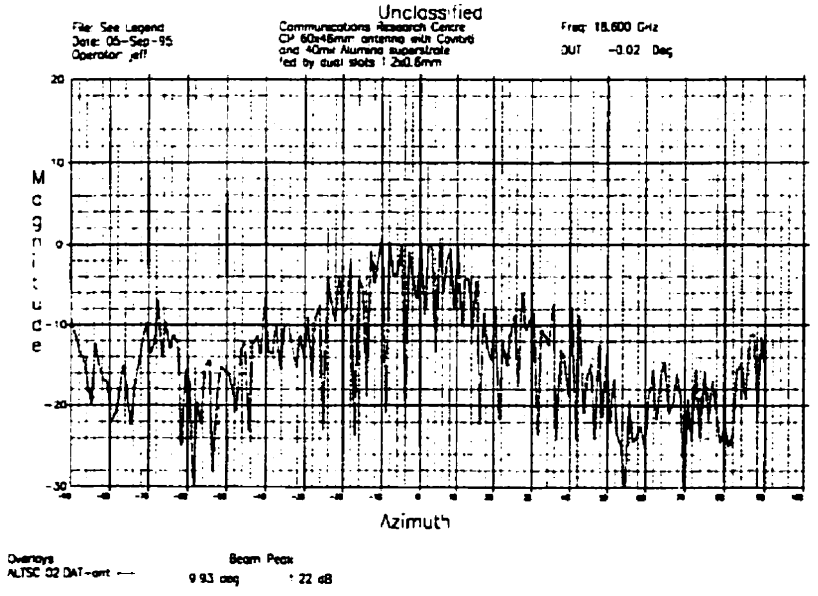


**Figure 2.15 Attempt at Producing Circular Polarization with parasitically coupled slots**

### 2.2.3 Implementation of a Near Square Patch

Having failed to produce acceptable circular polarization with classical perturbation methods or through the use of a novel feed, efforts were concentrated on the use of an alternate radiating element to feed the cavity structure. The first attempt was made with a near square patch, which, it was hoped, would produce two orthogonal modes whose bevelled corners would result in a ninety degree phase difference. In order to obtain the radiation pattern of a near square patch at 19.7GHz, Ensemble was chosen as the quickest method of determining the validity of the design. Several tests were run with different patch dimensions and various degrees of bevelling. For 5880 Duroid of 1/32 inch thickness, the design was chosen to be 4.7x4.8mm in size with opposite corners bevelled 45degrees, by removing 1.1mm along each side. Unlike the rectangular patch attempted previously, the near square patch proved more amenable to circular polarized operation.

According to the computed analysis summarized in Figures 2.16-19 the element appears to be capable of achieving circular polarization. The return loss calculations presented in Figure 2.16 suggest only one resonant mode however, given the frequency step size used when calculating the results, it may be possible to miss a second resonance.

Figure 2.17 indicates that circular polarization should occur over a 3dB Axial Ratio bandwidth of about 600MHz. The resulting far-field radiation patterns of the orthogonal electric field components such as those in Figures 2.18-19 show the anticipated beam shape and comparable magnitudes.

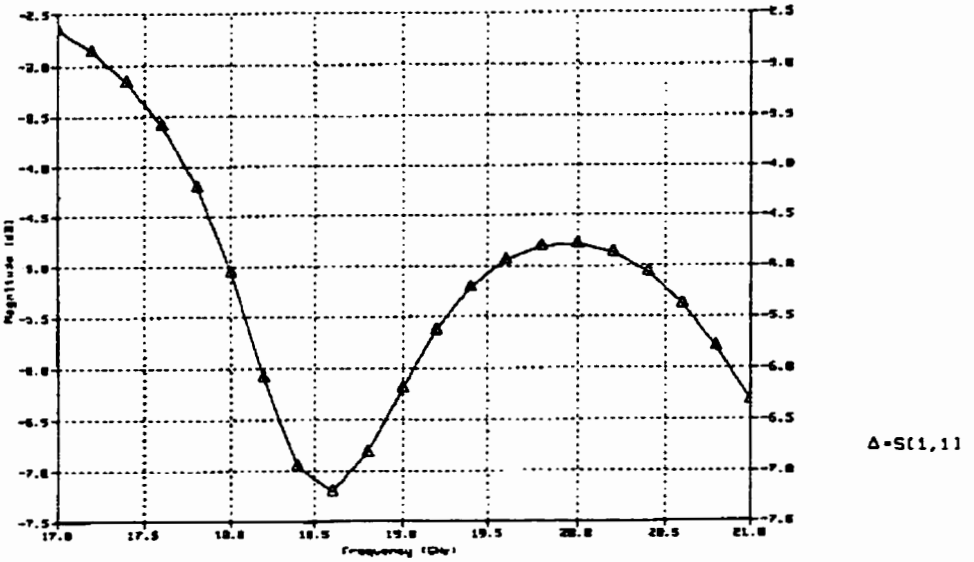


**Figure 2.16 Ensemble Simulated Return Loss of Aperture-Coupled Near Square Patch**

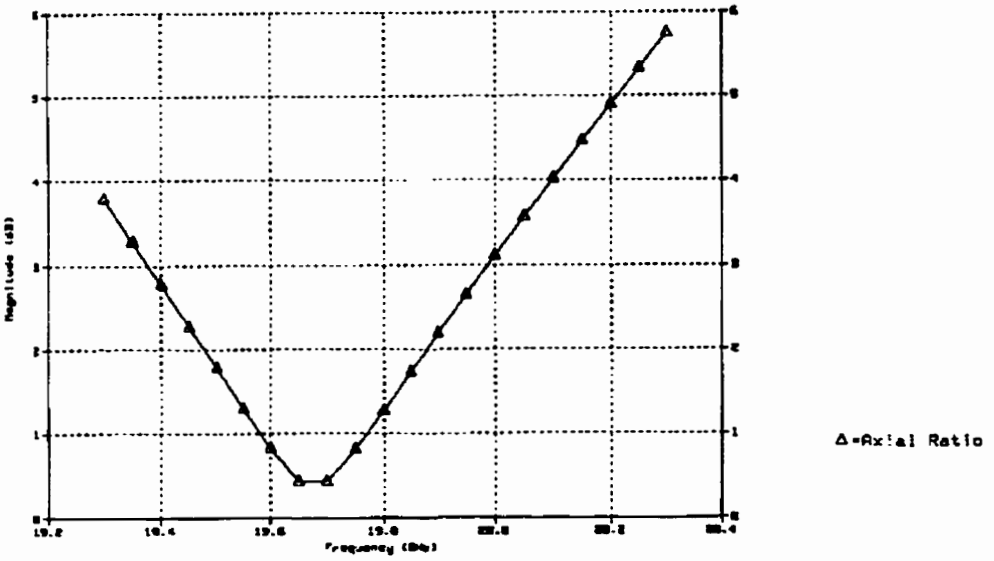


**Figure 2.17 Ensemble Simulated Axial Ratio of Aperture-Coupled Near Square Patch**

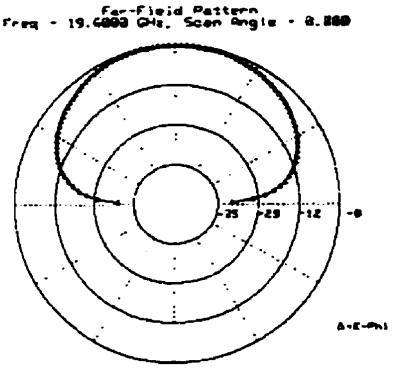

**Figure 2.18 Ensemble Simulated Far Field Pattern Eϕ; Phi=0 f=19.6GHz**

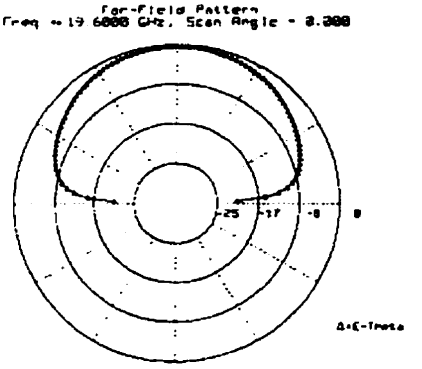

**Figure 2.19 Ensemble Simulated Far Field Pattern Eθ; Phi=0 f=19.6GHz**

Initial physical testing showed that the simulations were accurate in terms of the potential for circular polarization, but that the current geometry had an axial ratio bandwidth of less than 300MHz. Results for the operating bandwidth from 18.8-19.2GHz are shown in Figures 2.20-22. The discrepancy in the achievable bandwidth may be attributable to phase error at the cavity aperture or possibly a misalignment of the feed.

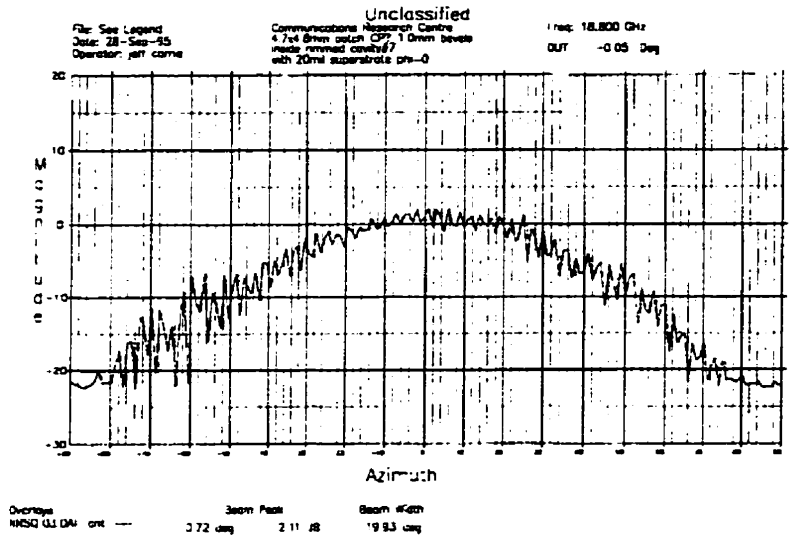


**Figure 2.20 Circular Polarization achieved with a Near-Square Patch-fed Cavity f=18.8GHz**

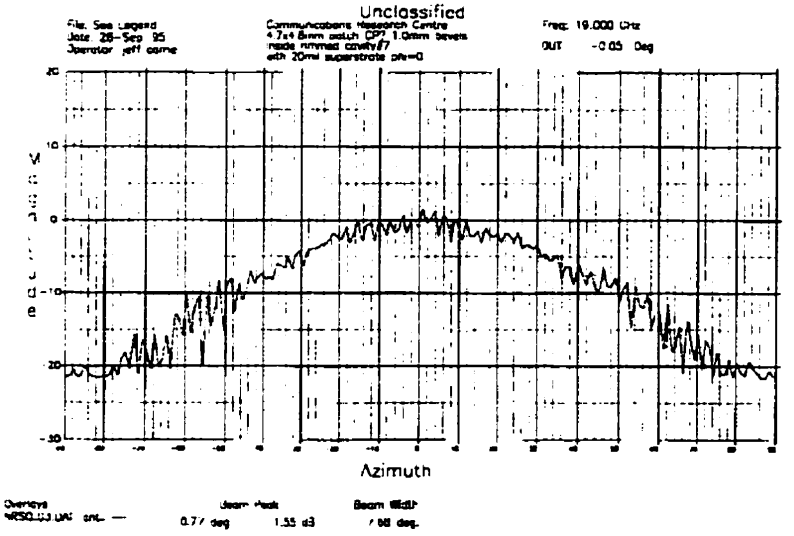


**Figure 2.21 Circular Polarization achieved with a Near-Square Patch-fed Cavity f=19.0GHz**

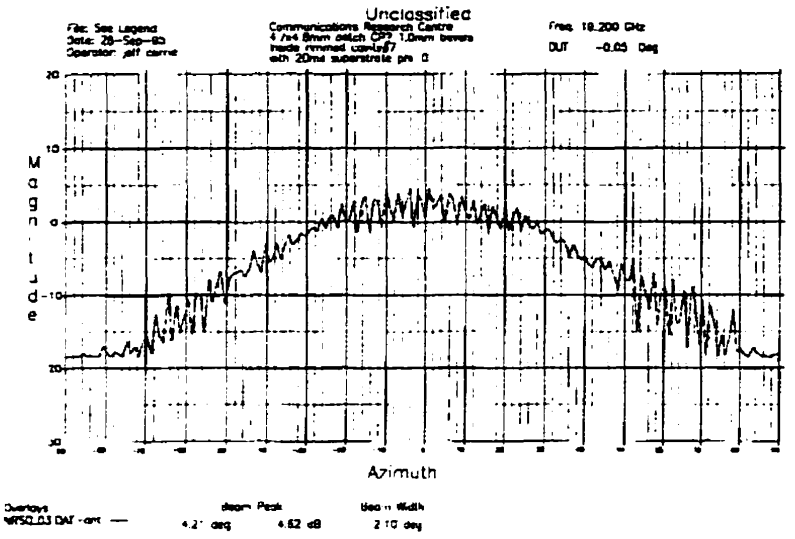


**Figure 2.22 Circular Polarization achieved with a Near-Square Patch-fed Cavity f=19.2GHz**

### 2.2.4 Implementation of a Cross-Shaped Dielectric Resonator

The third option was that of a dielectric cross as presented in [53] and pictured in Figure 2.23. The geometry consists of two rectangular dielectric resonators orthogonal to each other in a cross formation. The cross is then positioned at a fourty-five degree angle to an aperture coupling slot excited by a microstrip feedline. Previously an FD-TD technique has been used to analyze this geometry[5,6,7]. Using the same technique a dielectric cross has been suggested for use at K-Band.

The geometry is chosen so that the two arms of the cross radiate fields which are equal in amplitude and 90 degrees out of phase, thus circularly polarized radiation. When viewed

on a Smith chart, the two radiating arms will appear with one showing a slight capacitive reactance while the other arm shows a slight inductive reactance. Essentially we are attempting to design the cross such that the individual arms of the cross produce impedances which are directly proportional in magnitude with a ninety degree phase difference. Initial designs of the geometry achieved promising results with respect to the gain and the Axial Ratio bandwidth. Impedance analysis suggests the dielectric resonator to have a much wider operational bandwidth than the microstrip patches. In addition, DRAs typically have lower electrical losses and a high radiation efficiency due to the lack of conductor and surface wave losses. As a result, efforts were concentrated on developing the Dielectric Cross as the feed element for the cylindrical cavity.

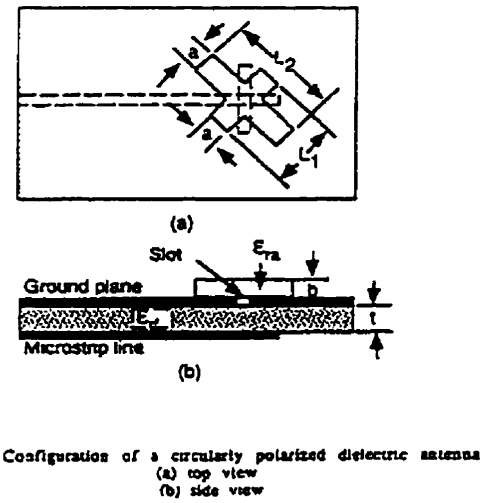


Configuration of a circularly polarized dielectric antenna
(a) top view
(b) side view

**Figure 2.23 Configuration of the Circularly Polarized Aperture-Coupled Dielectric Cross [53]**

Initial designs were fabricated from unclad duroid of medium permittivity ($\varepsilon_r$=10.8) and physically tested. Some tuning of the feed line's stub length was required to tune out the reactive component of the impedance. Physical testing seemed to indicate that the single

slot feed was sufficient for exciting circular polarization, pictured in Figure 2.24 and that the alignment of the dielectric cross was not crucial. The cross was also tolerant of fabrication imperfections. Given the small size of the cross, the interior edges were more rounded than perfectly square. It was noted that each arm had its own resonance on the Smith Chart, one with a capacitive reactance and one with an inductive reactance.

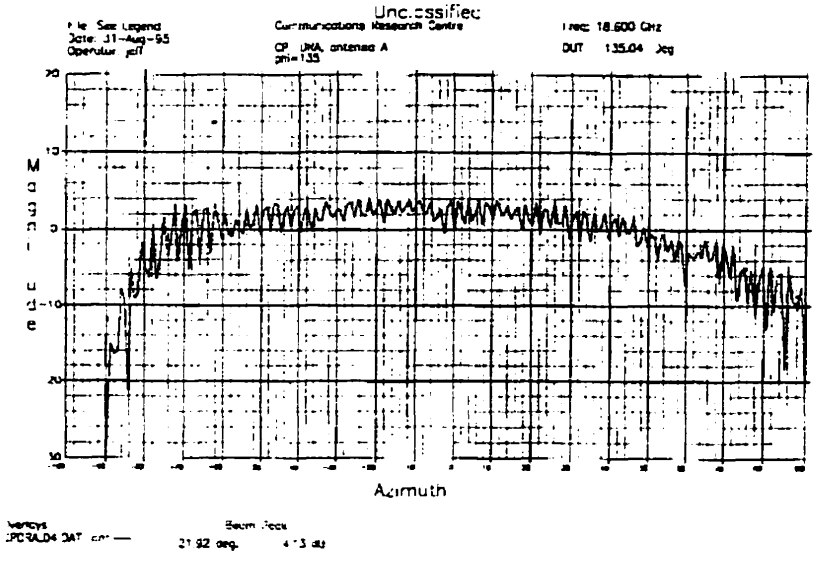


**Figure 2.24 Circular Polarization Produced by a Cross-Shaped Dielectric Resonator**

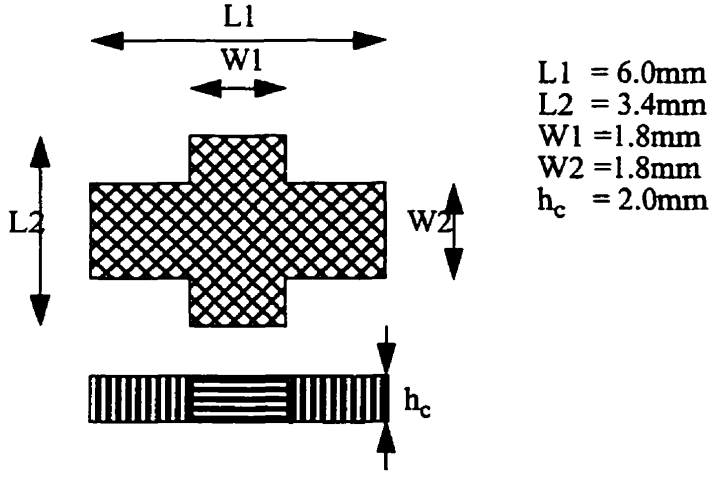


**Figure 2.25 Dimensions of the Optimized Cross**

Further design iterations at MacQuarie University produced the dielectric cross of Figure 2.25 with dimensions L1=6mm, L2=3.4mm, W1=W2=1.8mm and h=2.0mm. The feed line is fabricated on 25mil thick copper clad Rogers 6010Duroid ($\varepsilon_r$=10.2) with a 50Ω feedline of width 0.65mm extending 1.3mm past the centre of a 2.6x0.6mm slot. The slot used is smaller than the slot in the linear polarized cavity antenna. For aperture coupling an increased slot length typically lowers the input resistance, increases the coupling and lowers the backlobe radiation with minimal effect on the operating frequency. Typically the slot length is less than a half wavelength in order that the slot radiation does not interfere with the desired radiation pattern. Increasing the slot width tends to decrease the operating frequency while an increased tuning stub length increases the inductive reactance component.

In order to verify that the TLM code could be used to design the dielectric cross, the geometry predicted by Dr. Esselle's FD-TD technique was then modelled using Panacea. Using the transmission line matrix code we could analyze an entire geometry without performing several physical fabrications and tests. Return loss measurements are calculated at the specified feed port and the near field measurements can be used to produce the far field patterns using the free space Green's function. The computational analysis required that the rotated dielectric cross be modelled using a stepwise approximation, as a triangular meshing, more amenable to the 45 degree rotation of the cross was not available. Figure 2.26 shows the meshing of the cross, where the X and Y axes are scaled in unit mesh sizes. That is, the cross is centred at (45,45) within a 90x90 mesh. The mesh size is 0.2mm in each dimension. Simulation seemed to bear out the physical observation that imperfections in the cross fabrication were forgiveable. Return loss simulations pictured in Figure

2.27 showed the existence of two modes, one operating on each arm of the dielectric cross. Simulation of the individual arms resulted in the diagrams of Figure 2.28 which show the longer arm to have a slightly inductive reactance while the shorter arm reveals a slightly capacitive reactance. This reinforces that we have produced the necessary relative impedances, equal and in phase quadrature, necessary for circular polarization.

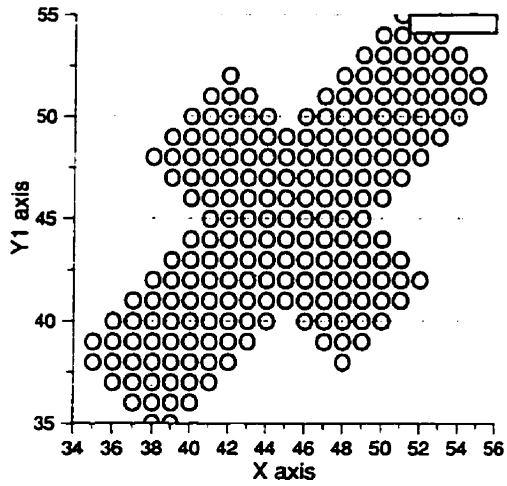


**Figure 2.26 TLM Stepped Approximation of the Dielectric Cross**

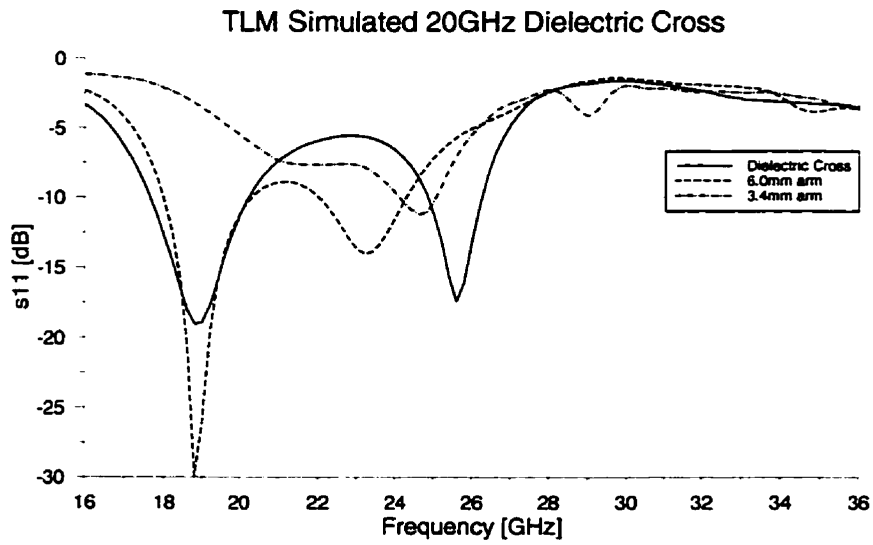


**Figure 2.27 TLM Simulated Return Loss of the 20GHz Dielectric Cross**

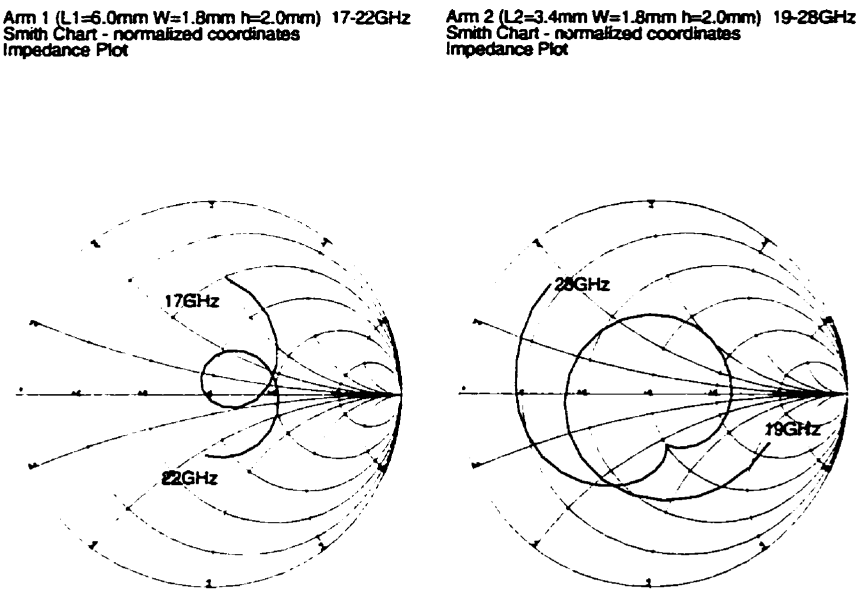


**Figure 2.28 TLM Simulation of Individual arms of the 20GHz Dielectric Cross**

Continuing the simulation with the geometrical meshing of Nx=90, Ny=90, Nz=30 where each mesh segment is 0.2mm and 3000 time steps, the near to far field transformations are made in both principal planes and show the electric field components to be equal and roughly 90 degrees out of phase with each other. As expected, the dielectric resonator has a wide beamwidth similar to that of a dipole antenna. The backplane radiation appears to be focused into a small lobe. These values are the result of using the free space Green's function when performing the near to far field transformation and therefore are not valid. Since our principal interest is with the forward radiation, we will ignore these values. It is hoped that the slotted ground plane used for the feed will minimize the actual backlobe. Figures 2.29-32 show the magnitude and phase of the orthogonal fields simulated in both H-plane ($\phi$=0) and E-plane ($\phi$=90) cuts. Figure 2.33 shows that the magnitude equality extends for quite some way however, the phase equivalence soon deteriorates and is the limiting factor in allowing the radiation of clean CP.

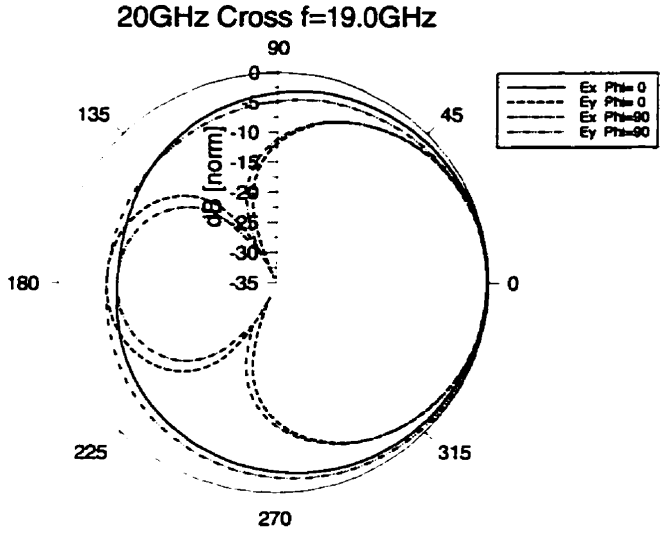


**Figure 2.29 TLM Simulated Far Field Pattern of the Dielectric Cross f=19.0GHz**

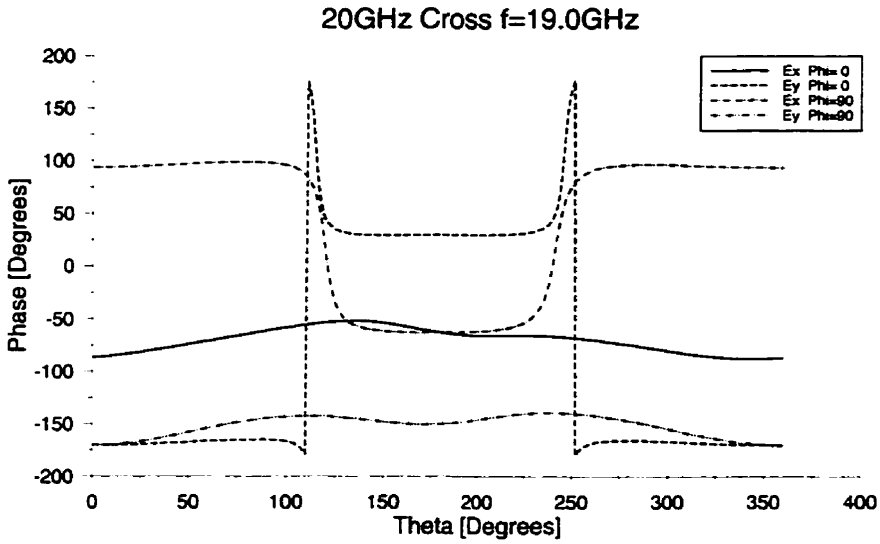


**Figure 2.30 TLM Simulated Phase Difference of the Dielectric Cross f=19.0GHz**

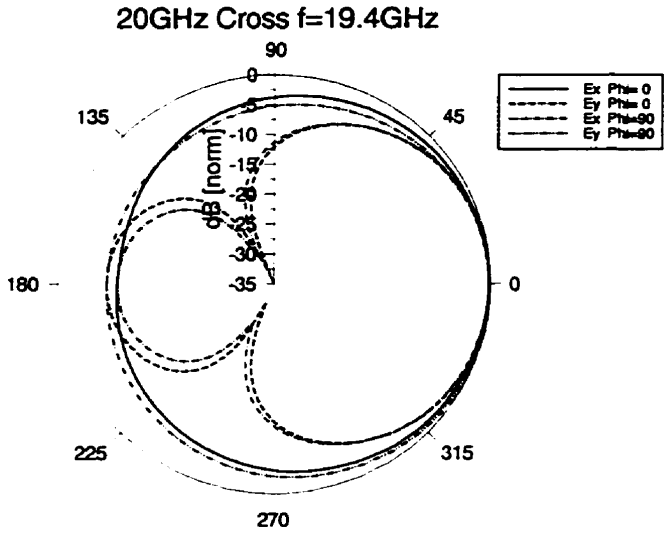


**Figure 2.31 TLM Simulated Far Field Pattern of the Dielectric Cross f=19.4GHz**

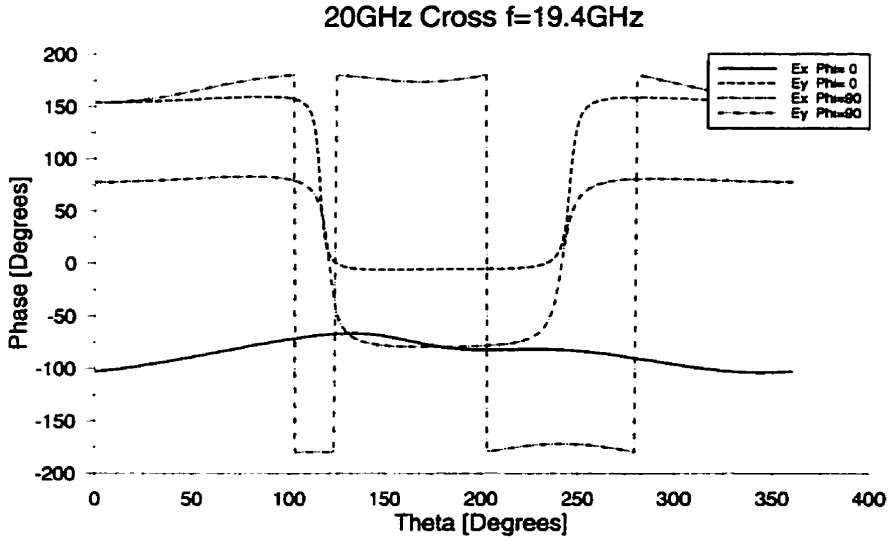


**Figure 2.32 TLM Simulated Phase Difference of the Dielectric Cross f=19.4GHz**

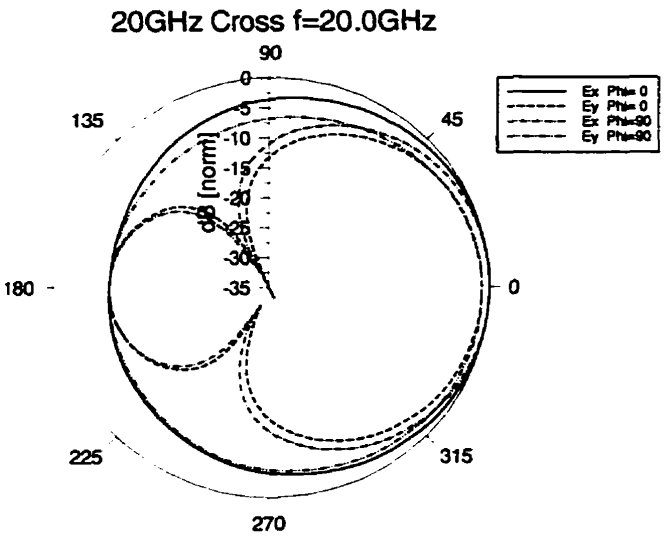


**Figure 2.33 TLM Simulated Far Field Pattern of the Dielectric Cross f=20.0GHz**

Circular polarization is defined by Balanis[54] to be a subset of elliptical polarization which more accurately describes the imperfect radiation of the antenna. Elliptical polarization is characterized by an electric field with two orthogonal components not necessarily equal in magnitude though they can be, provided the time-phase difference is neither an even multiple of 180 degrees (linear polarization) or an odd multiple of 90 degrees (circular polarization). Simulation has shown that the antenna definitely radiates elliptical polarization. We define the polarization to be near circular by characterizing the radiation in terms of its axial ratio. In the ideal circular case, the time harmonic electric field traces out a circle, however, mismatches in magnitude and phase cause the trace to become more elliptical, with one mode becoming more dominant. Balanis defines the axial ratio to be equivalent to the ratio between the two axes of the ellipse traced out in time. For circular polarization, this equates to an axial ratio of 1 (0dB).

Elliptical polarization is illustrated in Figure2.34, where the rotating electric field vector sweeps out an ellipse. The direction of propagation is normal to the diagram and the axial ratio is calculated as the ratio of the major and minor axes.

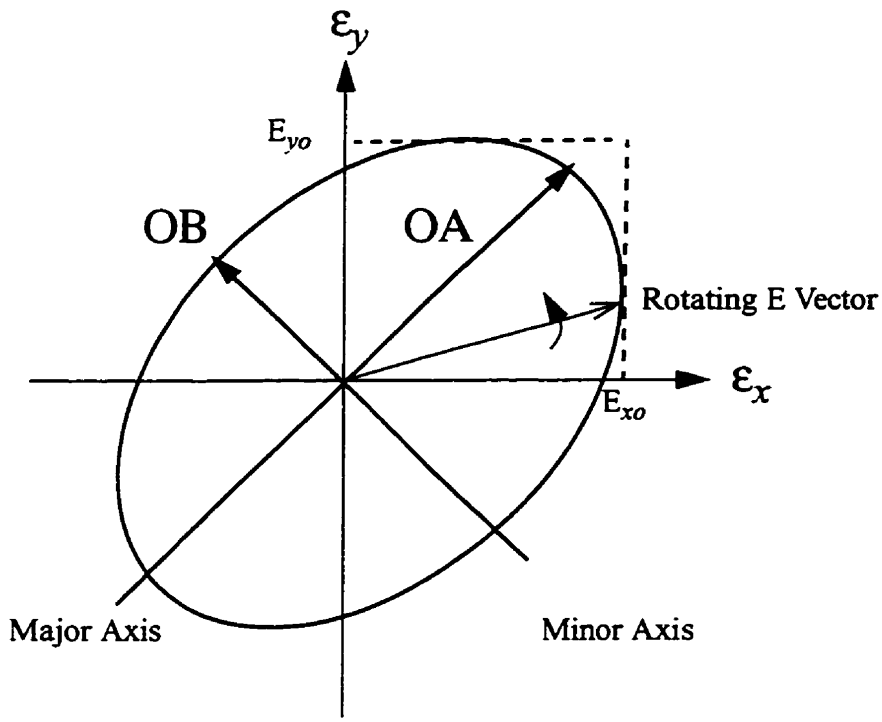


**Figure 2.34 Elliptical Polarization Trace**

$$AR = \frac{OA}{OB}$$

where:

$$OA = \left[\frac{1}{2}\left\{E_{xo}^2 + E_{yo}^2 + \left[E_{xo}^4 + E_{yo}^4 + 2E_{xo}^2 E_{yo}^2 \cos(2\Delta\phi)\right]^{\frac{1}{2}}\right\}\right]^{\frac{1}{2}}$$

and:

$$OB = \left[\frac{1}{2}\left\{E_{xo}^2 + E_{yo}^2 - \left[E_{xo}^4 + E_{yo}^4 + 2E_{xo}^2 E_{yo}^2 \cos(2\Delta\phi)\right]^{\frac{1}{2}}\right\}\right]^{\frac{1}{2}}$$

The axial ratio results produced by the microstrip coupled cross simulation are calculated using the appropriate field components. These results are summarized in Table 1. While the TLM code outputs the components in terms of $\theta$ and $\phi$, orthogonality allows direct substitution. That is for the $\phi$=0 xz plane, a unit vector along the x axis equates to a unit vector in $\theta$, while a unit vector along the y axis equates to a unit vector in $\phi$. Similar orthogonalities exist in the other principal plane (yz, $\phi$=90) where the unit vector along y corresponds to a unit vector in $\theta$ while a unit vector along the *negative* x axis corresponds to a unit vector in $\phi$.

Magnitudes are expressed in decibels and so must be returned to unity scale before being inserted into the above equations as $E_{x0}$ and $E_{y0}$with $\Delta\phi = (\phi_y - \phi_x)$.

**TABLE 1. Far Field components for the microstrip cross 19-20GHz phi=0;**

| Frequency (GHz) | \|Ex\| (dB) | ϕ[Ex] (rad) | \|Ey\| (dB) | ϕ[Ey] (rad) | Axial Ratio |
|---|---|---|---|---|---|
| 19.0 | -113.436 | -1.50789 | -113.233 | -2.97004 | 0.97dB |
| 19.2 | -113.518 | -1.64823 | -113.183 | 2.99879 | 0.66dB |
| 19.4 | -113.494 | -1.78974 | -113.281 | 2.68566 | 2.09dB |
| 19.6 | -113.389 | -1.93772 | -113.525 | 2.37737 | 3.55dB |
| 19.8 | -113.248 | -2.09449 | -113.903 | 2.07737 | 4.99dB |
| 20.0 | -113.106 | -2.25945 | -114.390 | 1.78832 | 6.40dB |

Although far field data was not calculated below 19GHz it is not unreasonable to assume that the magnitude and phase relationships are fairly symmetric and that the axial ratio bandwidth is on the order of 800MHz.

Physical testing of the antenna was performed with various cavities and dielectric radomes. Using the network analyzer, the return loss was monitored. These results are summarized in Figures 2.35-38 and show the improved match as the dielectric radome is increased towards a quarter guided wavelength (approximately 40 mil) as for the case of the linear polarized cavity. Observe that there is a slight lowering in operating frequency as the superstrate thickness increases. This extra dimension of freedom allows us to fine tune the operating frequency. A TLM analysis of this will be performed for the 30GHz cavity element.

Using a cavity of diameter 3.05cm with a height of 0.79cm and a dielectric radome of 40 mil, the antenna performed as shown in Figures 2.39-42. The radiation patterns shown suggest a 3dB axial ratio bandwidth on the order of 700MHz, comparable to what was predicted with the TLM code. As with the linear element the gain and frequency of operation of the entire antenna will increase with the appropriate cavity height. Antenna gain is on the order of 13dB, although there is a drop of 0.5dB over the operating range. Measurements are 3dB lower as a result of the test setup which utilizes a rotating linear horn to simulate a circular polarized source. Since only one half of the power is transmitted, gain is reduced by 3dB. The effect of the cavity is definitely noticeable as it focuses the main beam to a half-power beamwidth of 30 degrees. A further iteration utilized the same element inside a smaller cavity (cavity height 0.737mm with a diameter of 2.6cm) topped

with a 50mil Alumina superstrate which increased the centre frequency of operation from 18.5 GHz to 20.2 GHz while retaining the same 700MHz Axial Ratio bandwidth.

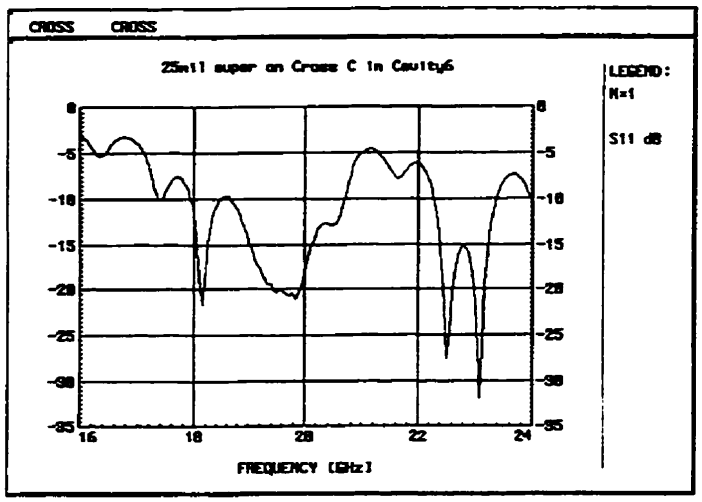


**Figure 2.35 Return Loss produced by the Cross-fed Cavity, Radome thickness=25mil**

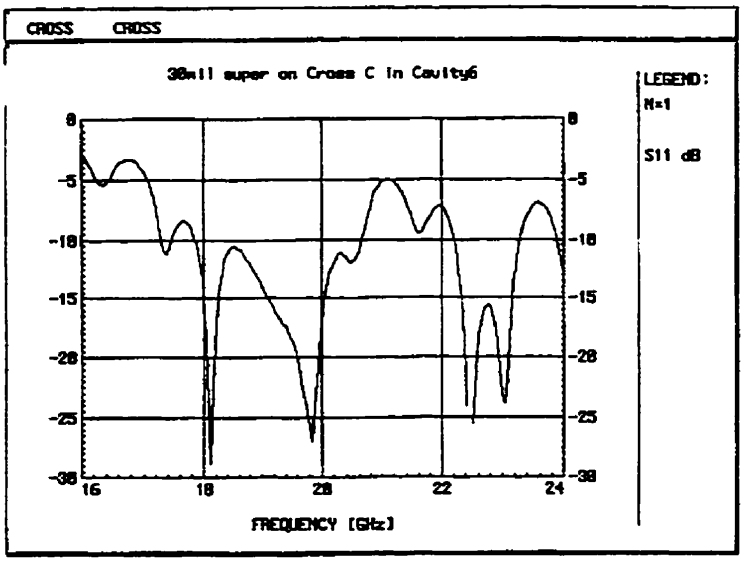


**Figure 2.36 Return Loss produced by the Cross-fed Cavity, Radome thickness=30mil**

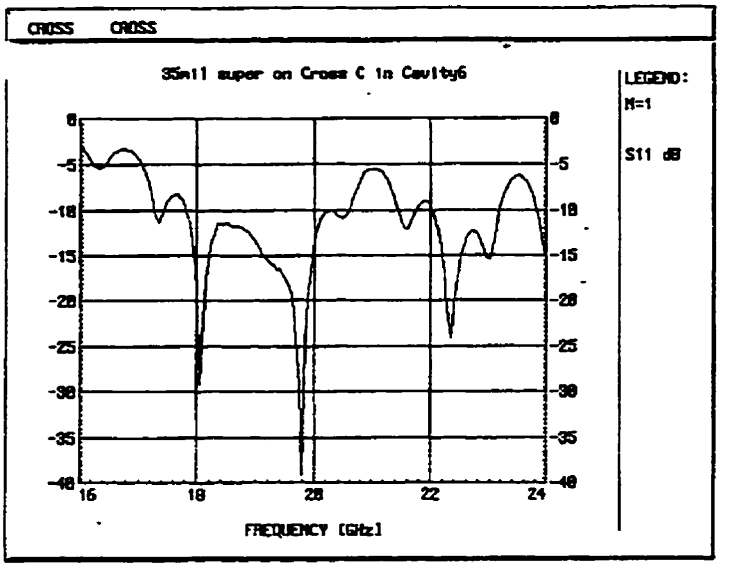


**Figure 2.37 Return Loss produced by the Cross-fed Cavity, Radome thickness=35mil**

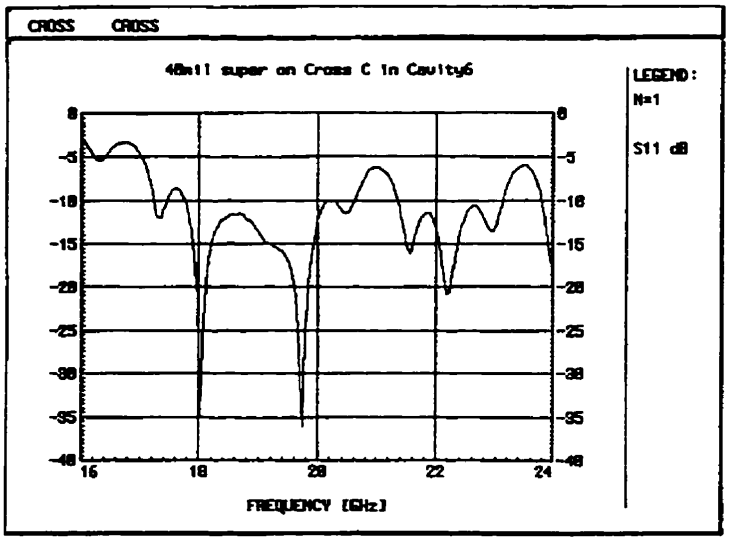


**Figure 2.38 Return Loss produced by the Cross-fed Cavity, Radome thickness=40mil**

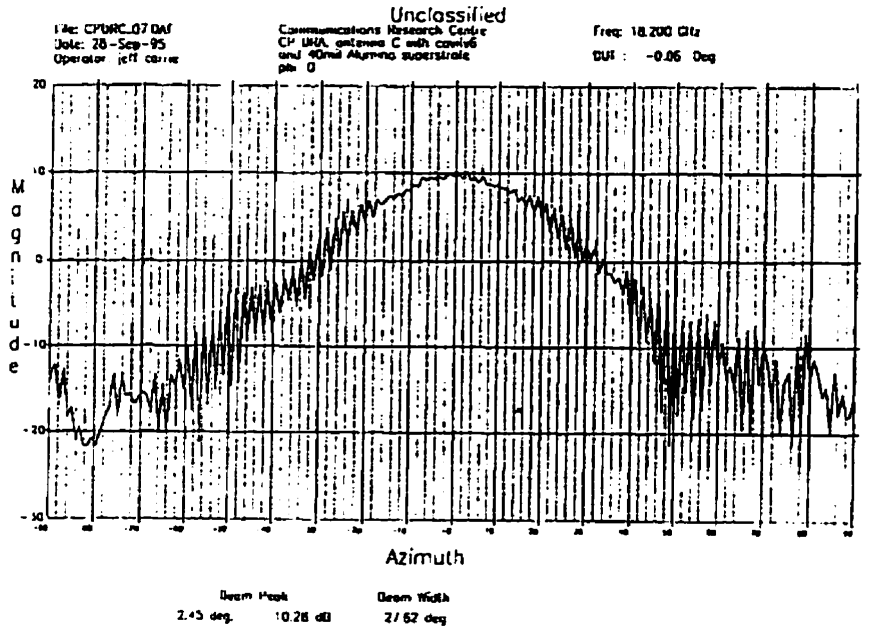


**Figure 2.39 Circular Polarization produced by the Cross-fed Cavity, f=18.2GHz**

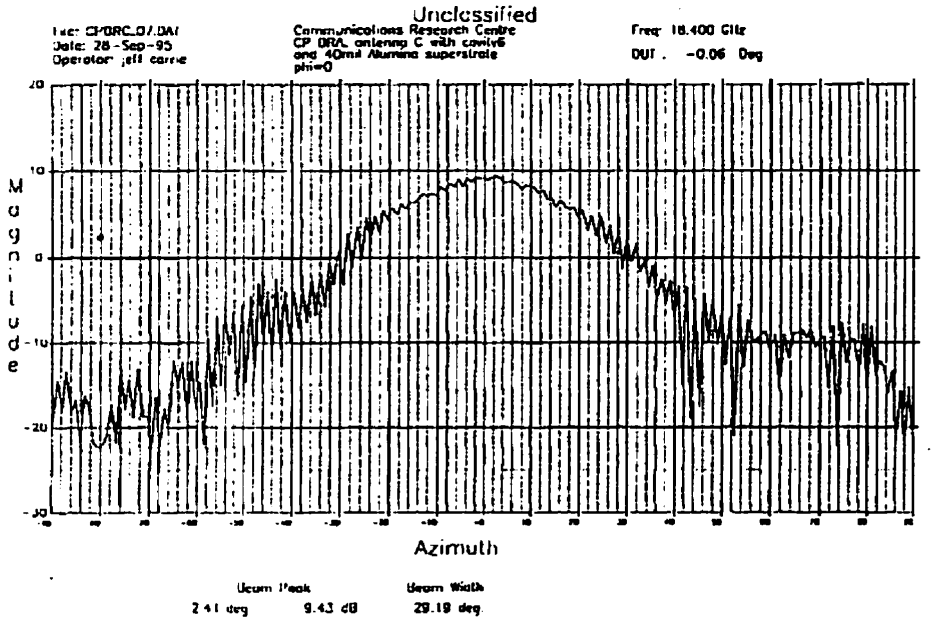


**Figure 2.40 Circular Polarization produced by the Cross-fed Cavity, f=18.4GHz**

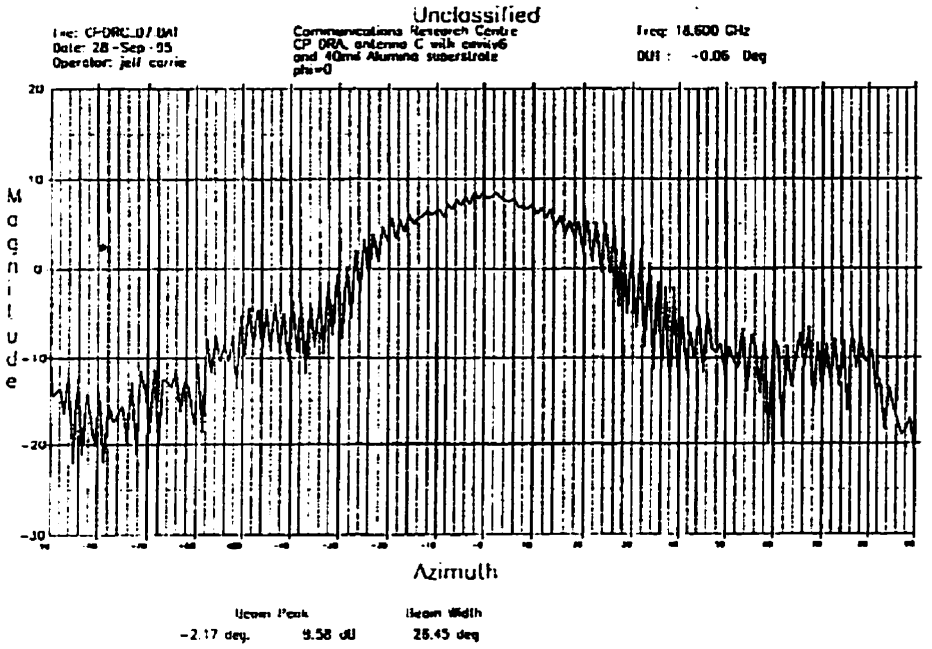


**Figure 2.41 Circular Polarization produced by the Cross-fed Cavity, f=18.6GHz**

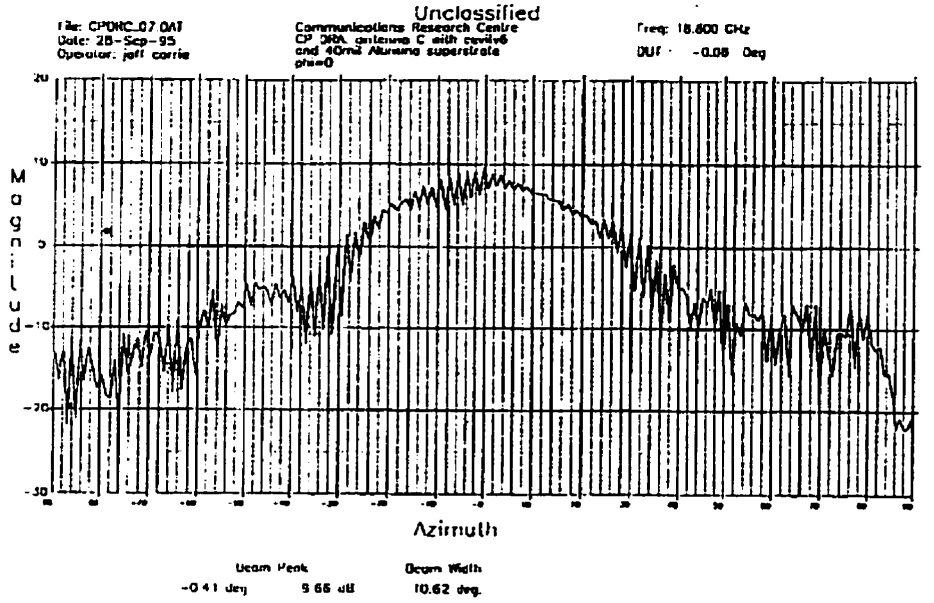


**Figure 2.42 Circular Polarization produced by the Cross-fed Cavity, f=18.8GHz**

## 2.3 Summary

In this chapter several antenna elements were considered for receive applications. A brief history of the evolution of the working linearly polarized element was provided as well as a description of the cavity geometry. Numerical methods used to analyze the antenna geometries were discussed with emphasis on the Transmission Line Matrix (TLM) method.

Several attempts were made to achieve a circularly polarized element. Perturbations of the existing geometry as well as novel feed techniques and redesign of the microwave patch were attempted with moderate success. The dielectric resonator cross was introduced and simulated with the TLM code. Physical results were presented for a dielectric cross excited cavity geometry capable of producing circular polarization over a 700MHz bandwidth. The final geometry was shown in Figures 2.25 and 2.42.

Numerical simulation of the full cavity was not performed owing to memory restrictions required to analyze the physically large structure. These results have been previously discussed in [11].

In the following chapters attempts will be made to scale the elements up to the operating frequency of 30GHz suitable for use in transmit antenna applications. Axial Ratio Bandwidth for the transmit antenna is anticipated to encompass a full 1GHz operating bandwidth.

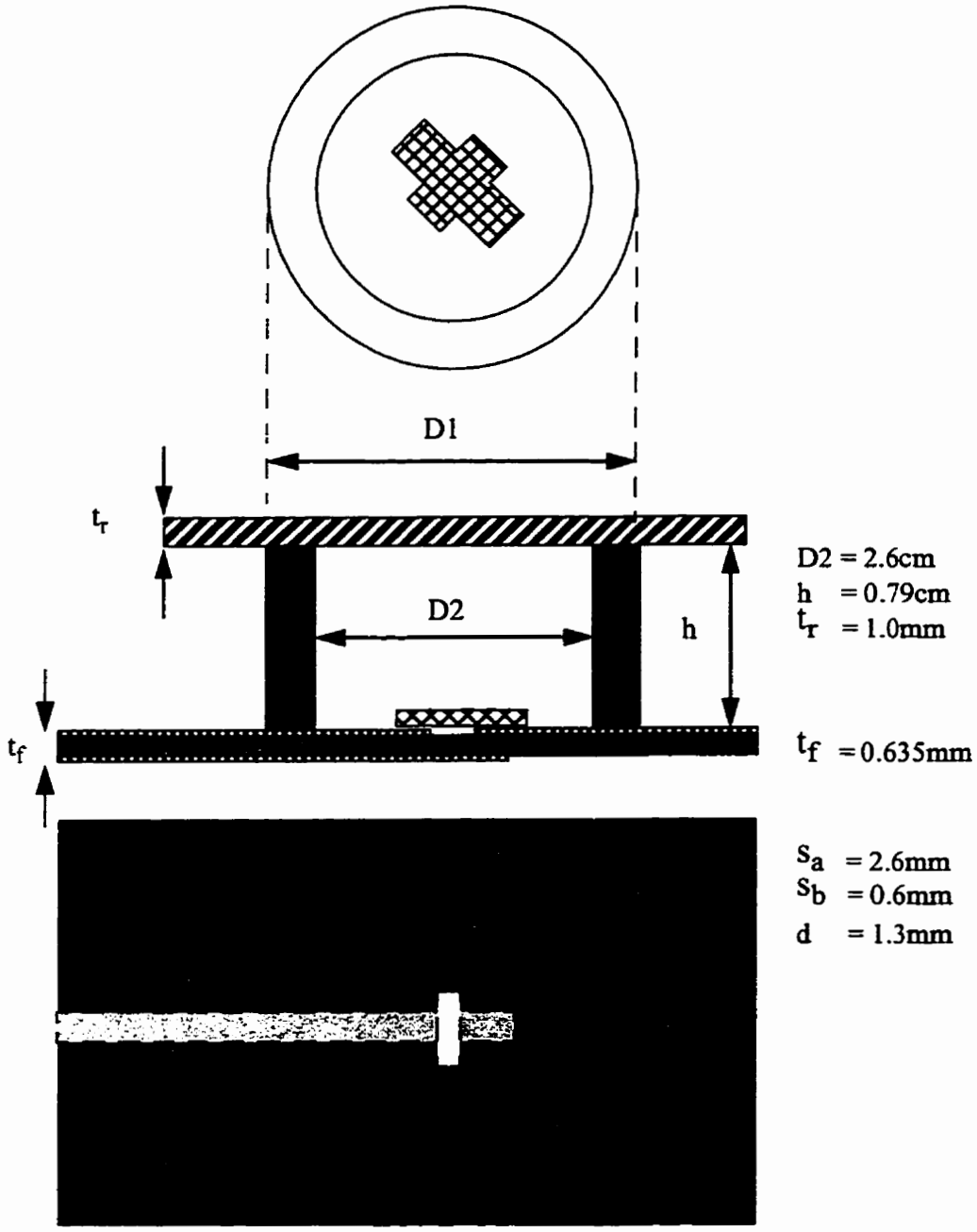


**Figure 2.43 Geometry of the Cross-fed Cavity Element**

# Transmit Antenna Elements

## 3.0 Transmit Antenna Elements for use in 30GHz Applications

The design of linear and circularly polarized antennas for use in 30GHz transmit applications evolves from previous work with receive antenna elements. Rather than this being a simple matter of scaling however, the higher frequency applications are more prone to error and are more sensitive to design variations and misalignment. In this chapter a linearly polarized microstrip patch fed cavity is developed based on a scaled model of the K-band receive element. This design would have to be reiterated to adjust for frequency shifting and the suppression of higher side lobe levels than previously encountered. To overcome the high sidelobe levels, several techniques were attempted to minimize the effects of parasitic modes and suspected phase imbalances. These attempts would finally lead to an optimized geometry. Circularly polarized efforts included calculation of a near square microstrip patch as was attempted for receive applications however, the majority of effort was concentrated on using the TLM method to design a dielectric resonating cross. The cross is then inserted into the cavity geometry and the dimensions are then optimized for a 1GHz axial ratio bandwidth. After having optimized the microstrip-fed structure, initial steps are taken to translate the cavity geometry from a microstrip feed to a stripline feed. Finally, conclusions are drawn for the performance of the receive elements along with suggestions on improving the performance of the prototype stripline structure.

## 3.1 Linearly Polarized Elements

As in the receive antenna case, a linearly polarized cavity backed patch is to be optimized for use as a radiating element amenable for use in an array environment. Again the cavity is to be no larger than 2 free space wavelengths in diameter and will be approximately a half wavelength in height. The cavity will be excited by an aperture-coupled microstrip patch and an alumina radome will be used to match the cavity to free space. Initial design work and testing involved two microstrip patch designs, a scaled version of the previous 19.7 GHz model, as well as an empirically calculated patch as per Bahl[18]for use at 29.5GHz.

Preliminary results supported the empirically calculated patch, although the return loss had a devastating effect on the antenna gain. In spite of the use of a slot-coupling program for accurate modeling of the feed line, the actual response was far from what had been predicted. These initial results were comparable to early attempts with the linear receive element. The characteristics of concern were the high shoulders evident in the E plane pattern cut. It was hoped that these shoulders would be lowered by improved design of the element. While the gain was not directly calculated, the principal plane beamwidth indicated good directivity. It was necessary to extend the feed line as well as to decrease the patch size to improve the reflection parameter response and increase the operating frequency of the antenna element. The patch dimensions were cut to become 3.94x2.76mm and the feed line built on 0.025" thick 6010 duroid was adjusted to be 0.728mm thick and extend 4mm beyond the centre of the 2.73mmx0.4mm slot. The larger slot length increases the inductive reactance seen by the antenna. The resulting reflection analysis showed an improved match over approximately a 6.5% bandwidth with typical co and

cross-polarization patterns in the two principal planes reproduced below in Figures 3.1 and 3.2.

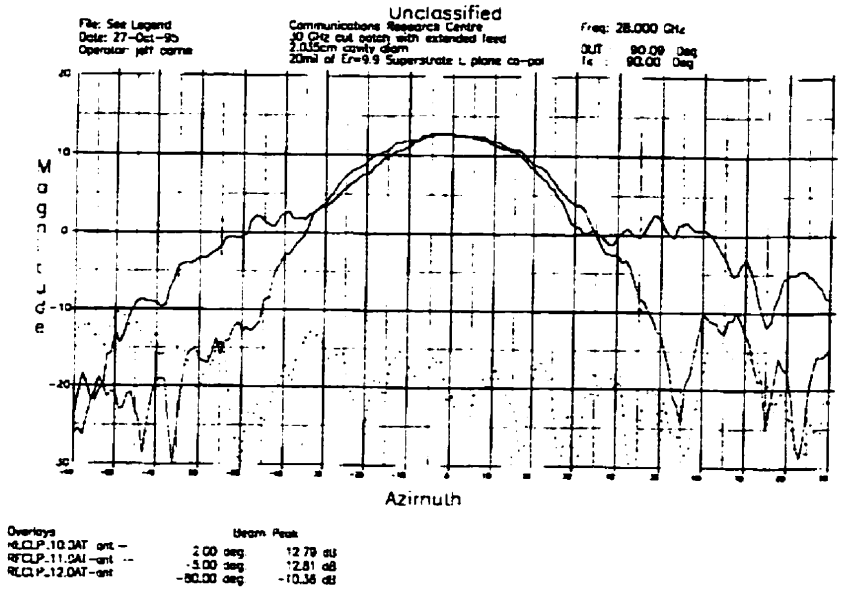


**Figure 3.1 Radiation Pattern of the initial patch fed cavity, f=28.0GHz**

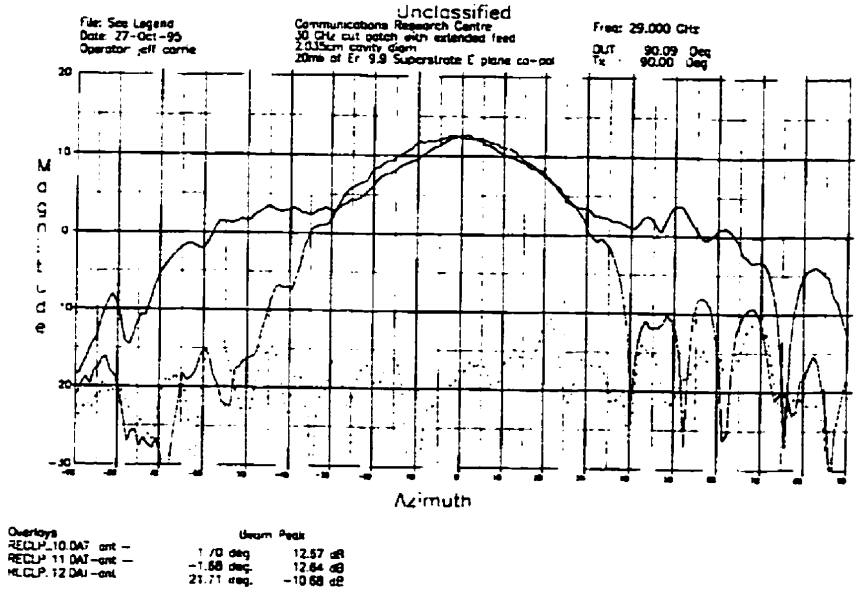


**Figure 3.2 Radiation Pattern of the initial patch fed cavity, f=29.0GHz**

As was the case with the receive antennas, the cavity has lowered the operating frequency of the entire element. The frequency band of operation ranges from 28 to 29 GHz, indicating that either the present cavity height of 0.52cm or the patch dimensions would have to be adjusted. The gain has improved, but the operating frequency is still lower than desired and the E plane shoulders still appear, especially at the higher end of the operating band.

There may have been several explanations for the appearance of shoulders in the radiation pattern. Three cases were considered, the possibility of surface waves, due to currents on the cavity walls leaking out of the cavity, the possibility of a parasitic TM mode interfering with the principal TE11 mode, and the cavity dimensions being prone to phase error at the radome.

It is possible that currents leaking out of the cavity, would not have a return path to ground and may instead radiate upon reaching the edge of the radome. The first attempt at rectifying this possibility involved cutting a choke around the perimeter of the cavity. The purpose of this groove was to act as an infinite resistance (open circuit) reflecting the current. In order to simulate the open circuit the groove was cut 0.1wavelengths across and a quarter wavelength deep, such that the total path in and out of the groove is a half wavelength. The resulting radiation patterns as seen in Figure 3.3 indicated that the groove had no effect on suppressing the shoulders. (Note that at this time there were difficulties with the receiver which caused dropouts to occur at several angles. This accounts for the spikes in the radiation pattern). An alternate method of minimizing the current was to extend the ground plane, in order to better simulate an infinitely distant boundary. Typically, a finite ground plane causes scattering at the edge, which if not physically covered with absorber

will show up as a ripple in the radiation pattern. The results of this experiment were no better than the previous attempt with the choke.

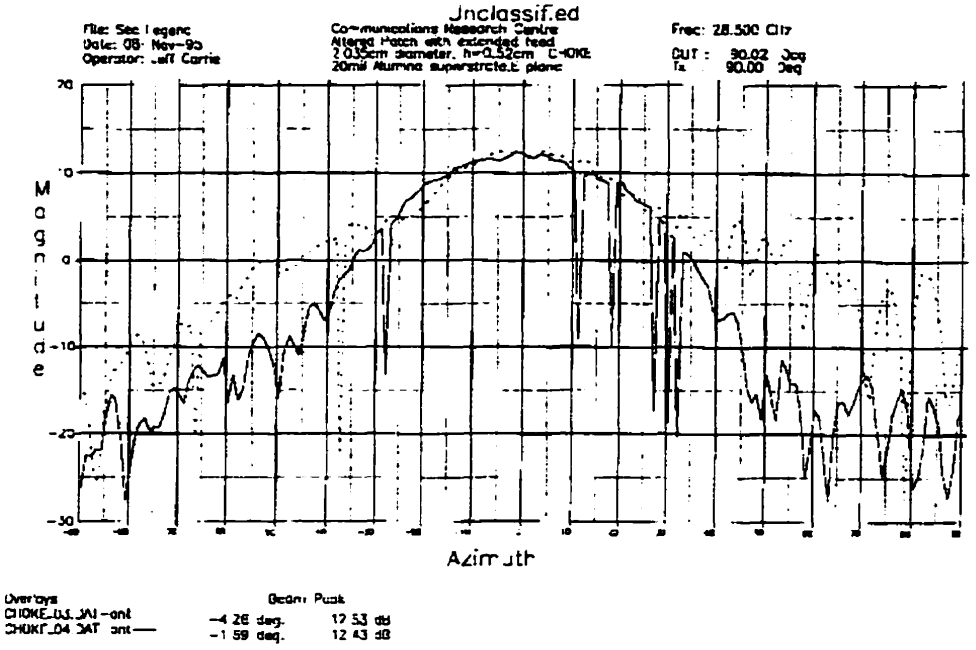


**Figure 3.3 Radiation Pattern of the Patch-fed Cavity with Choke**

In the event that a parasitic TM01 mode was being radiated, which would account for the shoulders, an attempt was made to disrupt the mode through the use of conducting strips placed along the E-plane. This attempt to disrupt parasitic modes failed to reduce the E-plane shoulders. Another attempt was made with metal posts which proved equally unsuccessful. In light of this, it may be possible that several parasitic modes are operating, and that no simple method will disrupt them. It was hoped that the cavity dimensions may help to minimize the shoulders during the course of optimization.

The cavity height was found to be of critical importance in optimizing the radiating element in K-Band applications. Initial heights at Ka-Band had simply been scaled from the earlier model and were a likely candidate to be optimized with respect to gain. Because of the high frequency and small cavity thicknesses some reworking of the original launching structure was also necessary for stability. Also of importance is the cavity diameter, the cavity backed elements are intended for use in an array environment. Present specifications required two free space wavelength separation between elements. As a result the diameter of the cavity would need to be decreased to allow the proper spacing. The reduced diameter of the cavity is expected to affect side lobe levels, and there will likely be a trade-off between element gain and mutual coupling losses.

Several cavity heights with various diameters were machined in different thicknesses and extensive testing was undertaken. The thinner cavity thicknesses increased the operating frequency to a higher operating range, as expected but while there was some improved suppression of the sidelobes, they were still noticeable.

The next step was to examine the cavity diameter. The cavity itself may be creating the parasitic TM mode. If this is the case, we should also see a contribution to the H-plane cross-polarization. Up to this point however, the cross-polarization levels have seemed reasonable. Decreasing the cavity diameter to 1.7cm likely reduced phase error at the aperture even more and was successful in minimizing the sidelobes below the previous levels without altering the operating bandwidth significantly. Despite the smaller aperture, gains remained at a respectable 13dB. One concern is the drop in gain of 2dB over the entire 1GHz operating band. The radiation patterns for E and H as well as cross polarization levels are shown in Figure 3.4. As mentioned before, there have been some problems with

the receiver locking on to data points at several frequencies and so large spikes in the measured patterns should be ignored.

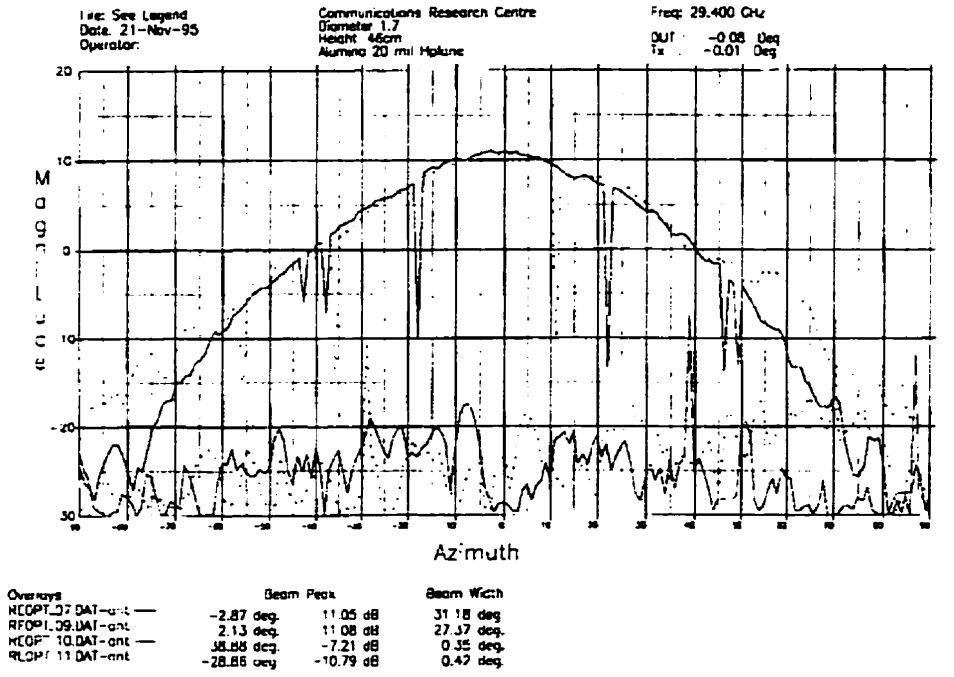


**Figure 3.4 Radiation pattern of the optimized Linear Polarized Cavity f=29.4GHz**

Suppression of the sidelobes is not fully explained, however the beam shapes are not unlike the E plane cuts of large angle flared horns. It is possible that in minimizing the cavity size we have managed to slightly correct for some phase difference, similar to the phase difficulties encountered by large angled horns.

The final design in Figure 3.5 consists of the 3.94x2.76mm patch inside a cavity of 1.7cm diameter and 0.46cm height. The feed line is built on 0.025" thick 6010 duroid and was adjusted to be 0.728mm thick and extend 4mm beyond the centre of the 2.73mmx0.4mm slot. The cavity is covered with a 20mil thick Alumina superstrate. Applications for this

antenna are shown in [55]. Gain enhancement techniques have been attempted in [9] and [32].

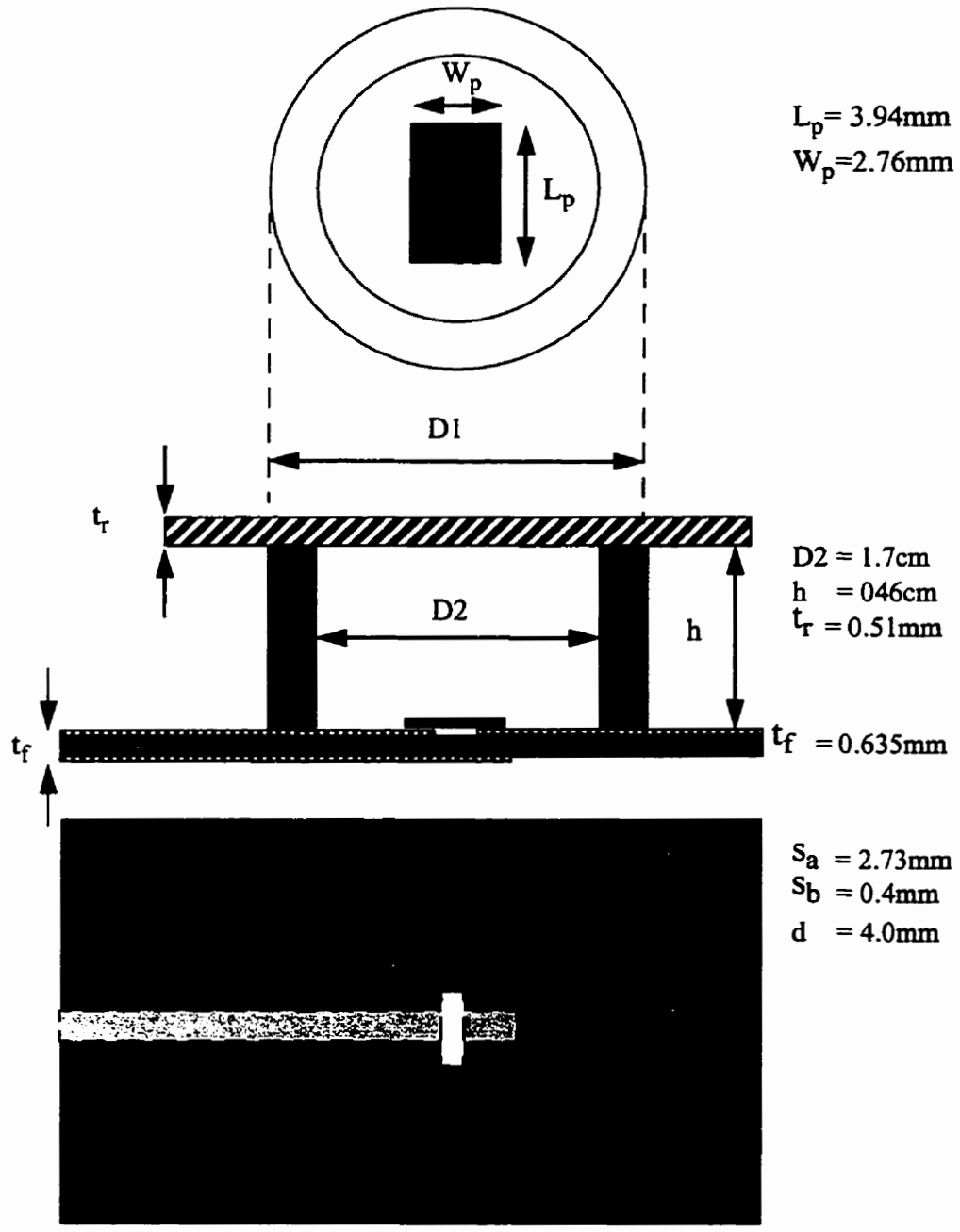


**Figure 3.5 Optimized Linearly-Polarized Cavity Geometry**

As the use of a dielectric cross for circular polarization has been successful, it is interesting to note the performance of a dielectric resonator in linearly polarized applications. Although a comparison between microstrip and dielectric resonators is beyond the intent of the research, they have been considered as an alternative to the microstrip patch. Broadband dielectric resonators have been used in [56,57,58] with several different shapes proposed in [59] and numerical techniques to calculate their efficiency[60]. Petosa et.al. have done extensive work in this area[61] including insight into the use of inhomogeneous crosses where the dielectric resonator uses a high permittivity section to increase coupling efficiency from the aperture-feed[62].

TLM code has been used to investigate the possibility of using a rectangular dielectric resonator as the cavity feed element. Several iterations were run and indicated good results for a 4.0 x2.2x1.2mm block cut from 6010 ($\varepsilon_r$=10.8) duroid and fed by a 0.784mm wide line built on 10mil thick 5880 duroid ($\varepsilon_r$=2.2) extending 0.7mm past the centre of a 5.0x0.6mm slot. Initial testing indicated that the dielectric resonator appeared to operate slightly below the frequency predicted by the source code. This discrepancy is likely to be associated with the circular cavity being represented as a square in the TLM simulation. The pattern shown in Figure 3.6 does appear to be consistent with the performance of the rectangular patch, showing good beam symmetry as well as low cross polarization levels, although the same degree of success as with the optimized patch was not achieved.

There is still some optimization to be done, before a final comparison may be done between the two elements, however for the purposes of the thesis the rectangular patch is sufficient and is preferable with respect to the simplicity of the design.

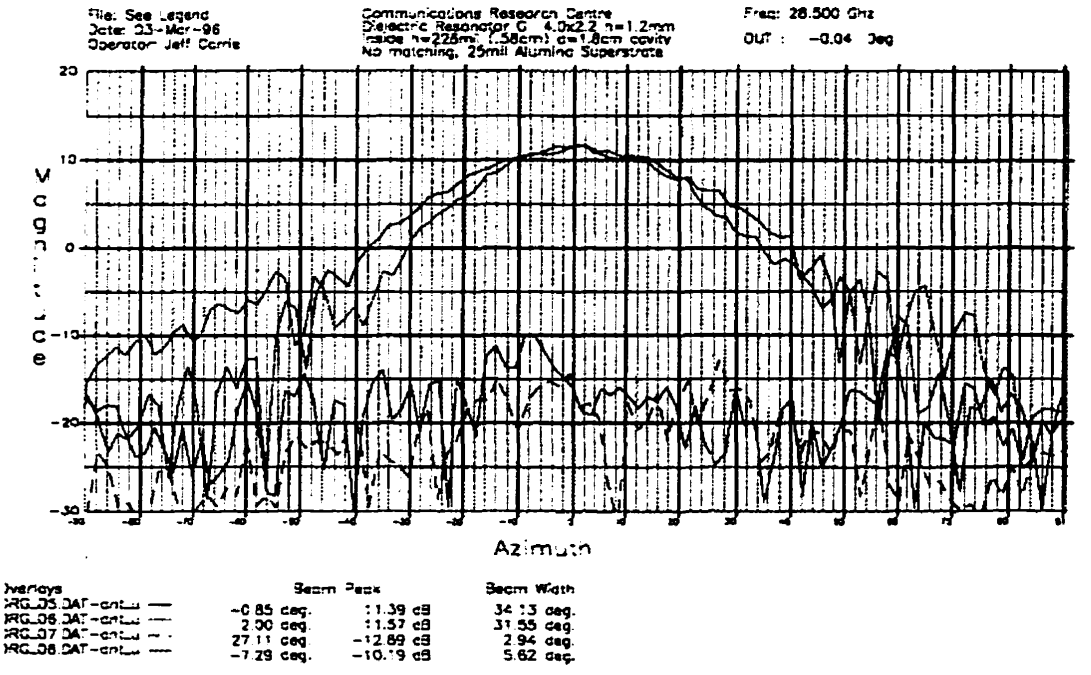


**Figure 3.6 Radiation Pattern of a Dielectric Block fed Cavity, f=28.5GHz**

## 3.2 Circularly Polarized Elements Fed with Microstrip

### 3.2.1 Attempts with a Near Square Microstrip Patch

As in the 20Ghz case, Ensemble was used to design a near square patch to radiate CP. Ensemble determined the patch size of 3.0x3.1mm with 1mm bevels as being capable of producing CP with a better than 3dB axial ratio over a 1GHz band. Initial testing seemed

to indicate otherwise and it was decided to create a dielectric cross capable of radiating CP to be the main element.

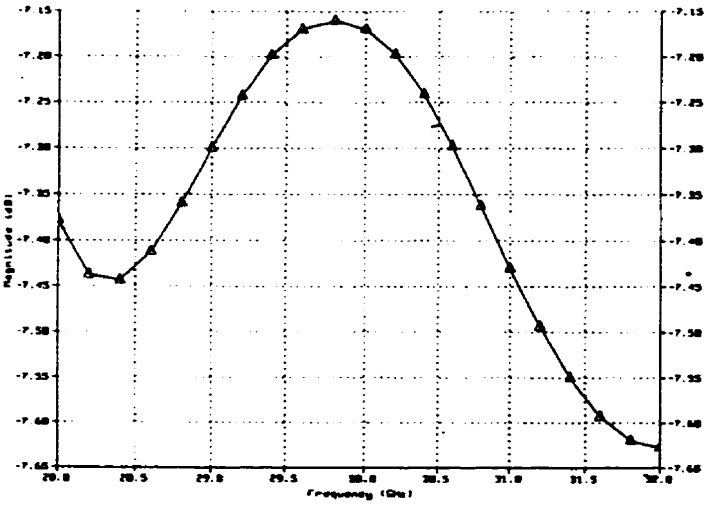

**Figure 3.7 Ensemble Simulated Return Loss of Aperture-Coupled Near Square Patch**

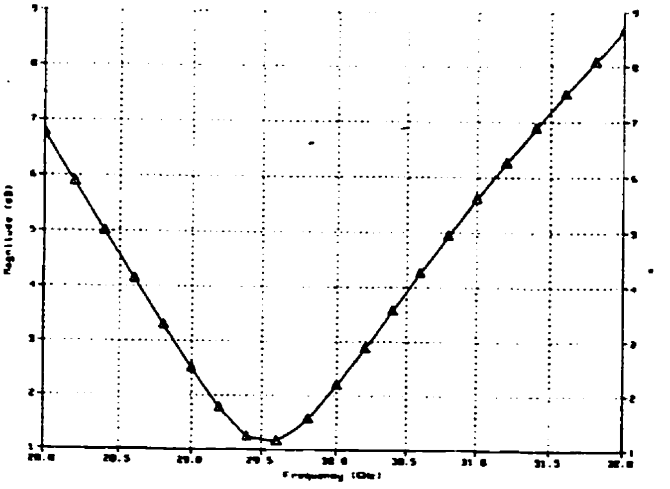

**Figure 3.8 Ensemble Simulated Axial Ratio of Aperture-Coupled Near Square Patch**

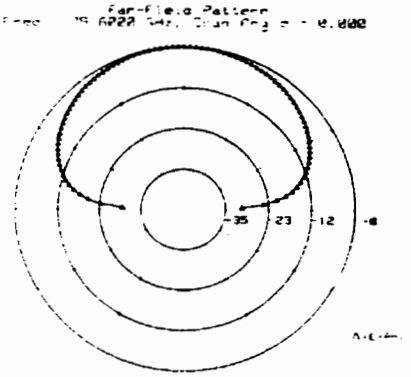

**Figure 3.9 Ensemble Simulated Far Field Pattern Eϕ; Phi=0 f=29.6GHz**

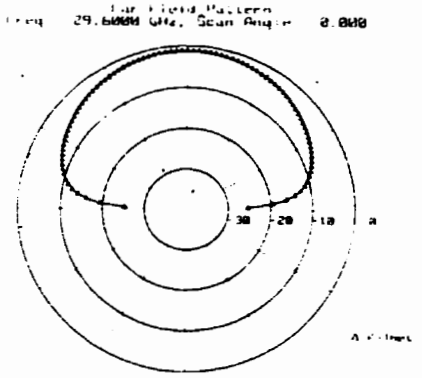

**Figure 3.10 Ensemble Simulated Far Field Pattern Eθ; Phi=0 f=29.6GHz**

### 3.2.2 Design and Test of the Cross-Shaped Dielectric Resonator

Earlier success at K-band with a dielectric cross allows a degree of optimism in being able to design a similar structure for Ka-Band. The design also holds the advantage of being more tolerant to misalignment than with the microstrip patch, since the feed position for the cross is not as crucial. Even the cardinal planes show excellent results in gain as well as Axial Ratio. The transmission line matrix code was used to analyze a scaled version of the receive cross and then optimized through the altering the available dimensions. Exact scaling of the cross was not possible due to memory constraints related to the meshing of

the geometry within the source code. Recall from Chapter 2 that increased meshing follows an $N^3$ relationship. Instead an initial approximate geometry was analyzed which indicated that the geometry would not radiate CP.

As a result, the effect of altering the geometry height, width and arm lengths was investigated to attempt to equalize the field magnitudes and maintain a phase difference of 90 degrees. Utilizing a space of Nx=90 Ny=90 Nz=30, several computer iterations produced two possible designs the first measuring L1=6.8mm L2=2.6mm W=1.0mm h=1.2mm and the second measuring L1=5.2mm L2=2.4mm W=1.0mm and h=1.2mm Of these two the second design performed the better, probably due to the longer lengths being less effected by machine tolerances during fabrication. TLM return loss is summarized in Figure 3.11, which shows the presence of two orthogonal modes, similar to the receive antenna case in Figure 2.26, although the match requires some improvement.

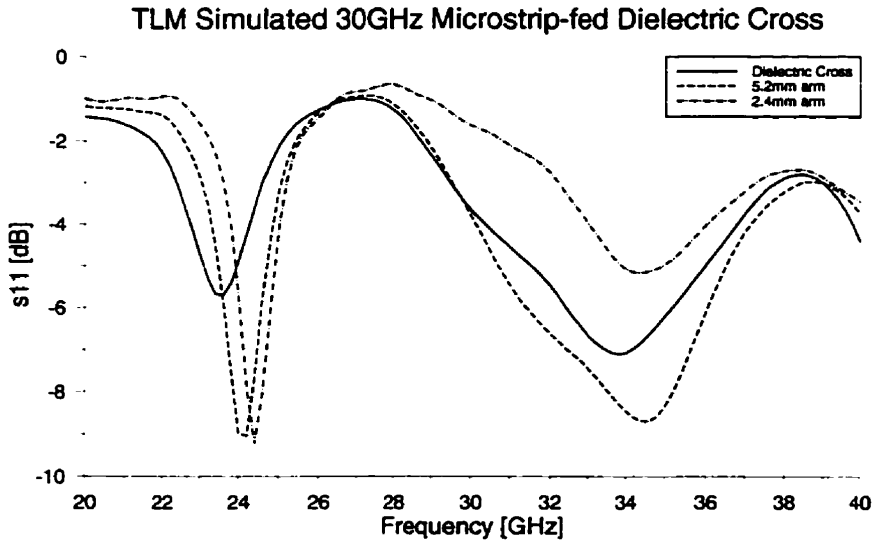


**Figure 3.11 TLM Simulated Return Loss of the Microstrip-fed 30GHz Dielectric Cross**

Far field magnitude and phase results are captured in Figures 3.12-17. Table 2 summarizes the bore-sight axial ratio performance over the band from 30-32 GHz. It is expected that the cavity geometry will lower the operating frequency.

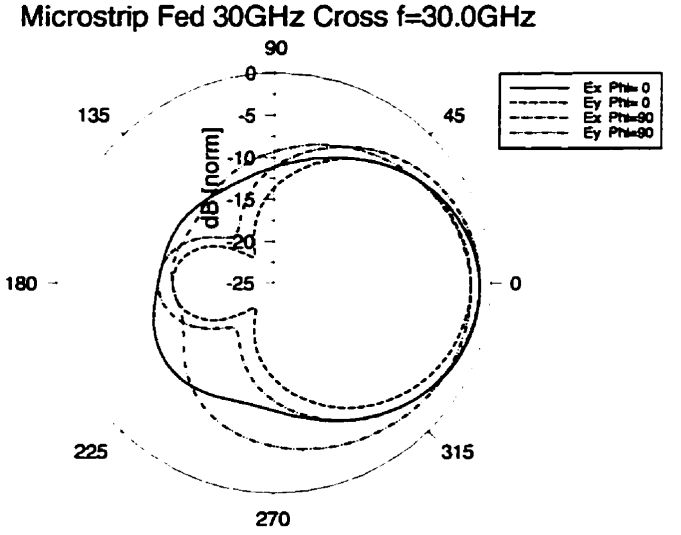


**Figure 3.12 TLM Simulated Far Field Pattern of the Dielectric Cross f=30.0GHz**

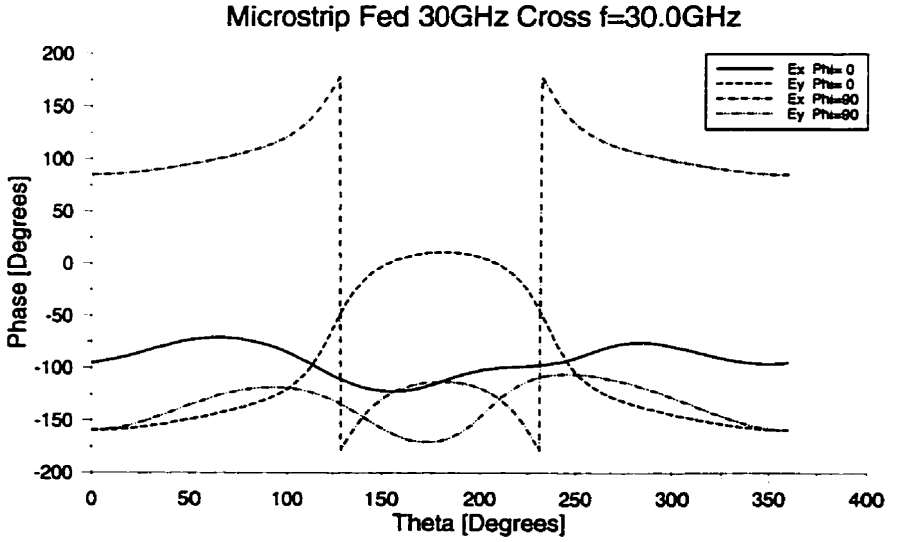


**Figure 3.13 TLM Simulated Phase Difference of the Dielectric Cross f=30.0GHz**

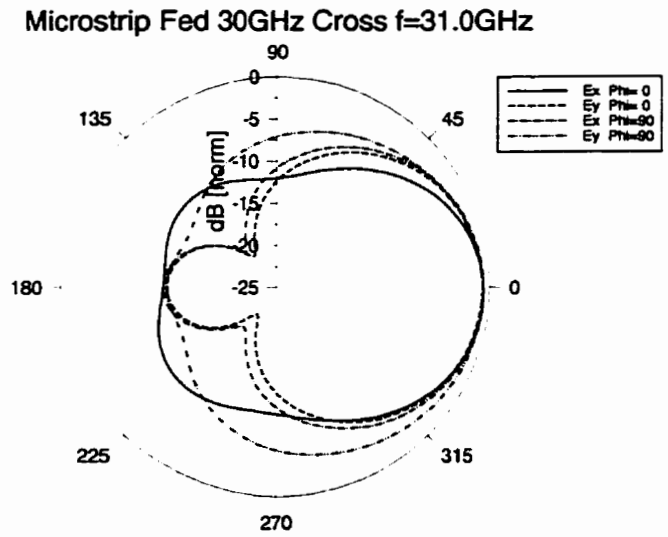


**Figure 3.14 TLM Simulated Far Field Pattern of the Dielectric Cross f=31.0GHz**

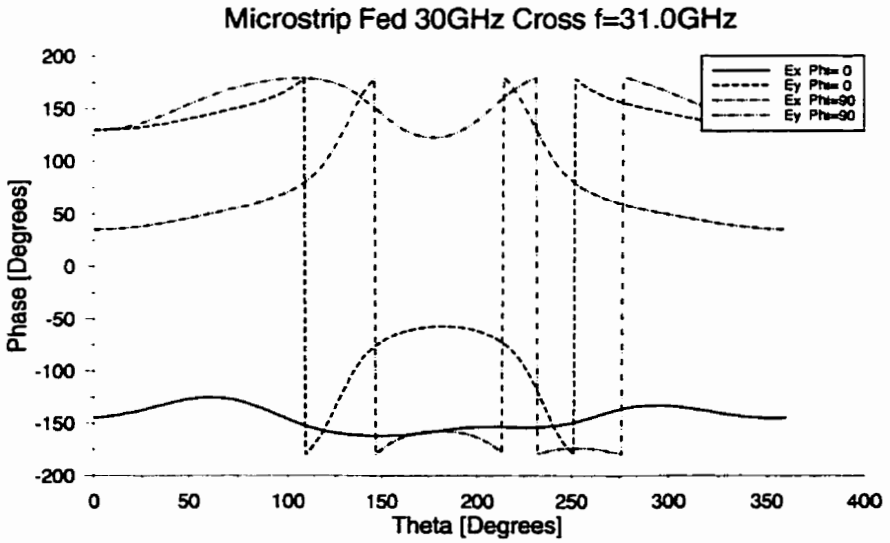


**Figure 3.15 TLM Simulated Phase Difference of the Dielectric Cross f=31.0GHz**

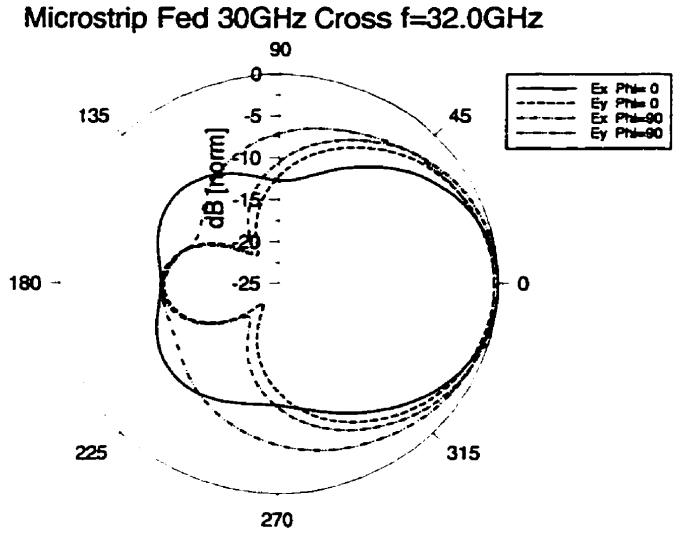


**Figure 3.16 TLM Simulated Far Field Pattern of the Dielectric Cross f=32.0GHz**

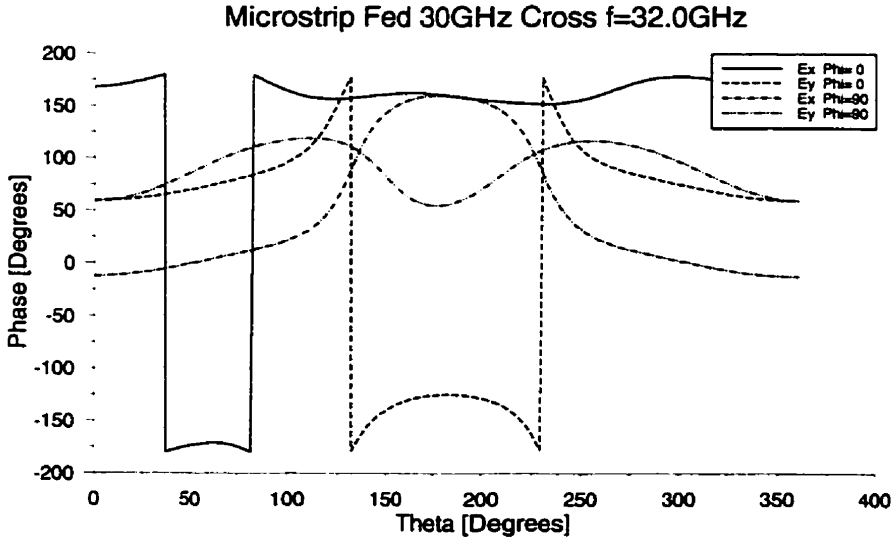


**Figure 3.17 TLM Simulated Phase Difference of the Dielectric Cross f=32.0GHz**

TABLE 2. **Far field components for the microstrip cross 29-32GHz phi=0;**

| Frequency (GHz) | \|Ex\| (dB) | ϕ[Ex] (rad) | \|Ey\| (dB) | ϕ[Ey] (rad) | Axial Ratio |
|---|---|---|---|---|---|
| 29.0 | -119.719 | -0.69260 | -122.406 | -1.53711 | 7.55 dB |
| 30.0 | -118.463 | -1.65494 | -119.510 | -2.77816 | 4.17 dB |
| 31.0 | -117.883 | -2.52647 | -118.011 | 2.26551 | 0.70 dB |
| 32.0 | -117.117 | 2.92695 | -117.576 | 1.03826 | 2.85 dB |

The designs of the microstrip cross were not physically tested on their own, rather it was decided that it was preferable to install them directly into the cavity first and then make any necessary adjustments to the cross design and aperture feed. Simulation shows approximately a 2GHz axial ratio bandwidth for the cross which is a great improvement over the simulation results of the receive antenna.

### 3.2.3 Simulation and Design of the Cross-fed Cavity

TLM simulation was also performed for the cross fed cavity, again with 3000 time steps on a 0.2mm mesh spacing and geometry of Nx=180 Ny=180 and Nz=45 these results are best summarized in Table 3. It appears that the cavity lowers the axial ratio bandwidth of the radiating element from 2GHz to 1.2GHz although this is still sufficient for the project requirements. The return loss for both cross and cavity are compared in Figure 3.18. Here the effect of the cavity is pronounced. Matching appears to have improved and the operating bandwidth has shifted to a lower frequency with the above noted reduction in perceived axial ratio bandwidth.

**TABLE 3. Far Field components for the microstrip cavity 28-32GHz phi=0;**

| Frequency (GHz) | \|Ex\| (dB) | ϕ[Ex] (rad) | \|Ey\| (dB) | ϕ[Ey] (rad) | Axial Ratio |
|---|---|---|---|---|---|
| 28.0 | -108.451 | 0.85802 | -106.295 | -0.19834 | 5.20 dB |
| 28.2 | -108.180 | 0.51643 | -106.126 | -0.74270 | 3.45 dB |
| 28.4 | -107.685 | 0.15368 | -106.122 | -1.26445 | 2.06 dB |
| 28.6 | -107.161 | -0.24654 | -106.176 | -1.76677 | 1.08 dB |
| 28.8 | -106.821 | -0.68147 | -106.217 | -2.25960 | 0.61 dB |
| 29.0 | -106.802 | -1.13748 | -106.247 | -2.75617 | 0.69 dB |
| 29.2 | -107.171 | -1.59699 | -106.348 | 3.01673 | 1.19 dB |
| 29.4 | -107.932 | -2.04029 | -106.642 | 2.49026 | 2.05 dB |
| 29.6 | -109.007 | -2.44588 | -107.259 | 1.95298 | 3.29 dB |
| 29.8 | -110.188 | -2.79557 | -108.323 | 1.95298 | 4.93 dB |
| 30.0 | -111.132 | -3.09165 | -109.949 | 0.90640 | 6.93 dB |

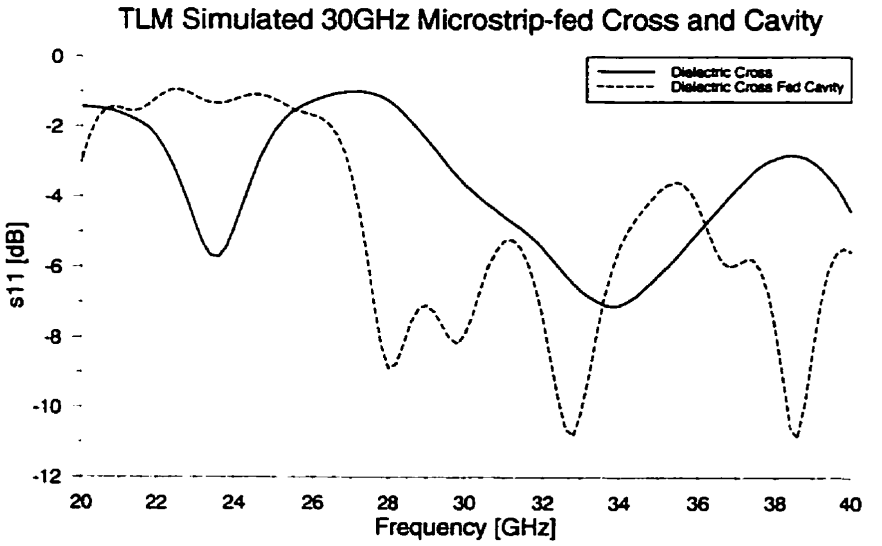


**Figure 3.18 TLM Simulated Return Loss of the 30GHz Dielectric Cross and Cavity**

Simulated results of the radiation patterns in Figures 3.19-29 are of interest compared to the wide beamwidth patterns produced by simulation of the cross itself. One can see the distinct focusing of the beam as produced by the cavity and that the half power beamwidth has shrunk considerably. As expected, the operating frequency has dropped and there appears to be a 3dB axial ratio bandwidth from 28.3 to 29.5GHz although beam symmetry does appear to weaken at the upper end of the band. In fact, by 30GHz it is obvious that the power has spread to other beams indicating interference from other radiating modes.

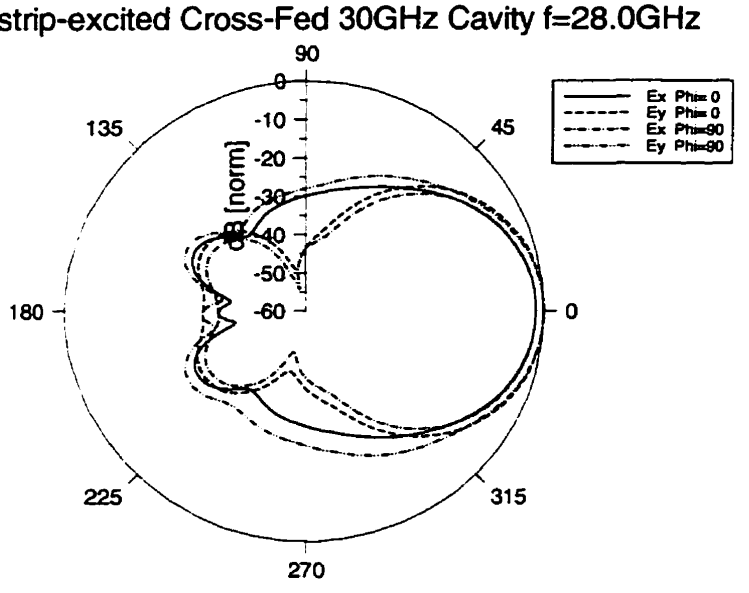


**Figure 3.19 TLM Simulated Far Field Pattern of the Cross-fed Cavity f=28.0GHz**

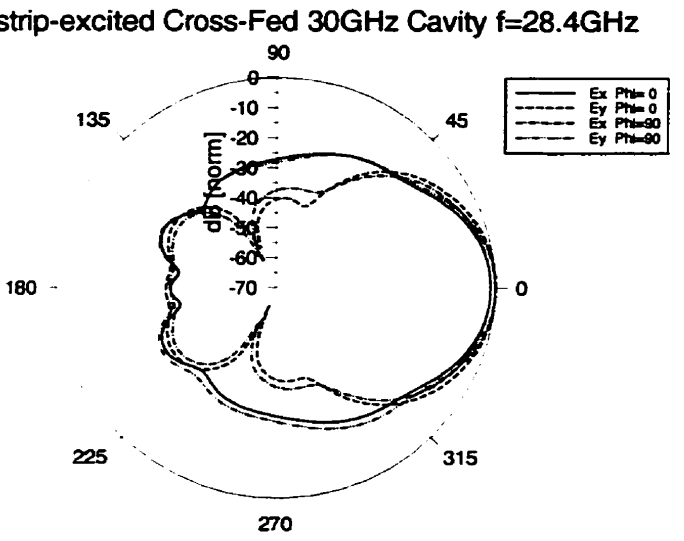


**Figure 3.20 TLM Simulated Far Field Pattern of the Cross-fed Cavity f=28.4GHz**

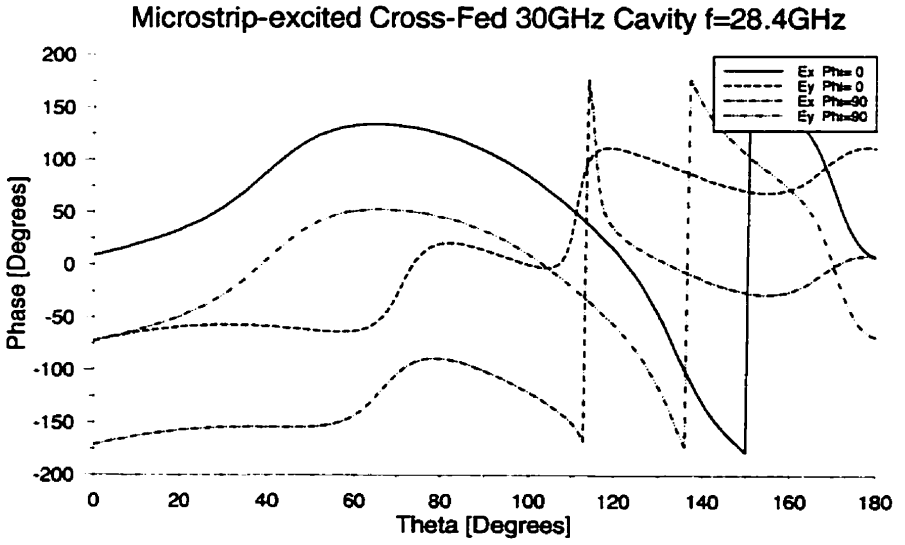


**Figure 3.21 TLM Simulated Phase Difference of the Cross-fed Cavity f=28.4GHz**

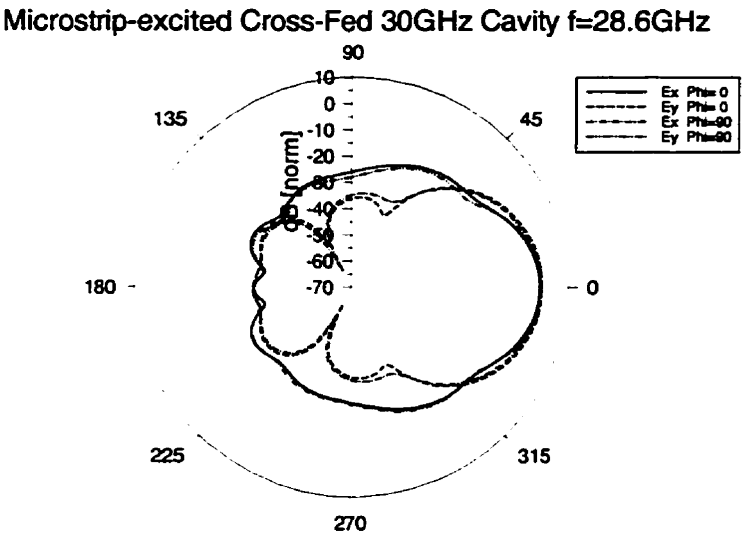


**Figure 3.22 TLM Simulated Far Field Pattern of the Cross-fed Cavity f=28.6GHz**

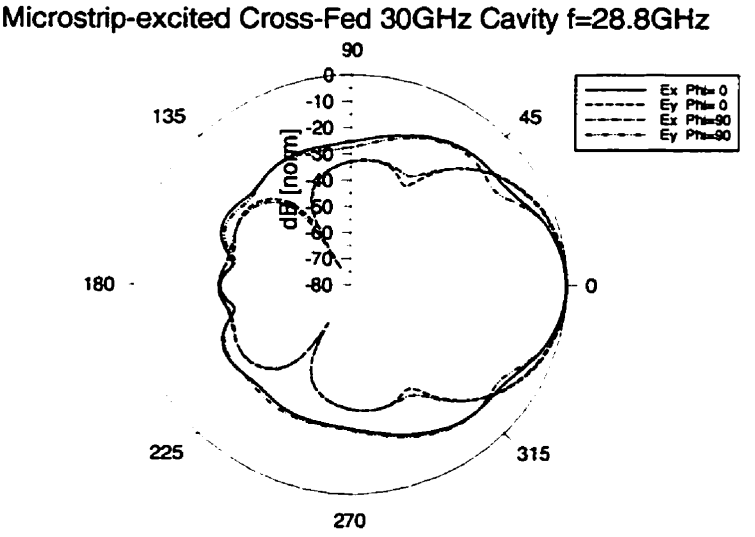


**Figure 3.23 TLM Simulated Far Field Pattern of the Cross-fed Cavity f=28.8GHz**

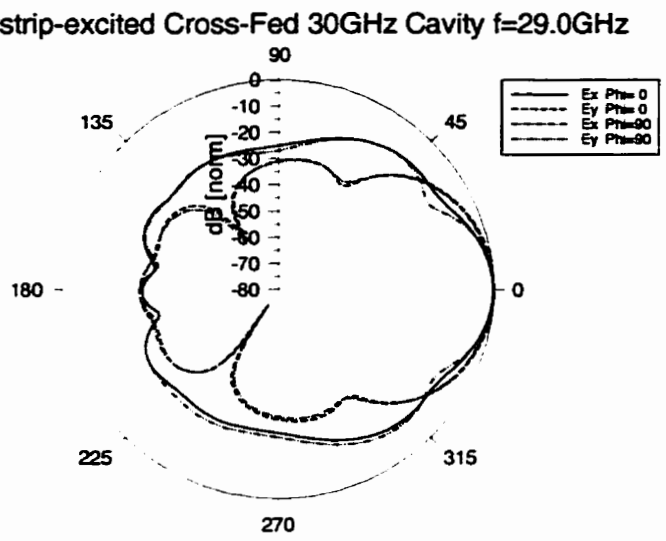


**Figure 3.24 TLM Simulated Far Field Pattern of the Cross-fed Cavity f=29.0GHz**

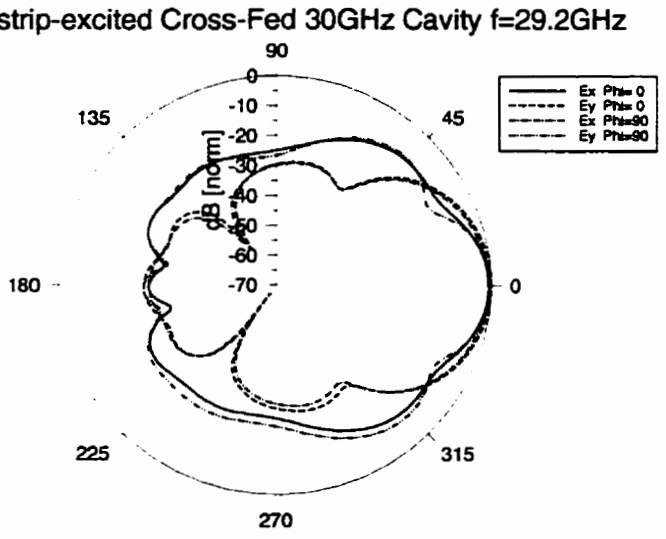


**Figure 3.25 TLM Simulated Far Field Pattern of the Cross-fed Cavity f=29.2GHz**

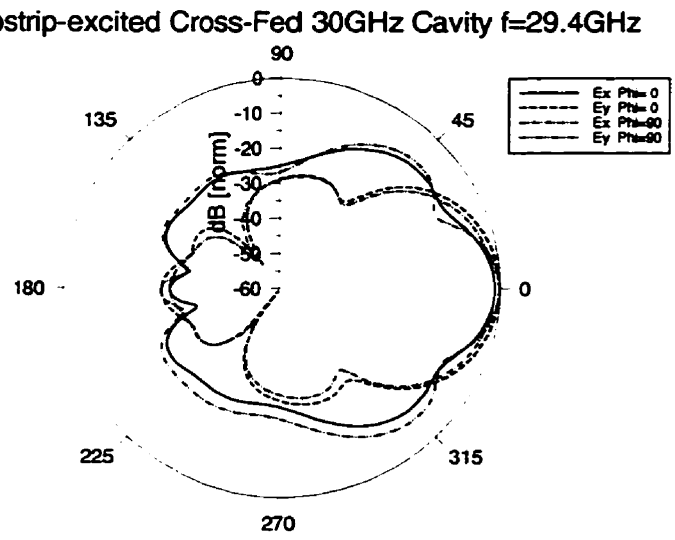


**Figure 3.26 TLM Simulated Far Field Pattern of the Cross-fed Cavity f=29.4GHz**

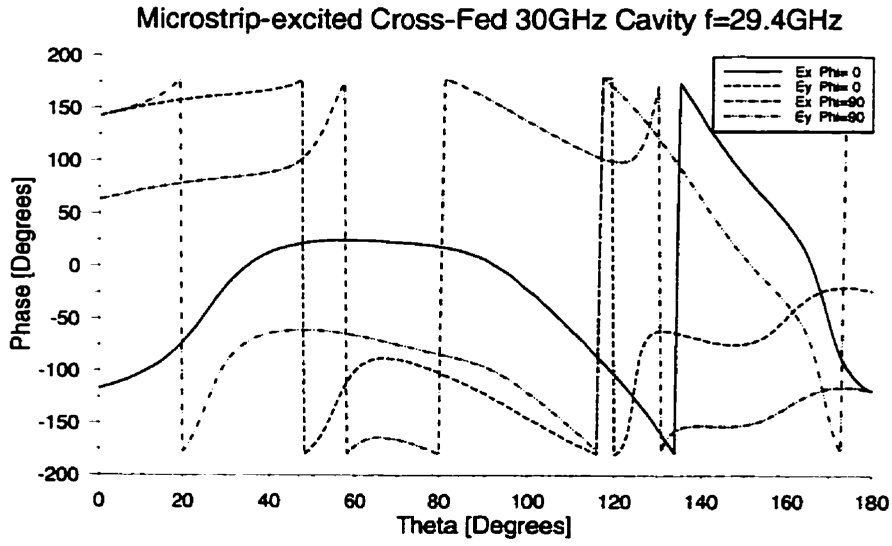


**Figure 3.27 TLM Simulated Phase Difference of the Cross-fed Cavity f=29.4GHz**

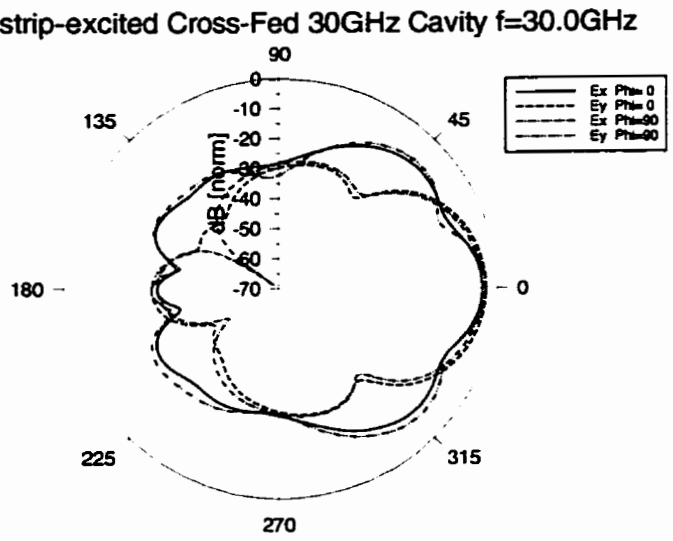


**Figure 3.28 TLM Simulated Far Field Pattern of the Cross-fed Cavity f=30.0GHz**

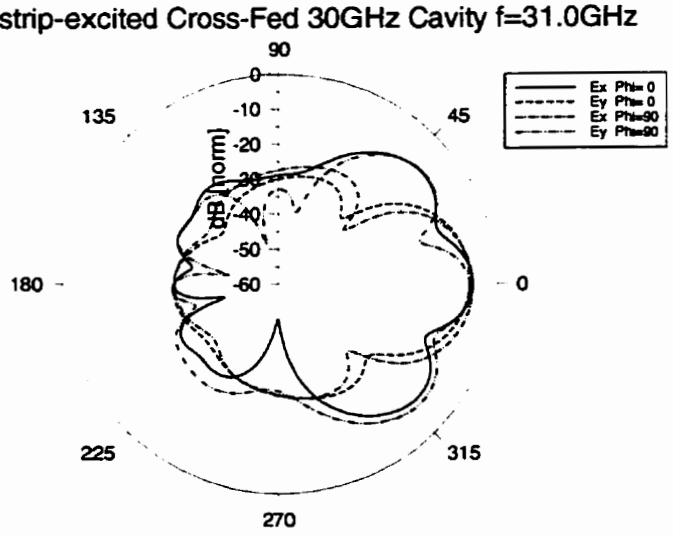


**Figure 3.29 TLM Simulated Far Field Pattern of the Cross-fed Cavity f=31.0GHz**

Physical testing produced the following results.

For the designed cross of 6.8x2.6mm of 1.2mm height inside a 1.8cm diameter, 0.56 cm high cavity a 600MHz axial ratio bandwidth was achieved centred at 28.5GHz. The operating frequency was increased by shaving the height of the cross to 1.1mm. This corresponded to an increase in the operating frequency to 28.8 GHz, with no noticeable effect on the axial ratio bandwidth.

It is believed that increasing the axial ratio bandwidth is dependent on maintaining the 90 degree phase shift between electric field components since the field magnitudes seem to change at a slower rate. A second 1.2mm high cross was tested by filing the cross arms to 5.26mm and 2.46mm (from the original 6.8x2.6mm lengths) this had the effect of not only increasing the centre frequency to 28.9GHz, but also of increasing the axial ratio bandwidth to 700MHz. Filing the second cross down to a 1.1mm height as well as improved matching of the cavity with different thicknesses of dielectric radome increased the operating frequency of the second cross to the optimal 29.5GHz with a 1GHz axial ratio bandwidth. Some frequency shift of the antenna with respect to radome height can be seen from the following return loss measurements of the optimized geometry. (Figures 3.30-34) For all figures, the cavity used measures 0.56cm in height and 1.8cm in diameter. These results correspond with several TLM simulations which were later performed on the stripline fed cavity.

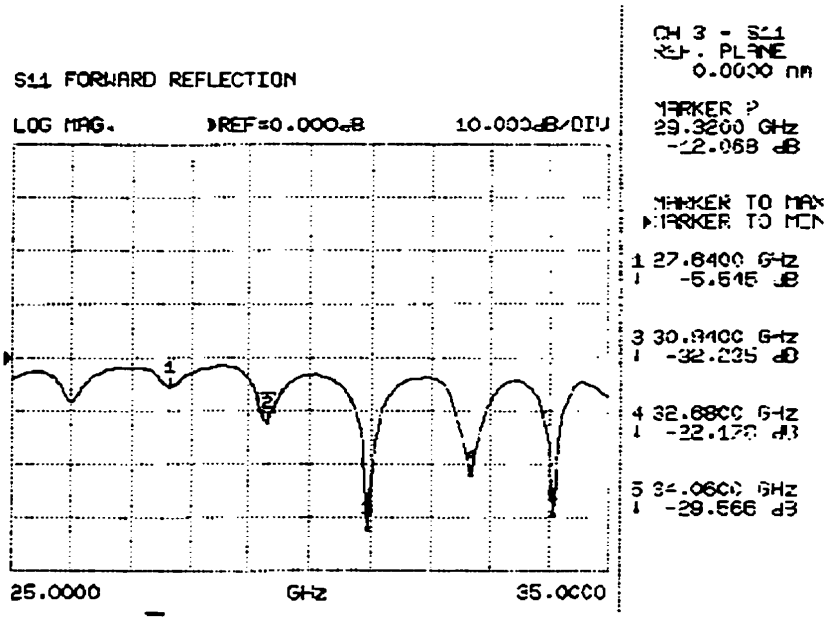


**Figure 3.30 Return Loss produced by the Cross-fed Cavity, Radome thickness= 0mil**

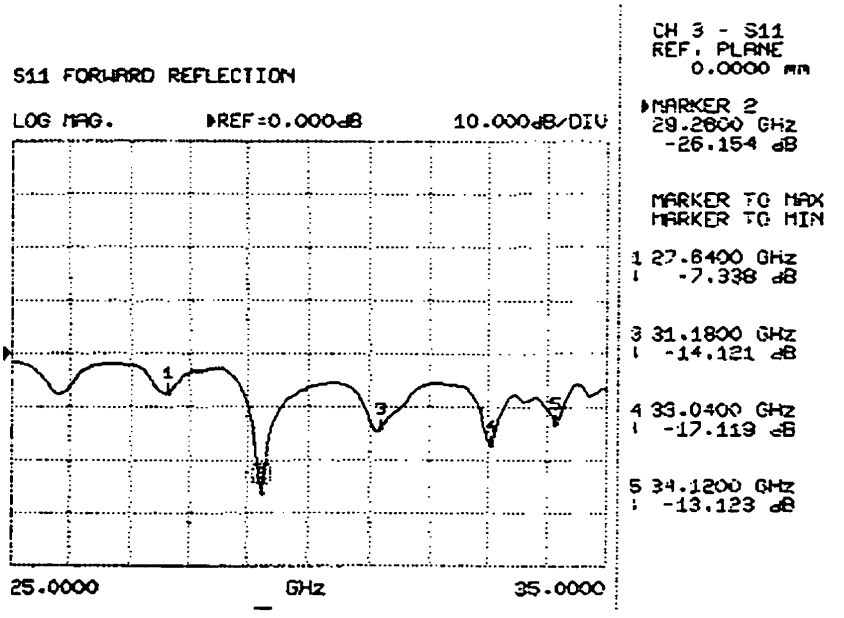


**Figure 3.31 Return Loss produced by the Cross-fed Cavity, Radome thickness=10mil**

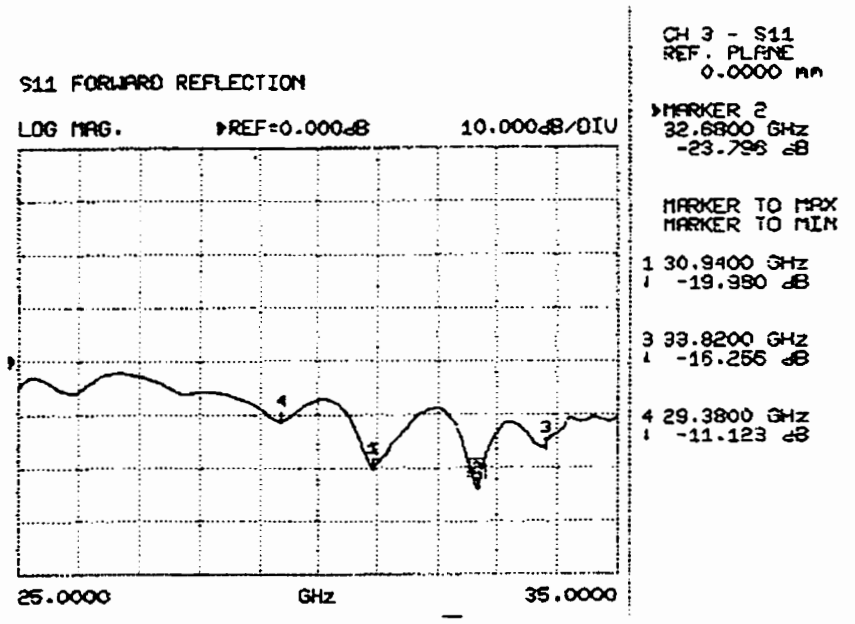


**Figure 3.32 Return Loss produced by the Cross-fed Cavity, Radome thickness=20mil**

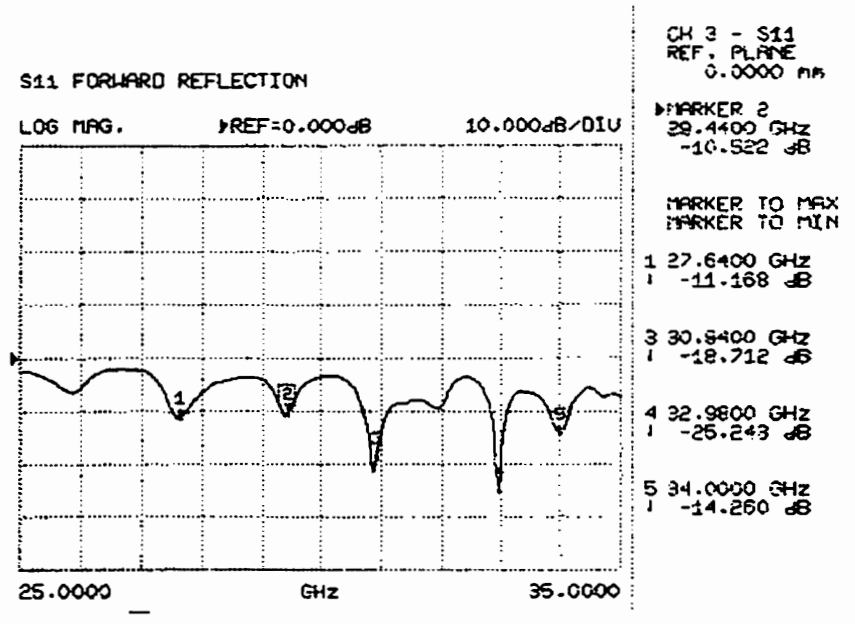


**Figure 3.33 Return Loss produced by the Cross-fed Cavity, Radome thickness=25mil**

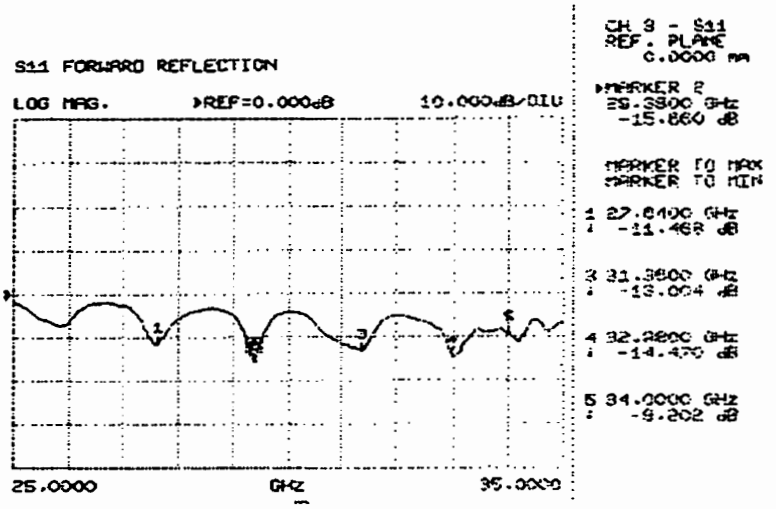


**Figure 3.34 Return Loss produced by the Cross-fed Cavity, Radome thickness=30mil**

Circular polarization patterns produced by the cross-fed cavity are displayed in Figures 3.35-40. They show that the quality of the CP is good for a wide bandwidth although after 45 degrees from boresight the degradation is quicker than with the cross alone. Gain values listed are not exact, but based on the HPBW of 30 degrees we can assume a gain of 15dB. It appears that the antenna is still troubled with the wide gain variation over the operating range. The optimized geometry now consists of the previously identified dielectric cross inserted in a 0.56cm high cavity of 1.8cm diameter with a 15mil Alumina radome. The cross is excited by a 0.728mm wide 50Ω feedline built on a 25mil thick Rogers6010 Duroid (Er=10.2) with a 3.72mm stub extending 3.72mm past the centre of a 2.4 x0.4mm slot.

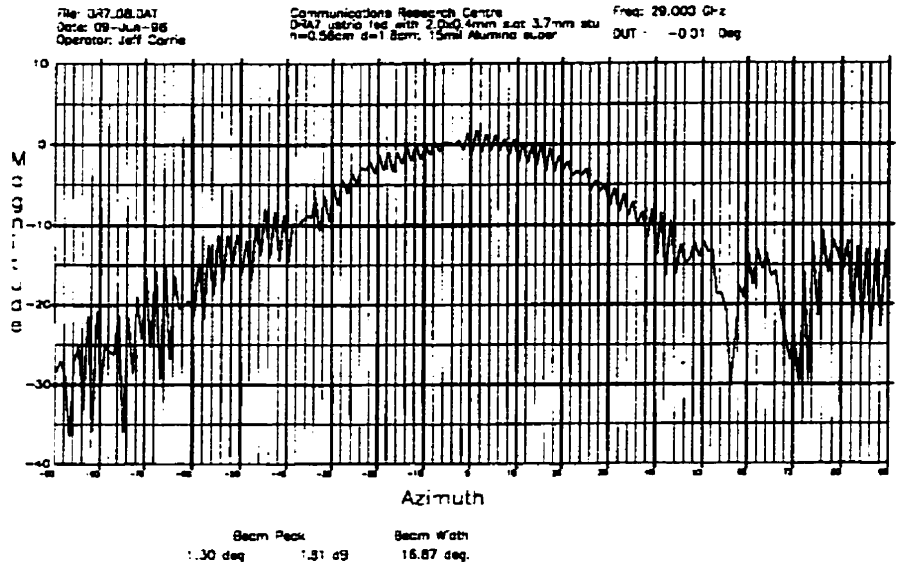


**Figure 3.35 Circular Polarization produced by the Cross-fed Cavity, f=29.0GHz**

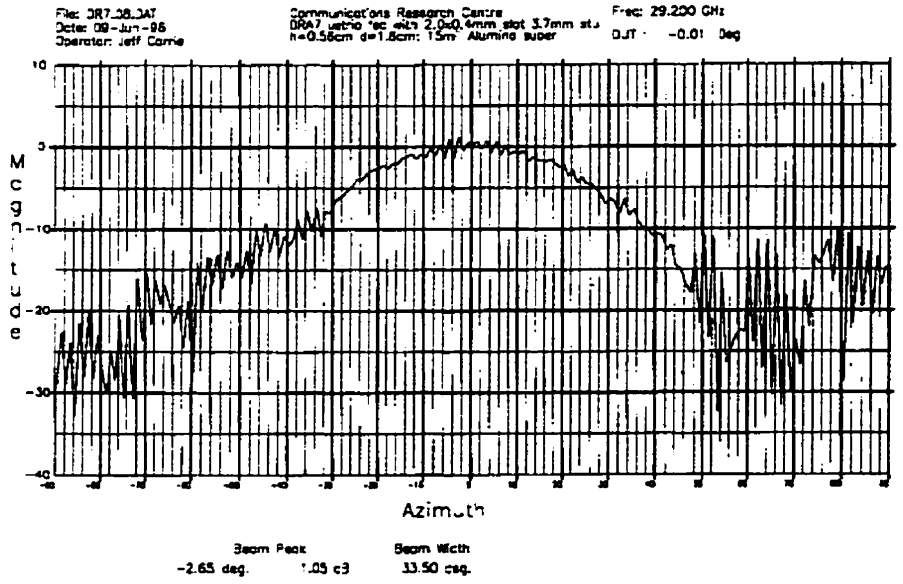


**Figure 3.36 Circular Polarization produced by the Cross-fed Cavity, f=29.2GHz**

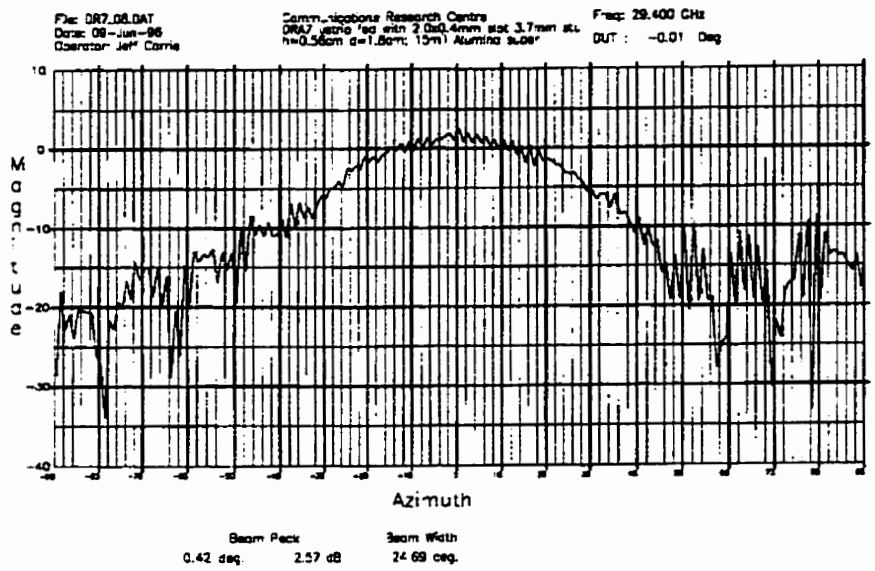


**Figure 3.37 Circular Polarization produced by the Cross-fed Cavity, f=29.4GHz**

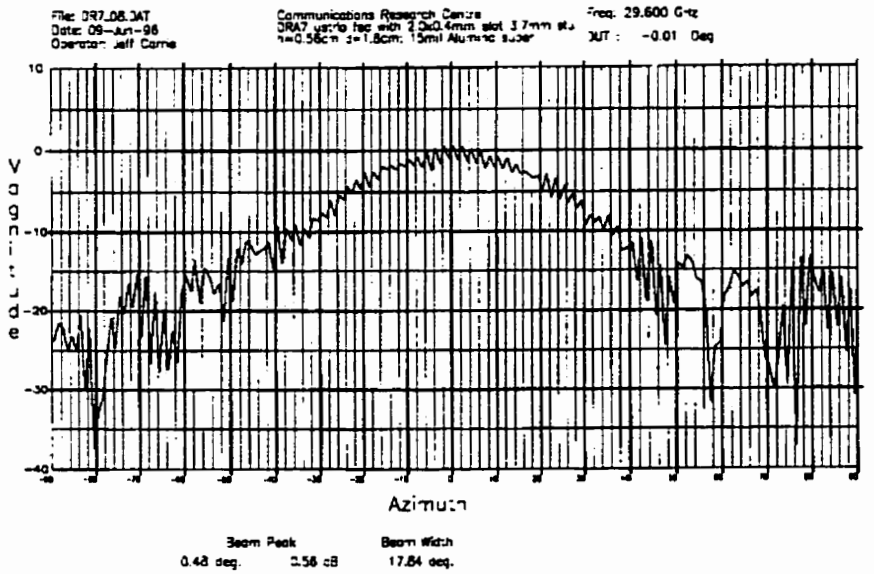


**Figure 3.38 Circular Polarization produced by the Cross-fed Cavity, f=29.6GHz**

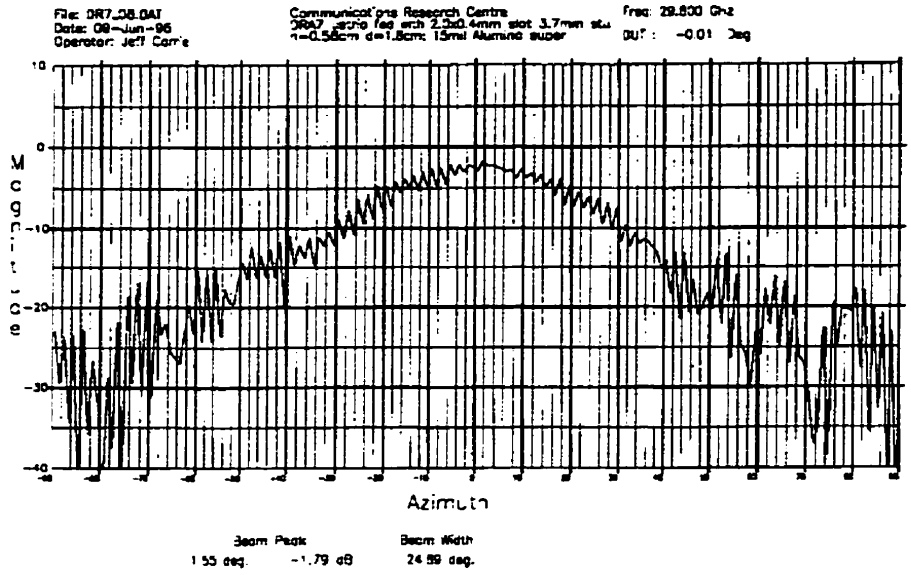


**Figure 3.39 Circular Polarization produced by the Cross-fed Cavity, f=29.8GHz**

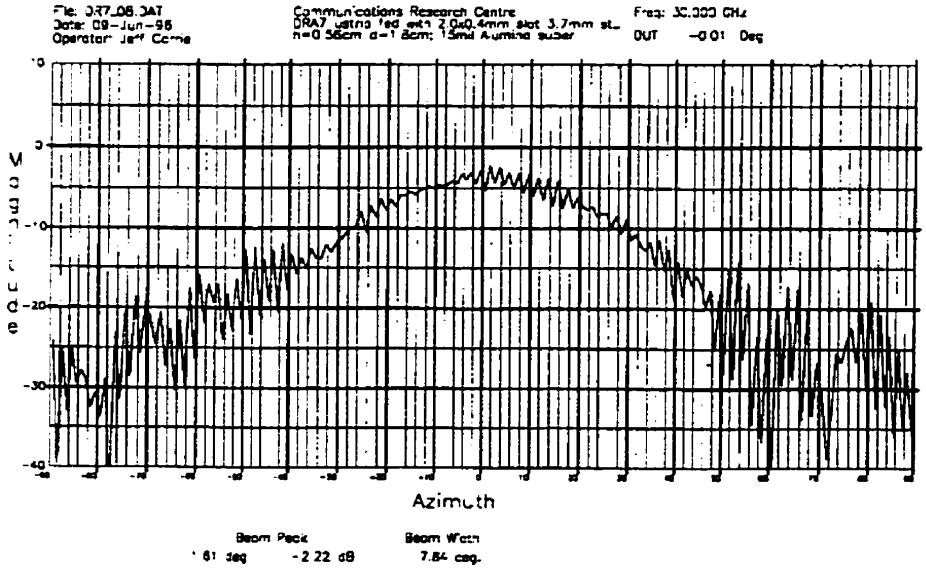


**Figure 3.40 Circular Polarization produced by the Cross-fed Cavity, f=30.0GHz**

The optimized dimensions are therefore as listed in Figures 3.41-42.

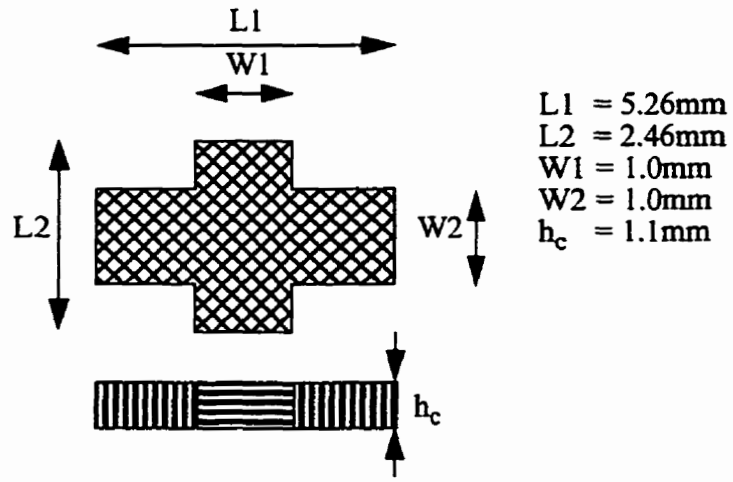


**Figure 3.41 Optimized Dimensions of the Dielectric Cross**

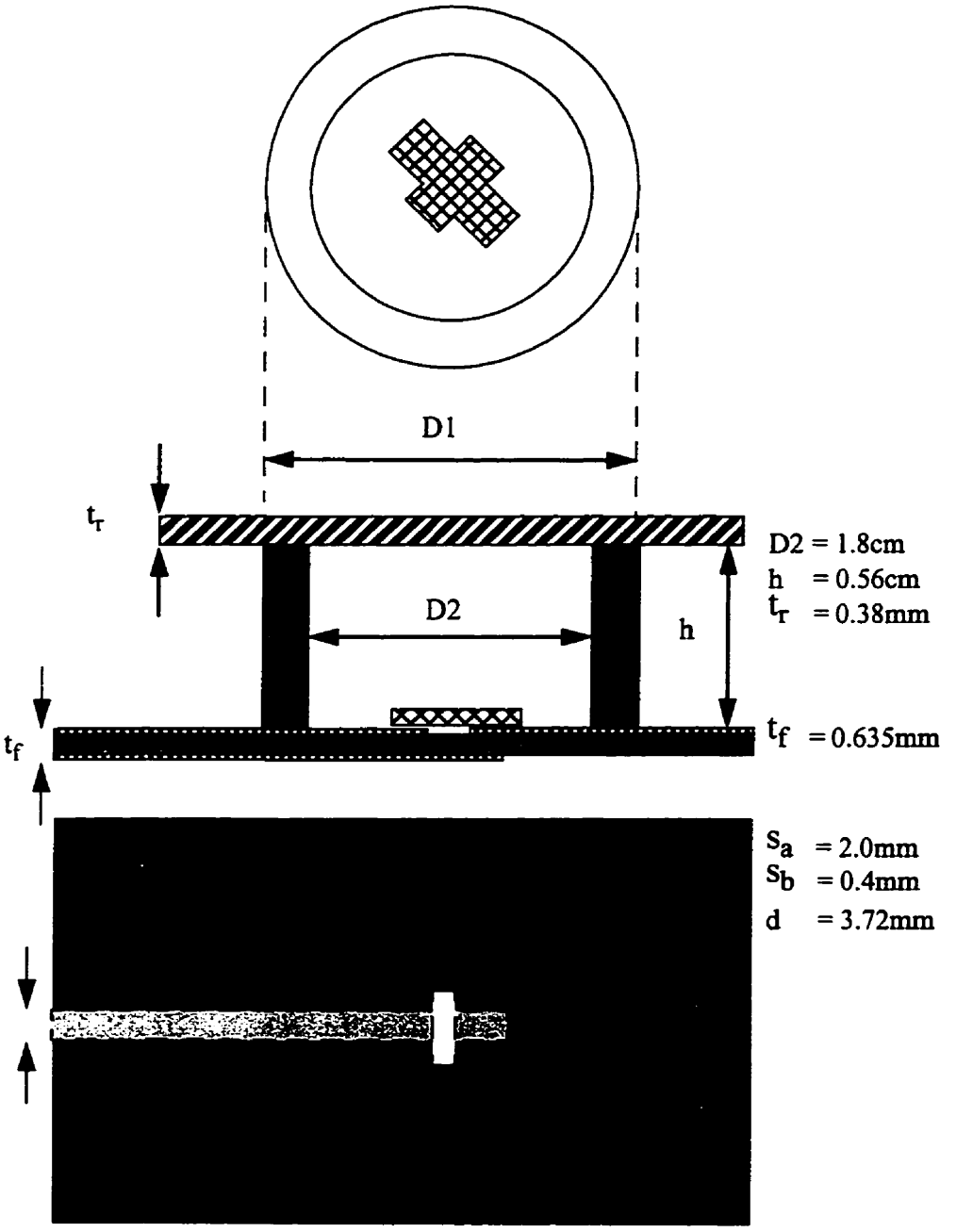


**Figure 3.42 Optimized Microstrip-fed Cavity Geometry**

## 3.3 Circularly Polarized Elements Fed with Stripline

Stripline eliminates parasitic feedline radiation and back radiation from the slot. This is done at the cost of trapping the back radiation between two ground planes which result in parallel plate modes. These parallel plate parasitics are typically disrupted through the use of shorting pins which in an array environment also isolate the individual elements and maintain the quality of the circular polarization. Although we have chosen to limit ourselves to the feeding of the dielectric cross, techniques have been investigated for slot-coupled patches[63] which were not pursued in this investigation.

### 3.3.1 Simulation of the Stripline-fed Cross

As the next step in the evolution of the antenna, TLM analysis of a stripline structure was begun. There are some concerns with respect to the validity of the reflection analysis since the substrate heights do not conform to the 0.2mm tolerances enforced by the program; however, the degree of coupling should not dramatically affect the overall radiation patterns produced. Stripline geometries have not been optimized but are merely presented as first iterations of the microstrip element making the transition to a stripline geometry. Initial feed design was used according to [64]. For the dielectric cross alone results are similar to the microstrip case with approximately a 2GHz bandwidth existing from 30-32GHz.

Return loss calculations in Figure 3.43 appear consistent, with dual modes operating around 29GHz and 33GHz. Radiation patterns and phase differences (Figures3.44-49)

show circular polarization to occur around 31GHz. This is affirmed through the calculations in Table 4.

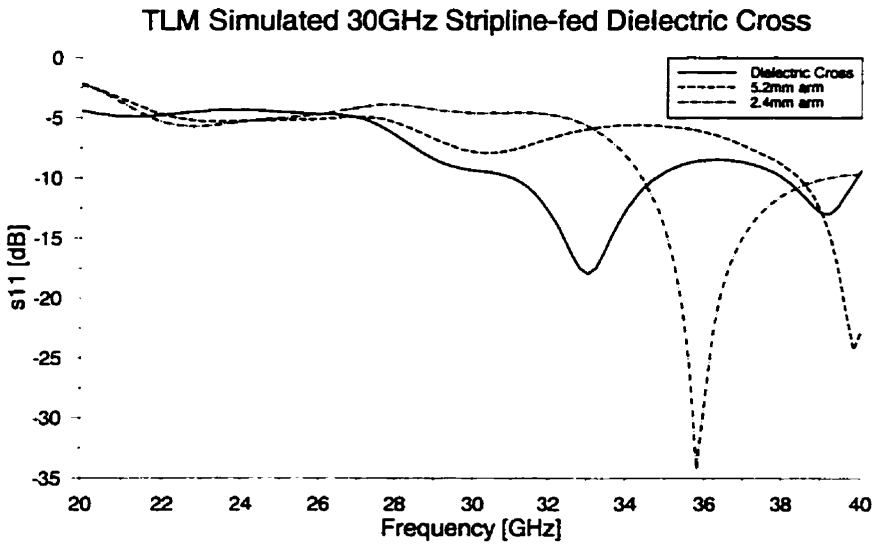


**Figure 3.43 TLM Simulated Return Loss of the Stripline-fed 30GHz Dielectric Cross**

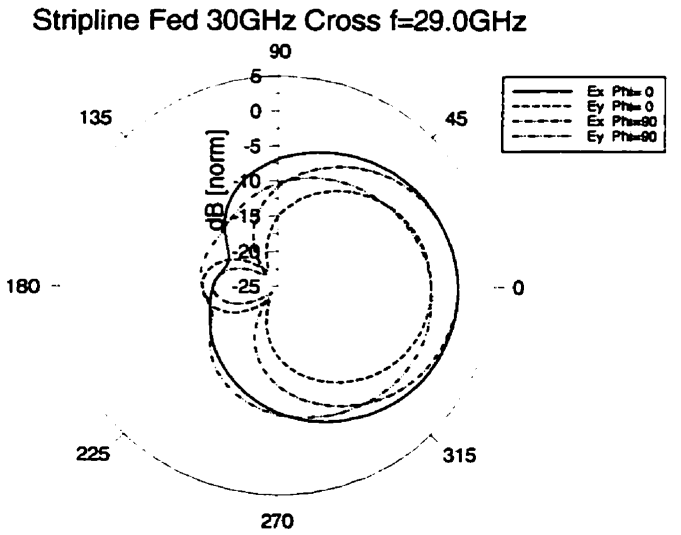


**Figure 3.44 TLM Simulated Far Field Pattern of the Dielectric Cross f=29.0GHz**

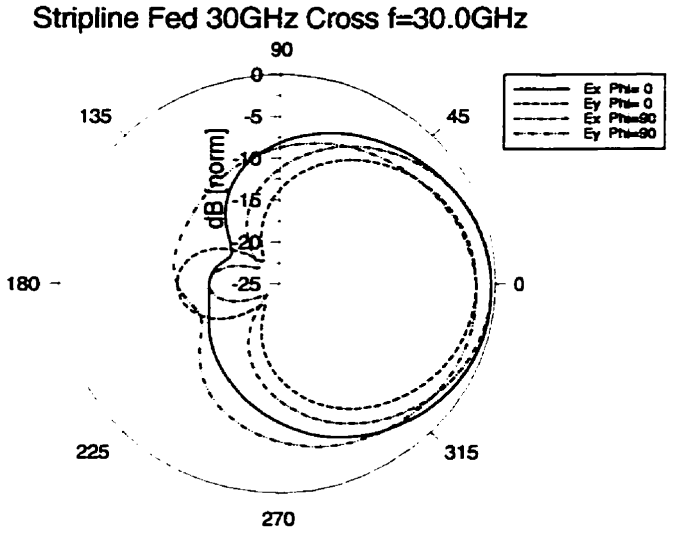


**Figure 3.45 TLM Simulated Far Field Pattern of the Dielectric Cross f=30.0GHz**

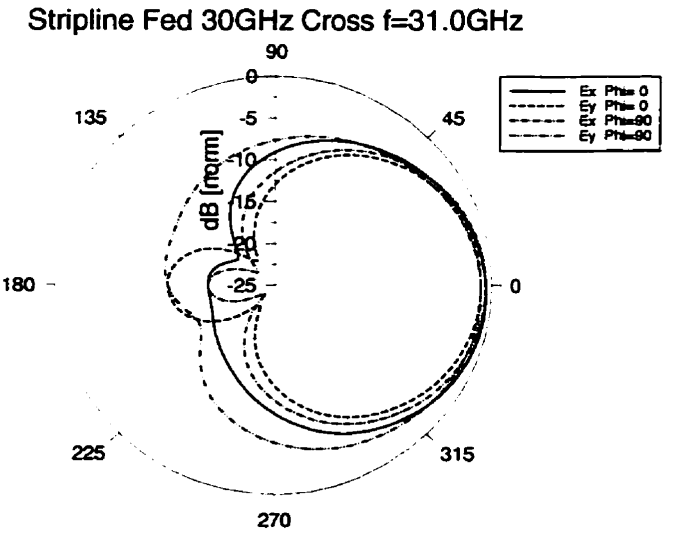


**Figure 3.46 TLM Simulated Far Field Pattern of the Dielectric Cross f=31.0GHz**

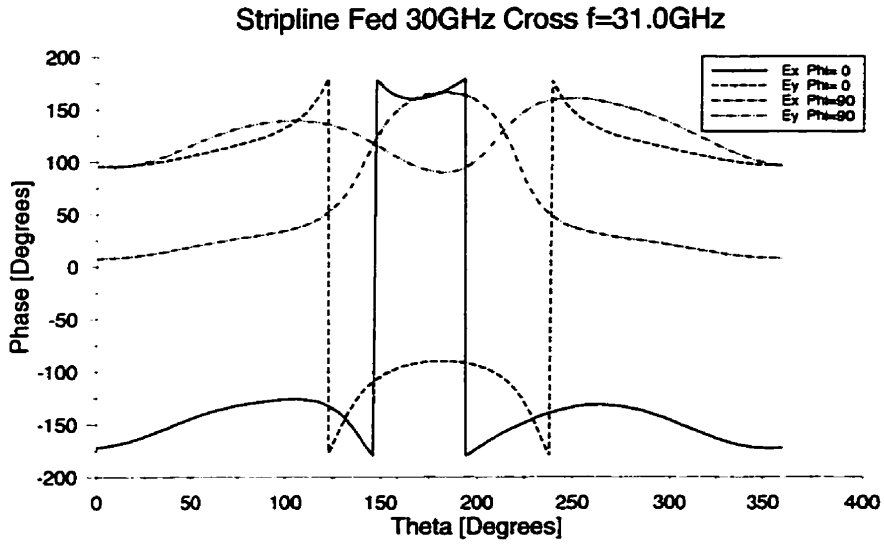


**Figure 3.47 TLM Simulated Phase Difference of the Dielectric Cross f=31.0GHz**

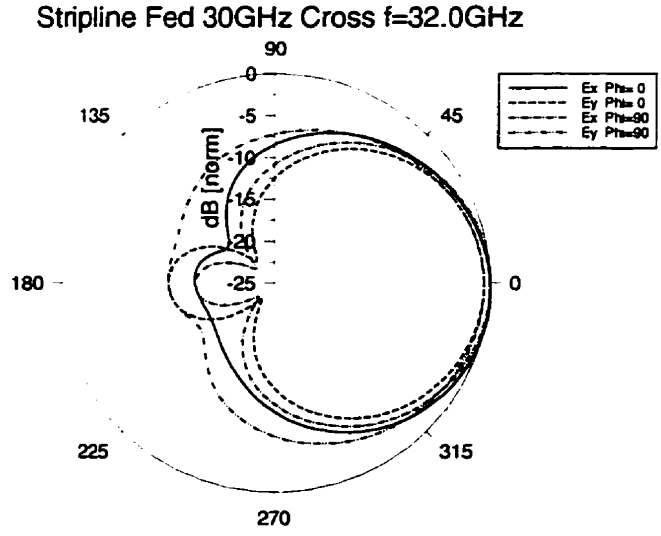


**Figure 3.48 TLM Simulated Far Field Pattern of the Dielectric Cross f=32.0GHz**

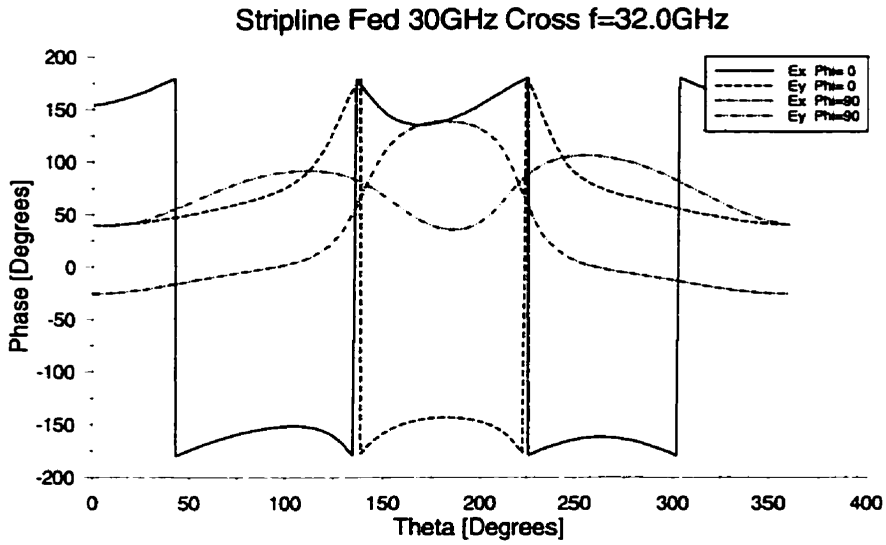


**Figure 3.49 TLM Simulated Phase Difference of the Dielectric Cross f=32.0GHz**

**TABLE 4. Far Field components for the stripline cross 29-32GHz phi=0**

| Frequency (GHz) | \|Ex\| (dB) | ϕ[Ex] (rad) | \|Ey\| (dB) | ϕ[Ey] (rad) | Axial Ratio |
|---|---|---|---|---|---|
| 29.0 | -143.009 | -1.79711 | -146.834 | -2.72833 | 7.25 dB |
| 30.0 | -143.570 | -2.44582 | -145.340 | 2.60942 | 3.53 dB |
| 31.0 | -143.726 | -3.00572 | -144.301 | 1.67237 | 0.65 dB |
| 32.0 | -143.005 | 2.69344 | -143.720 | 0.69878 | 3.87 dB |

### 3.3.2 Simulation and Testing of the Cross-fed Cavity

Simulation of the stripline fed cross within the cavity was also carried out. The return loss results of Figure 3.50 appear promising as the two modes identified operating in the cross-only simulation have closed together and are quite well matched to the element. As high-lighted in previous discussion, simulations with various thicknesses of superstrate were carried out and the increased height does produce a lowering of the operating frequency as shown in Figure 3.51. Also note the poorer return loss performance for thicker super-

strates. The 0.2mm superstrate is used and while this may not correlate with the quarter guided wavelength rule presented in Chapter 2, the dimension is the smallest the meshing size will allow. Unfortunately, the results obtained from the near to far field transformation (Figures 3.52-58) show that the potential for circular polarization is not there. Table 5 summarizes the axial ratio readings which minimize at 29.8GHz, higher than the microstrip feed simulation. Aside from the troubles simulating the proper superstrate height, given that the only change in the geometry is that of the feed method, it is suspected that the parasitic modes may be hindering the performance of the antenna. These parasitics are likely affecting the current distribution and disrupting the phase difference between the two wanted modes. As before the cavity lowers the operating frequency of the device.

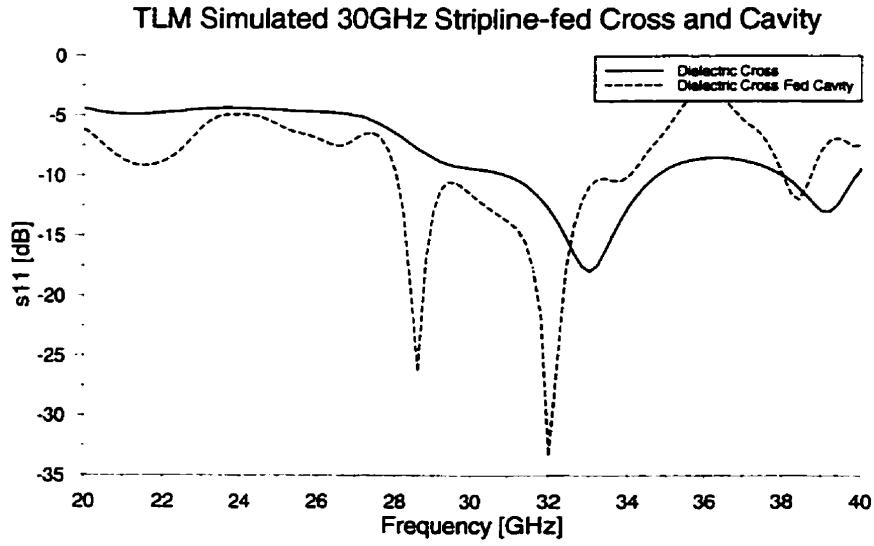


**Figure 3.50 TLM Simulated Return Loss of the 30GHz Dielectric Cross and Cavity**

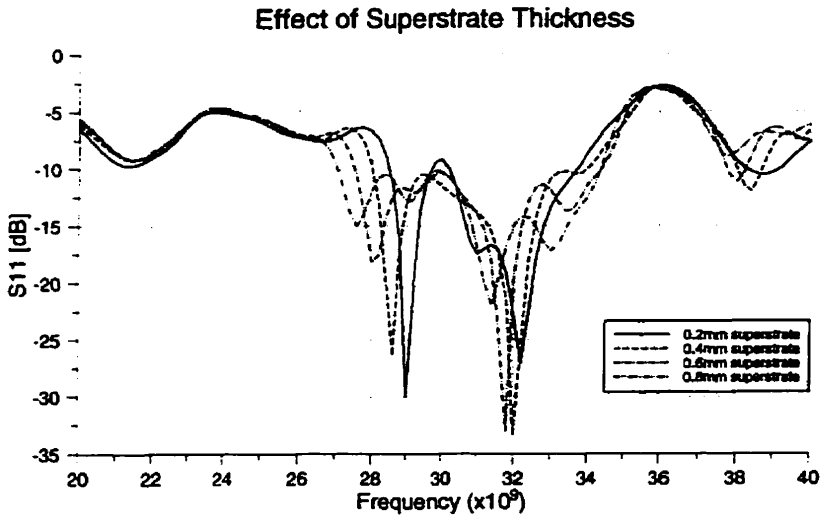


**Figure 3.51 TLM Simulated Return Loss for Several Superstrate Thicknesses**

**TABLE 5. Far Field components for the stripline 30GHZ cavity 28-32GHz phi=0;**

| Frequency (GHz) | \|Ex\| (dB) | ϕ[Ex] (rad) | \|Ey\| (dB) | ϕ[Ey] (rad) | Axial Ratio |
|---|---|---|---|---|---|
| 28.0 | -135.339 | -0.15726 | -137.689 | -0.47662 | 16.19 dB |
| 29.0 | -138.857 | -1.87557 | -135.500 | -2.71996 | 7.87 dB |
| 29.2 | -139.373 | -2.02669 | -135.235 | -3.10137 | 6.23 dB |
| 29.4 | -139.152 | -2.19207 | -134.842 | 2.78311 | 4.93 dB |
| 29.6 | -138.652 | -2.41414 | -134.515 | 2.35133 | 4.16 dB |
| 29.8 | -138.268 | -2.67716 | -134.477 | 1.88796 | 4.02 dB |
| 30.0 | -138.085 | -2.95075 | -134.917 | 1.40615 | 4.52 dB |
| 31.0 | -137.170 | 1.88476 | -142.221 | 0.29990 | 5.05 dB |
| 32.0 | -139.831 | 0.36340 | -136.352 | -1.90806 | 7.66 dB |

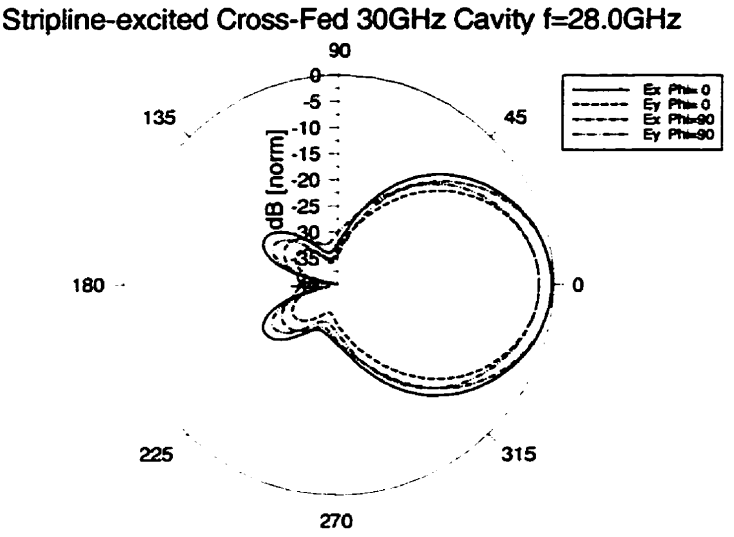


**Figure 3.52 TLM Simulated Far Field Pattern of the Cross-fed Cavity f=28.0GHz**

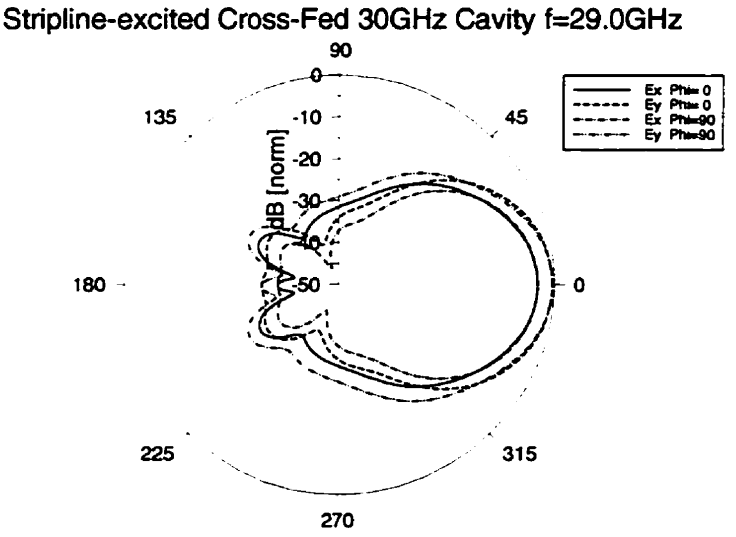


**Figure 3.53 TLM Simulated Far Field Pattern of the Cross-fed Cavity f=29.0GHz**

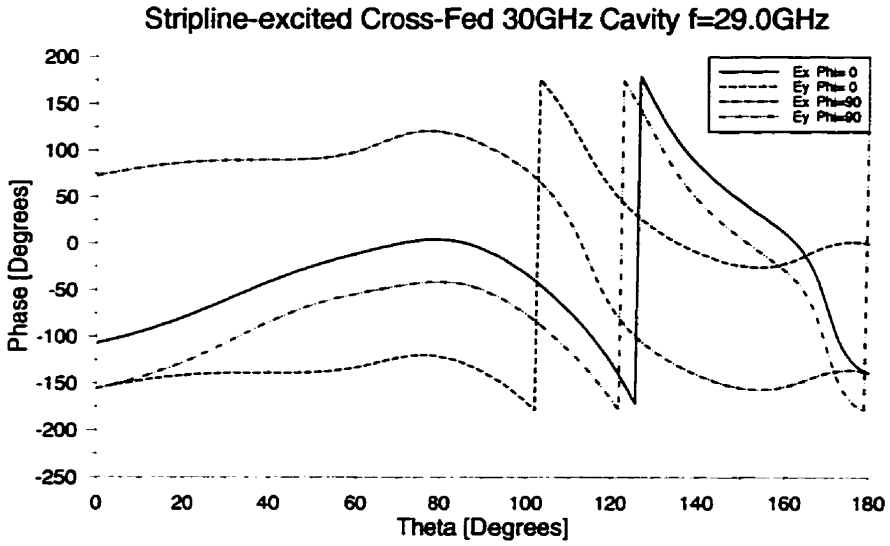


**Figure 3.54 TLM Simulated Phase Difference of the Cross-fed Cavity f=29.0GHz**

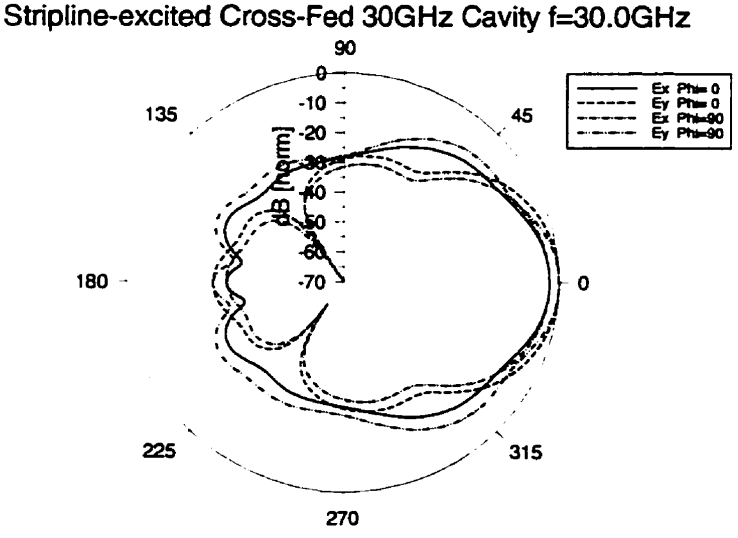


**Figure 3.55 TLM Simulated Far Field Pattern of the Cross-fed Cavity f=30.0GHz**

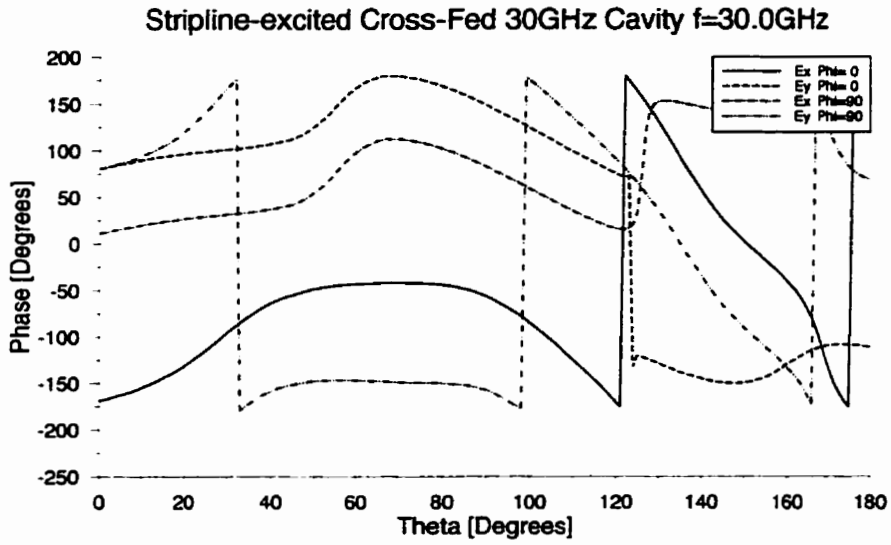


**Figure 3.56 TLM Simulated Phase Difference of the Cross-fed Cavity f=30.0GHz**

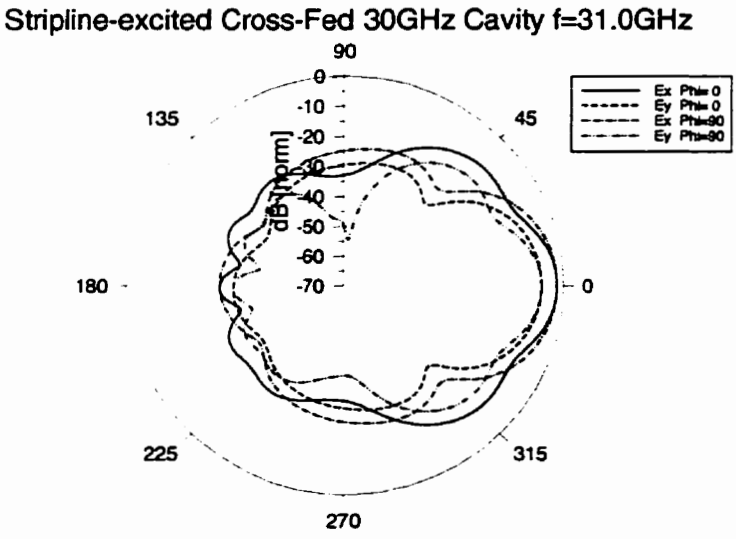


**Figure 3.57 TLM Simulated Far Field Pattern of the Cross-fed Cavity f=31.0GHz**

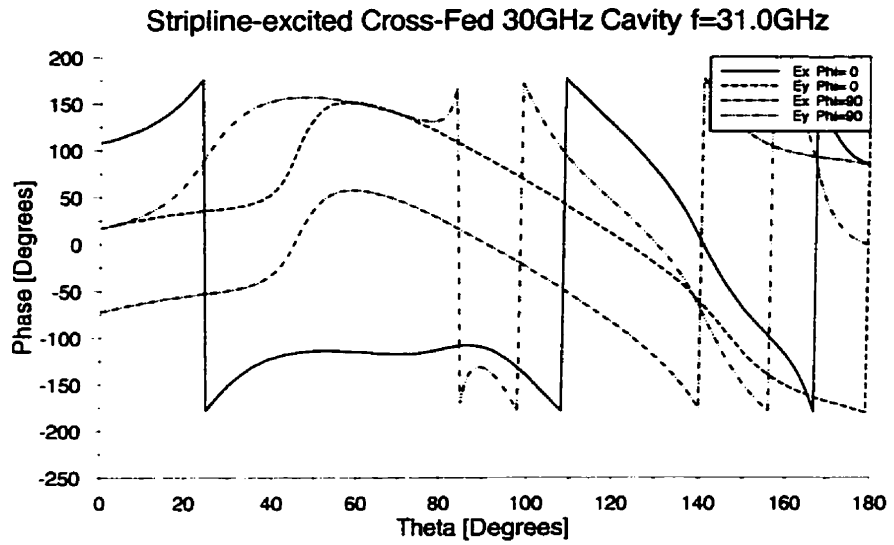


**Figure 3.58 TLM Simulated Phase Difference of the Cross-fed Cavity f=31.0GHz**

Greater axial ratio performance was expected based on the previous results with the microstrip fed cavity. It is possible that the excitation of parasitic modes within the cavity has caused the loss in axial ratio. The performance may be improved through better radome matching. Improvements to the return loss of the element may be introduced by an asymmetric stripline feed such as presented in [65]. Alternately, if parallel plate modes are evident, they may be disrupted through the use of shorting pins between the two ground planes. The ideal placement of the pins will be around the slot in the ground plane. Placement of the pins will be difficult given the small wavelength making the ideal separation ($0.1\lambda$) on the same order as the pin diameter. Physical testing does appear to show promise of circular polarization and the return loss of Figure 3.59 shows a reasonable match. Physical testing (Figures 3.60-62) showed the existence of CP across a limited bandwidth. As a result, further iterations will require a better feed and the implementation of shorting pins to attempt to disrupt the parasitics which interfere with the radiation pattern.

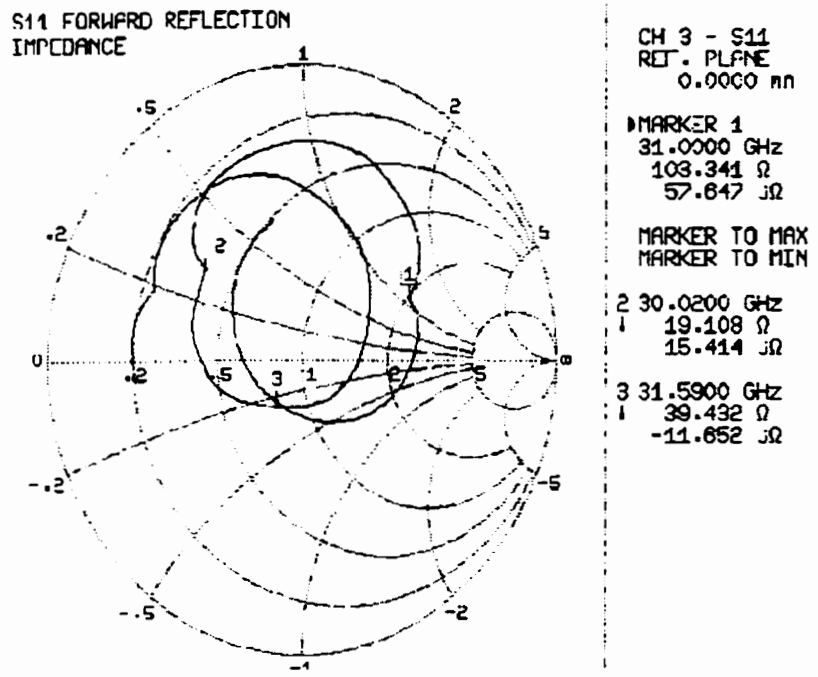


**Figure 3.59 Return Loss produced by the Cross-fed Cavity, Radome thickness=25mil**

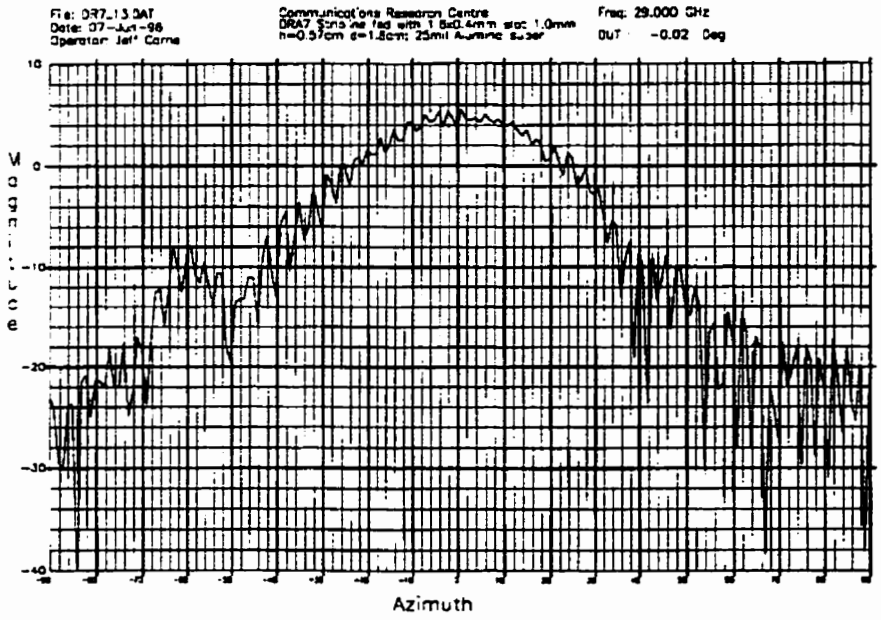


**Figure 3.60 Initial Circular Polarization produced by the Cross-fed Cavity, f=29.0GHz**

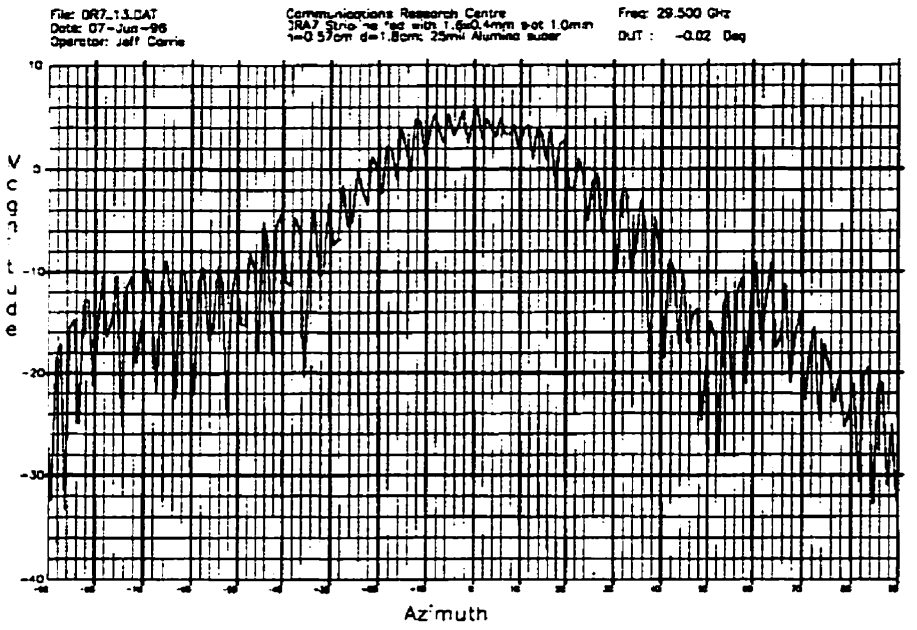


**Figure 3.61 Initial Circular Polarization produced by the Cross-fed Cavity, f=29.5GHz**

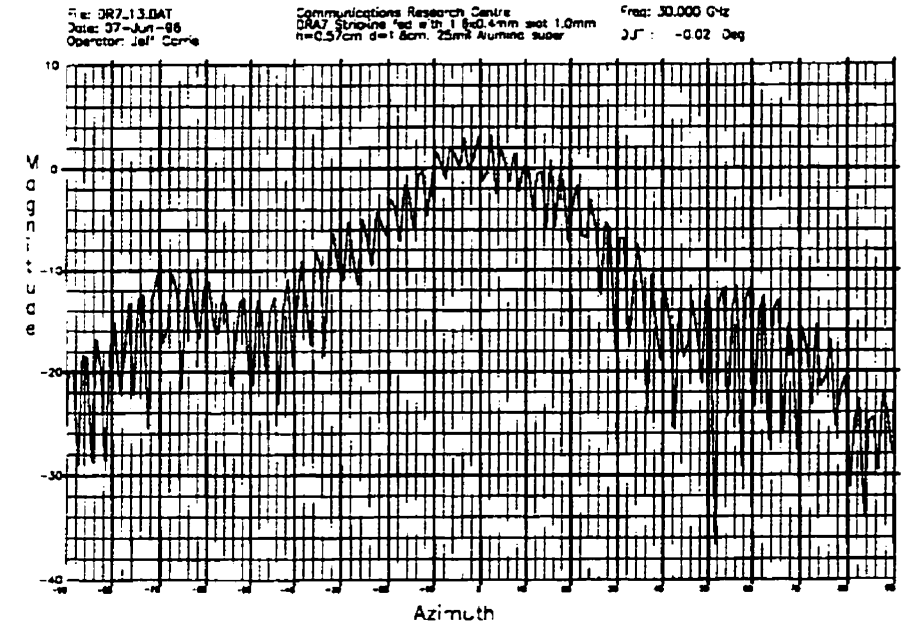


**Figure 3.62 Initial Circular Polarization produced by the Cross-fed Cavity, f=30.0GHz**

## 3.4 Summary

In this chapter several antenna elements were considered for linearly and circularly polarized transmit applications. Simple scaling of the linearly polarized receive antenna did not produce a working model. Redesign of the microstrip patch allowed for the change in operating frequency however, higher than expected sidelobe levels were present. A variety of methods were attempted to minimize side lobes which were inevitably reduced by minimizing the cavity diameter. In addition to the microstrip patch fed antenna, attempts were also made with a linearly polarized dielectric resonator. The option was physically verified although the optimization was not deemed necessary.

The use of a microstrip patch for circular polarization was once more analyzed and rejected in favour of the dielectric cross. The dielectric resonator cross was simulated with the TLM code for both microstrip and stripline feeding techniques. Physical results were presented for microstrip feeding and an optimized geometry was achieved which satisfied the design objective of having a 1GHz operating bandwidth from 29-30GHz. Initial attempts at migrating from microstrip to stripline feeding were met with poor results both in simulation and physical performance. It is believed that the introduction of parasitic modes within the cavity caused a disruption of the phase difference required for CP to operate. Optimization of the cavity radome will hopefully improve the antenna performance. Suggestions were made for improving the return loss of the antenna through improved ground continuity. These results have been discussed in previous literature [55,66]. Linearly polarized results have been presented in [55] with circularly polarized results and comparisons to TLM simulation summarized in [66].

The circularly polarized elements presented in this chapter have been used in a phased array environment presented in [67]. In addition, the dielectric resonator elements presented in this thesis have been further investigated in [68]. In the following chapter the thesis contributions will be summarized with conclusions drawn on the performance of the transmit and receive antennas. Future projects and research of interest will be outlined.

# Conclusions and Future Directions

## 4.0 Conclusions

In this thesis a transmission line matrix method has been used to model aperture coupled geometries, individual radiating elements as well as an entire cavity backed antenna. The goal of the research was to realize physical elements for use as linear and circularly polarized antennas in K band (20GHz) and Ka-Band (30GHz) applications. In accordance with this goal, the following information and results have been presented in this thesis.

- Use of an oversized patch was replaced with a single element fed cavity.
- Modifications of the linearly polarized cavity element proved to be ineffective as did the use of similar microstrip patch feeds. The exciting element was chosen to be a dielectric resonator capable of radiating circular polarization.
- A 20 GHz dielectric cross with arms measuring 6.0mm and 3.4mm each 1.8mm wide and 2.0mm high was developed and proved capable of radiating circular polarization.
- A transmission line matrix method was used to simulate the physical cross and proved to reflect the circularly polarized nature of the element. The TLM software was then used for future simulation and development.
- The element was then used to feed a cavity measuring 2.60 cm in diameter and 0.737 cm high. The antenna is fed using a 50Ω line on 25mil thick Rogers 6010 Duroid coupling through a 5.1mm x 0.6mm slot centred with respect to the cross. The feedline extends 1.3mm past the centre of the slot. The cavity was matched to free space using a

dielectric radome of 40mil thickness and proved capable of radiating circular polarization with an axial ratio of less than 3dB over an operating bandwidth of 18.2GHz to 18.8 GHz.

- Scaling of the linear polarized receive antenna element was not straight forward and required further optimization to produce a working element for transmit applications. The calculated patch size was modified to 3.94x2.76mm in order to radiate the proper frequency within the cavity geometry and this resulted in radiation patterns with high shoulders in one of the principal planes.
- High shoulders in the E-plane were similar to those produced by wide angle flared horns, these were minimized through reduction of the cavity diameter from 1.8cm to 1.7cm. The finalized cavity design measured 0.46mm in height and was topped with a alumina radome ($\varepsilon_r$=9.9) of 20mil. The entire geometry was fed with a 50Ω line on 25mil thick Rogers 6010 Duroid coupling through a 2.73mm x 0.4mm slot centred with respect to the patch and extending 4mm past the slot centre.
- A dielectric cross was simulated for use at 30GHz and used to simulate a full cavity element. Simulation resulted in the construction of a microstrip fed geometry where the 50Ω line couples through a 2.0x 0.4 mm slot with a matching stub of 3.72mm to the dielectric cross. The cross arms measure 5.26 x 2.46 mm with widths of 1.0 mm and heights of 1.1 mm. The aperture-coupled cross is inserted in a 0.56cm cavity with a diameter of 1.8cm and covered with a dielectric radome measuring 15mil in thickness.
- This architecture was then modified by replacing the microstrip feed with stripline. Preliminary results showed that the stripline geometry would require optimization and improved construct to ensure strong coupling to the device.

## 4.1 Future Directions

The research presented in this thesis has introduced several areas of interest which may be the basis for future investigation. Some of the more notable ones are highlighted.

- Improvements to the stripline geometry to ensure strong coupling to the device.
- Modifications to the TLM program to allow finer resolution of the dielectric cross and other irregularly shaped objects.
- Examination of the use of nonhomogeneous objects to improve coupling from the feed-line. This procedure would entail the construction of elements composed of two separate permittivities in a stacked block configuration.
- Simulation and physical comparison of simple two and four element arrays of cavity backed antennas described in the thesis.
- A study could be undertaken to examine the effects of fine and coarse meshing of antenna geometries. This is especially of concern with respect to stripline feeds as the higher frequencies have been typically defined by only one mesh width.

# References

[1] J. R. James and P. S. Hall, "Handbook of Microstrip Antennas", James and Hall (editors), Chapter 1 (Introduction), Peter Peregrinus Ltd.(1989).

[2] A.Adrian and D.H. Schaubert, "Dual Aperture-coupled Microstrip Antenna for Dual or Circular Polarisation", Electronics Letters, 5 November 1987, Vol.23, No.23, pp.1226-1227.

[3] H. Shoki, K. Kawabata and H. Iwasaki, "A Circularly Polarized Slot-coupled Microstrip Antenna Using a Parasitically Excited Slot", IEICE Trans. Vol. E 74, No.10, October 1991, pp. 3268-3273.

[4] H. Iwasaki and K. Kawabata, "A Circular Microstrip Antenna with a Cross or Slot for Circular Polarization", IEICE Trans. Vol. E 74, No.10, October 1991, pp. 3274-3279.

[5] K.P. Esselle, "Circularly Polarised Dielectric Resonator Antenna: Analysis of Near and Far Fields using FD-TD Method", 1995 URSI Digest, Newport Beach, California June 1995, p.28.

[6] K. Esselle, "Circularly Polarised Low Profile Rectangular DRA FD-TD and Experimental Results", IEEE AP-96 Symposium, Baltimore, MD. July 21-26,1996 pp. 577-580.

[7] K. Esselle, "The Finite-Difference Time-Domain Analysis of a Rectangular Dielectric Resonator Antenna", Journal of Electrical and Electronics Engineers, Australia, 1995, Vol.15 No.1 pp. 63-70.

[8] L. Shafai and A.A. Kishk, "Handbook of Microstrip Antennas", James and Hall (editors), Chapter 2 (Analysis of circular and microstrip antennas), Peter Peregrinus Ltd.(1989).

[9] H.Moheb and J. Shaker, "Performance Enhancement of EHF Cavity Backed Antenna Element", Proceedings of the Symposium on Antenna Technology and Applied Electromagnetics, ANTEM-96, 1996, Montreal, Canada, Conf. Proc. pp. 197-200.

[10] N.R.S. Simons, A. Sebak and A. Ittipiboon, "Analysis of Aperture-Coupled Microstrip-Antenna and Circuit Structures using the Transmission-Line-Matrix Method", IEEE Trans. AP, August 1995, v.37 No.4 pp. 27-37.

[11] J. Carrie, K. Esselle, D.J. Roscoe, A.Ittipiboon, A. Sebak and L. Shafai, "A K-Band Circularly Polarized Cavity-backed Dielectric Resonator", IEEE AP-96 Symposium, Baltimore, MD. July 21-26,1996 pp. 734-737.

[12] P.M. Frank, "Integrating Active Devices to Structures with Aperture-coupled, Microstrip Feeding", M Sc. Thesis, University of Manitoba, 1996.

[13] H. Legay, "Ka-Band Active Array", NSERC/SPAR CRD Project, Part I, Submitted by University of Manitoba, 1994.

[14] D.M. Pozar, "Microstrip Antenna Aperture-coupled to a Microstrip Line", Electronics Letters, 17 January 1985, Vol.21 No.2, pp.49-50.

[15] D.J. Roscoe, L. Shafai, A. Ittipiboon, M. Cuhaci and H. Moheb, "Novel Low Profile Antenna Candidates for EHF Portable Terminals", IMSC 1995 Symposium, pp. 318-323, Ottawa, Ont., June 1995.

[16] A.J.M.Soares, S.Barosso De Assis Fonseca and A.J. Giarola, "The Effect of a Dielectric Cover on the Current Distribution and Input Impedance of Printed Dipoles", IEEE Trans. AP, November 1984, v.32 No.11 pp. 1149-1153.

[17] S.T. Jellett and M.E. Bialkowski, "A Circularly Polarised MSAT Antenna Element with Increased Operational Bandwidth", IEEE AP-94 Symposium, Seattle, WA. June 19-24,1994 pp. 1044-1047.

[18] I.J. Bahl and P. Bhartia, "Microstrip Antennas", 1980 Artech House.

[19] M.A. Saed, "Efficient Method for Analysis and Design of Aperture-Coupled Rectangular Microstrip Antennas", IEEE Trans. AP, July 1993, v.41 No.7 pp. 986-989.

[20] J.Cheng N.I.Dib and P.B.Katehi, "Theoretical Modeling of Cavity-Backed Patch Antennas using a Hybrid Technique", IEEE Trans. AP, September 1995, v.43 No.2 pp. 1003-1013.

[21] S.A.Long, M.W. McAllister and L.C. Shen, "The Resonant Cylindrical Dielectric Cavity Antenna", IEEE Trans. AP, May 1983, v.31 No.5 pp. 406-412.

[22] A. Kumar and H.D. Hristov, "Microwave Cavity Antennas", Artech House.

[23] K.C. Gupta, R. Garg and I.J. Bahl, "Microstrip Line and Slotlines", 1979 Artech House.

[24] A. Ittipiboon, R.Oostlander, Y.M.M. Antar and M. Cuhaci, "A Modal Expansion Method of Analysis and Measurement on Aperture-Coupled Microstrip Antenna", IEEE Trans. AP, November 1991, v.39 No.11 pp. 1567-1574.

[25] J.R. Mosig and F.E. Gardiol, "Rayonnement d'une antenne microruban de forme abritraire" (Radiation of an arbitrarily shaped microstrip antenna), Ann. Telecommun. v.40 No.3-4, 1985, pp. 181-189.

[26] J.R. Mosig and F.E. Gardiol, "General Integral Equation Formulation for Microstrip Antennas and Scatterers", IEE Proc. Vol. 132 Pt. H No.7 Dec.1985, pp.424-432.

[27] J.R. Mosig, "Arbitrarily Shaped Microstrip Structures and their Analysis with a Mixed Potential Integral Equation", IEEE Trans. MTT Vol.36 No.2, February 1988, pp.314-323.

[28] P.L. Sullivan and D. H. Schaubert, "Analysis of an Aperture Coupled Microstrip antenna", IEEE Trans. AP August 1986, Vol.34 No.8 pp.977-984.

[29] X. Shen, G.A.E. Vandenbosch and A. R. Van de Capelle, "Study of Gain Enhancement Method for Microstrip Antennas using Moment Method", IEEE Trans. AP March, 1995, Vol.43 No.3 pp.227-231.

[30] L. Barlatey, J.R. Mosig and T. Sphicopolous, "Analysis of Stacked Microstrip Patches with a Mixed Potential Integrated Equation", IEEE Trans. AP, May 1990, v.38 No.5 pp. 608-615.

[31] F. Zavosh and J.T. Aberle, "Single and Stacked Circular Microstrip Patch Antennas Backed by a Circular Cavity", IEEE Trans. AP July, 1995, Vol.43 No.7 pp. 746-750.

[32] A. Ittipiboon, D. Roscoe, J.Carrie and L.Shafai, "Lens antenna with improved efficiency for millimeter-wave applications", Proceedings of the Symposium on Antenna Technology and Applied Electromagnetics, ANTEM-96, 1996, Montreal, Canada, Conf. Proc. pp. 193-196.

[33] M.A. Richard, K.B.Bhasin, and P.C. Claspy, "Superconducting Microstrip Antennas: An Experimental Comparison of Two Feeding Methods", IEEE Trans. AP, July 1993, v.41 No.7 pp. 967-974.

[34] S.D. Tangoski and D.M. Pozar, "Improved Coupling for Aperture-coupled Microstrip Antennas", Electronics Letters, 20 June 1991, Vol.27 No.13 pp. 1129-1131.

[35] P.B. Johns and R.L. Beurle, "Numerical Solution of 2-D Scattering Problems using a Transmission Line Matrix", Proc. IEE Vol.118 pp. 1203-1208, 1971.

[36] N.R.S. Simons, "Application of the Transmission-Line Matrix Method to Open Region Field Problems", M Sc. Thesis, University of Manitoba, 1992.

[37] N.R.S. Simons, "Development and Application of Differential-Equation based Numerical Techniques to Electro-magnetic Scattering and Radiation Problems", Ph.D. Thesis, University of Manitoba, 1994.

[38] W.J.R. Hoefore, "The Transmission Line Matrix (TLM) Method, in: Numerical Techniques for Microwave and Millimeter Wave Passive Structures", T. Itoh (editor), Wiley, New York, 1989.

[39] P.B. Johns, "A Symmetric Condensed Node for the Transmission Line Matrix Method", IEEE Trans. MTT April, 1987, Vol35 No.4 pp. 370-377.

[40] S. Akhtarzal and P.B. Johns, "Generalized Elements for the Transmission Line Matrix Method of Numerical Analysis", Proc. IEE December, 1975, Vol. 122 No. 12, pp. 1349-1352.

[41] Sanford and Munson, "Conformal VHF Antenna for Apollo-Soyuz Test Project", IEE International Conference publ.128 Antennas for Aircraft and Spacecraft, 1975 pp. 130-135.

[42] M. Haneishi, T. Nambara and S. Yoshida, "Study on Ellipticity Properties of Single-fed type Circularly Polarised Microstrip Antennas", Electronics Letters, 4 March, 1982 Vol.18 No.5, pp.191-193.

[43] W.F. Richards, Yuen T. Lo and D.D. Harrison, "An improved theory for Microstrip Antennas and Applications", IEEE Trans. AP January 1981, Vol.29 No.1 pp. 38-47.

[44] R.M. Sorbello and A. I.Zaghloul, "Wideband, High Efficiency Circularly Polarized Slot Elements", 1989 IEEE Int. Symposium AP pp. 1473-1476.

[45] P.C. Sharma and K.C. Gupta, "Analysis and Optimized Design of Single Feed Circularly Polarized Microstrip Antennas", IEEE Trans. AP November 1983, Vol.31 No.6 pp. 949-955.

[46] J. Huang, "A technique for an Array to Generate Circular Polarization with Linearly Polarized Elements", IEEE Trans. AP September 1996, Vol.34 No. 9, pp. 1113-1124.

[47] M. Haneishi and Y. Suzuki, "Handbook of Microstrip Antennas", James and Hall (editors), Chapter 4 (Circular Polarization and Bandwidth), Peter Peregrinus Ltd.(1989).

[48] M.I. Aksun, S. Chuang and Y.T. Lo, "On Slot-Coupled Microstrip Antennas and Their Applications to CP Operation- Theory and Experiment", IEEE Trans. AP August 1988, Vol.38 No.8 pp. 1224-1230.

[49] S.D. Tangoski and D.M. Pozar, "Design of Wideband Circularly Polarized Aperture-Coupled Microstrip Antennas", IEEE Trans. AP, February 1993, v.41 No.2 pp. 214-220.

[50] C.H.Tsao, Y.M.Hwang, F. Kilburg and F. Dietrich, "Aperture Coupled Patch Antennas with Wide-bandwidth and Dual-polarization capabilities", IEEE AP-88 Symposium, Syracuse, NY. June 6-10,1988 pp. 936-939.

[51] P.C. Sharma and K.C. Gupta, "Analysis and Optimised Design of Single-feed Circularly Polarised Microstrip Element", IEEE Trans. AP, Vol31, 1983.

[52] E. Aloni and R. Kastner, "Analysis of a Dual Circularly Polarized Microstrip Antenna fed by Crossed slots", IEEE Trans. AP, August 1994, v.42 No.8 pp. 1053-1058.

[53] A. Ittipiboon, D. Roscoe, R.K. Mongia and M. Cuhaci, "A CP Dielectric Guide Antenna with a single slot feed", Proceedings of the Symposium on Antenna Technology and Applied Electromagnetics, ANTEM-94, 1994, Ottawa, Canada, Conf. Proc. pp. 427-430.

[54] Constantine A. Balanis, "Antenna Theory, Analysis and Design", (1st Ed.) Harper and Rowe, New York, 1982.

[55] D.J. Roscoe, J. Carrie, A. Ittipiboon and L. Shafai, "A 30GHz transmit array for portable communications terminals", IEEE AP-96 Symposium, Baltimore, MD. July 21-26,1996 pp. 1116-1119.

[56] M.Haneishi and H. Takazawa, "Broadband Circularly Polarised Planar Array Composed of a pair of Dielectric Resonator Antennas", Electronics Letters, 9 May 1987, Vol.21, No.10, pp. 437-438.

[57] A. Ittipiboon, R.K. Mongia, Y.M.M. Antar, P. Bhartia and M. Cuhaci, "Aperture fed Rectangular and Triangular Dielectric Resonators for use as Magnetic Dipole Antennas", Electronics Letters, 11 November 1993, Vol. 29 No. 23, pp. 2001-2002.

[58] A. Ippitiboon, D. Roscoe and M. Cuhaci, "A General Radiation Field Computation of Dielectric Resonator Antennas", IEEE AP-94 Symposium, Seattle, WA. June 19-24,1994, pp. 760-763.

[59] R.K. Mongia, "Half-split Dielectric Resonator Placed on Metallic Plane for Antenna Applications", Electronics Letters, 30 March 1989, Vol. 25 No. 7 pp.462-464.

[60] R.K. Mongia, A. Ippitiboon, and M. Cuhaci, "Measurement of Radiation Efficiency of Dielectric Resonator Antennas", IEEE Microwave and Guided Wave Letters, Vol.4 No.3 March 1994 pp. 80-82.

[61] A. Petosa, D.J. Roscoe, A. Ittipiboon, and M. Cuhaci, "Antenna Research at the Communications Research Centre", IEEE Antennas and Propagation Magazine, Oct. 1996, v.38 No. 5, pp.7-18.

[62] A. Petosa, M. Cuhaci, A. Ittipiboon, N.R.S. Simons and R. LaRose, "Microstrip-Fed Stacked Dielectric Resonator Antenna", Proceedings of the Symposium on Antenna Technology and Applied Electromagnetics, ANTEM-96, 1996, Montreal, Canada, pp.705-708.

[63] P. Brachat and J.M. Baracco, "Dual-polarization, Slot-Coupled Printed Antennas fed by stripline", IEEE Trans. AP July 1995, Vol.43 No.7 pp.738-742.

[64] I.J.Bahl and Ramesh Garg, "A Designers Guide to Stripline Circuits", Microwaves, Jan 1978, pp. 90-96.

[65] N.I. Herscovici, N. K. Das, J. Klugman, "A Microstrip Array fed by a new type of multilayer Feeding Network", Microwave Journal, July 1995, pp. 124-134.

[66] J. Carrie, N.R.S. Simons, A. Ittipiboon, D.J. Roscoe, A. Sebak and L. Shafai, "A Ka-Band Circularly Polarized Dielectric Resonator modelled using the Transmission-Line-Matrix method", Proceedings of the Symposium on Antenna Technology and Applied Electromagnetics, ANTEM-96, 1996, Montreal, Canada, Conf. Proc. pp. 709-712.

[67] D.J. Roscoe, R. Douville, J.-F. Rivard, A. Ittipiboon, L. Shafai, A. Sebak, J. Carrie, M. Macki, A. Sebak, J. Wight, D. McPherson, E. Guetre and L. Chow, "Phased Array Technology for Circularly Polarized Ka-Band Satellite Antennas", Third Ka-Band Utilization Conference, 1997 Sorrento, Italy.

[68] A. Petosa, A. Ittipiboon, Y. M. M. Antar, D.J. Roscoe and M. Cuhaci, "Recent Advances in Dielectric-Resonator Antenna Technology", IEEE Antennas and Propagation Magazine, June 1998, v.40 No. 3, pp.35-48.

# IMAGE EVALUATION
# TEST TARGET (QA-3)

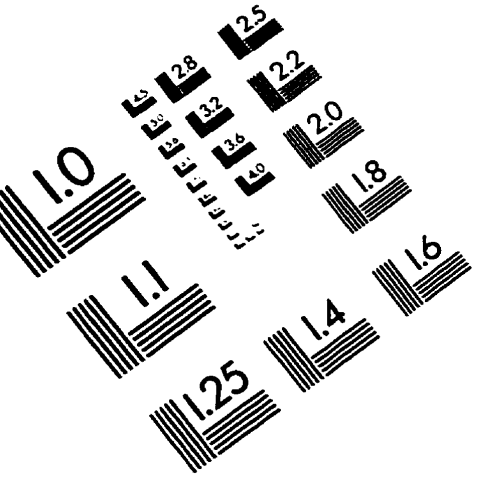


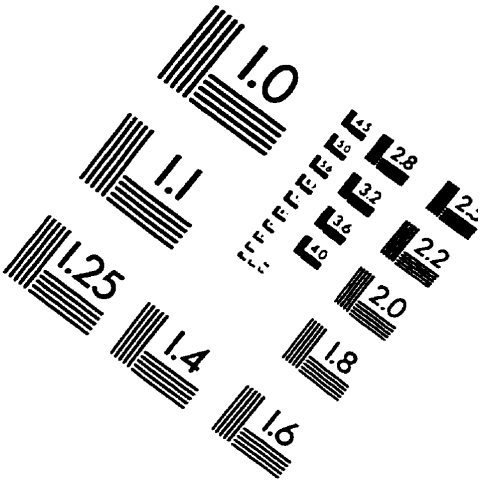


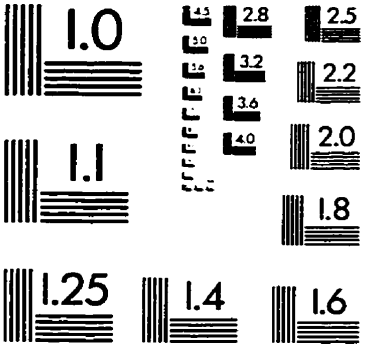


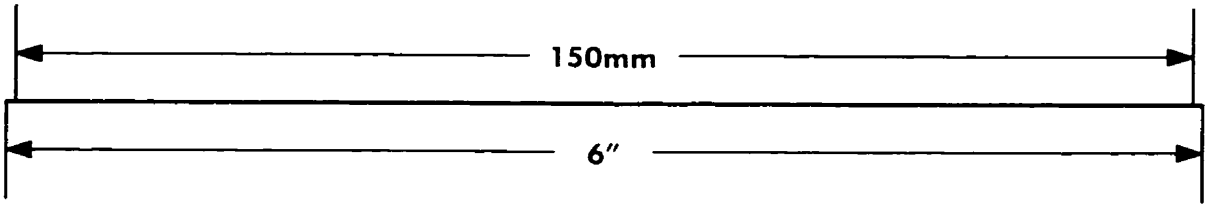


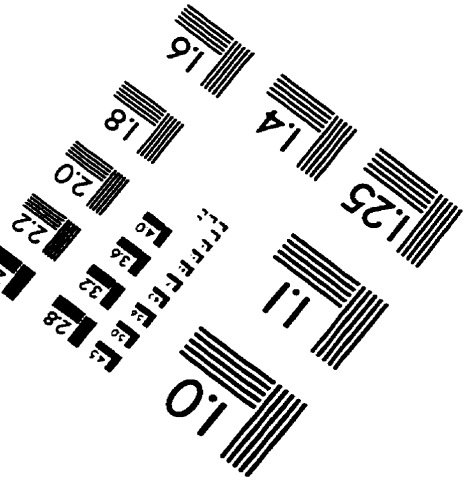


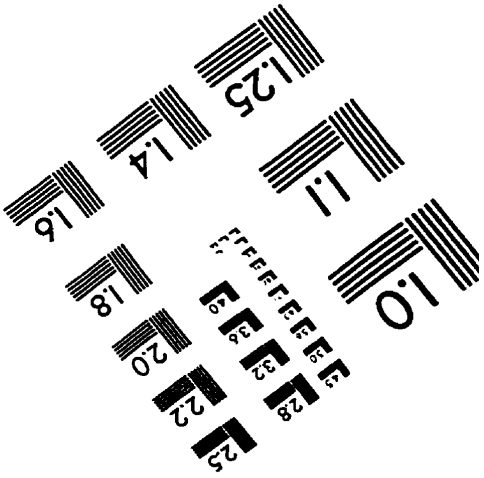


APPLIED IMAGE, Inc
1653 East Main Street
Rochester, NY 14609 USA
Phone: 716/482-0300
Fax: 716/288-5989